

Miniaturized and Parallel Synthesis of Compound Libraries for High-Throughput On-Chip Screening on Hydrophilic-Hydro- phobic Patterned Surfaces

Zur Erlangung des akademischen Grades eines

DOKTORS DER NATURWISSENSCHAFTEN

(Dr. rer. nat.)

von der KIT-Fakultät für Chemie und Biowissenschaften

des Karlsruher Instituts für Technologie (KIT)

genehmigte

Dissertation

von

Marius Brehm

1. Referent: Prof. Dr. Pavel Levkin
2. Referent: Priv.-Doz. Dr. Michael Hirtz

Tag der mündlichen Prüfung: 15.04.2021

Wo damals die Grenzen der Wissenschaft waren, da ist jetzt die Mitte.

Georg Christoph Lichtenberg

Inhaltsverzeichnis

| | |
|--|-------------|
| Inhaltsverzeichnis | i |
| Abstract | iv |
| Zusammenfassung | v |
| List of Figures | vi |
| Table Directory | xiv |
| List of Abbreviations | xv |
| Vorwort | xvii |
| 1 Theoretical Introduction | 1 |
| 1.1 Wettability of Surfaces | 1 |
| 1.2 The Droplet Microarray | 3 |
| 1.2.1 Manufacturing..... | 3 |
| 1.2.2 Applications..... | 5 |
| 1.3 Solid Phase Synthesis | 10 |
| 1.4 Photolabile Linkers | 11 |
| 1.5 Chemical Reactions | 14 |
| 1.5.1 Ugi-Reaction | 14 |
| 1.5.2 Suzuki-Miyaura-Reaction | 16 |
| 1.5.3 Thiolactone Aminolysis & Disulfide Exchange..... | 18 |
| 2 Experimental Part | 19 |
| 2.1 Reversible Wettability by Silanization | 19 |
| 2.1.1 Materials and Methods | 20 |
| 2.1.1.1 HEMA-co-EDMA Polymer Coating of Glass Slides ^[25] | 20 |
| 2.1.1.2 Surface Modification via Silanization | 20 |
| 2.1.1.3 Surface Desilanization by Immersion | 21 |
| 2.1.1.4 Water Contact Angle Measurements..... | 21 |

| | | |
|-----------|---|----|
| 2.1.1.5 | Wettability Cycles | 21 |
| 2.1.1.6 | Superhydrophobic-Hydrophilic Pattern Printed by Liquid Dispenser..... | 21 |
| 2.1.1.7 | Time-of-Flight Secondary Ion Mass Spectrometry (ToF-SIMS) ^[3] | 21 |
| 2.1.1.8 | Atomic Force Microscopy (AFM) ^[3] | 22 |
| 2.1.2 | Results and Discussion..... | 22 |
| 2.1.2.1 | Investigation of Different Polymer Porosities | 22 |
| 2.1.2.2 | Process of Silanization | 23 |
| 2.1.2.3 | Desilanization Process | 25 |
| 2.1.2.4 | Reversible Wettability | 27 |
| 2.1.2.5 | Spatial Control of Desilanization | 30 |
| 2.1.2.6 | Application of Other Substrates | 34 |
| 2.1.3 | Conclusion | 36 |
| 2.2 | Application of Droplet Microarrays for Solid Phase Synthesis | 37 |
| 2.2.1 | Nanomolar Synthesis in Droplet Microarrays for UV-Triggered On-Chip Cell Screening | 37 |
| 2.2.1.1 | Materials and Methods | 39 |
| 2.2.1.1.1 | Patterning and Functionalization of the Polymer with Photolinker..... | 39 |
| 2.2.1.1.2 | Photorelease and LC-MS Analysis of Products..... | 39 |
| 2.2.1.2 | Results and Discussion..... | 40 |
| 2.2.1.2.1 | Loading and Photorelease..... | 40 |
| 2.2.1.2.2 | Raman Microscopy of Linker-Modified DMA..... | 42 |
| 2.2.1.2.3 | Biocompatibility and Selectivity of UV-Release | 44 |
| 2.2.1.2.4 | Exemplary Reactions for LC-MS Analysis | 48 |
| 2.2.1.2.5 | Copying of the Array for MALDI-TOF Analysis..... | 52 |
| 2.2.2 | Sequence-Defined Oligomers via Ugi/Thiol-ene Cycles..... | 56 |
| 2.2.2.1 | First Ugi Cycle | 57 |
| 2.2.2.2 | Thiol-Ene Reaction with 3-Mercaptopropionic Acid | 61 |
| 2.2.2.3 | Second Ugi Cycle | 62 |

| | | |
|----------|---|-----------|
| 2.2.2.4 | Thiol-Ene Reaction with Cysteaminium Chloride | 65 |
| 2.2.3 | Pd-Catalysed Synthesis of Biphenyls and Screening for Estrogenic Activity | 67 |
| 2.2.3.1 | Results and Discussion | 68 |
| 2.2.3.2 | YES-Assay..... | 77 |
| 2.2.3.3 | MALDI-ToF from Conductive Droplet Microarrays..... | 81 |
| 2.2.4 | Conclusion | 83 |
| 3 | Summary..... | 84 |
| 4 | Outlook..... | 87 |
| 5 | Appendix..... | 88 |
| 5.1 | Spectra | 88 |
| 5.1.1 | Thickness of Polymer Coating via Optical Profilometry | 88 |
| 5.1.2 | Raman Spectra and LC-MS Chromatograms of Chapter 2.2.1 | 90 |
| 5.1.3 | LC-MS Chromatograms of Chapter 2.2.2..... | 98 |
| 5.1.4 | LC-MS Chromatograms of Chapter 2.2.3..... | 112 |
| 5.2 | Bibliography | 121 |

Abstract

Superhydrophobic surfaces are an interesting phenomenon and were studied extensively in the last decades. With the most famous example in nature, the lotus leaf, their water-repellent and self-cleaning properties inspired scientist to produce such surfaces artificially and use them for corrosion inhibition, anti-biofouling, oil-water separation or controlling of cell adhesion in life sciences. As more complex projects require more flexibility in the control of surface wettability, many methods for (reversibly) switching between a hydrophilic and a hydrophobic state were introduced, but lacked either inherent stability of these states, needed UV-irradiation or only allowed for an insufficient change of wettability. Therefore, a new methodology for a fast, stable and reversible switch of surface wettability is introduced as first project of this work in chapter 2.1. It is based on the silanization of a hydrophilic, nanoporous HEMA-co-EDMA polymer coating or a smooth silicon wafer and the rapid removal of this modification via fluoride anions. Since both steps are completely reversible as monitored by ToF-SIMS analysis, multiple cycles between a superhydrophobic and hydrophilic surface were possible with each step performed in less than 2 minutes. The fluoride anions were applied as a solution via immersion of the whole surface or spatial application via automated liquid dispensing or brushes. The presented work allows for a fast and simple manufacturing of hydrophilic-superhydrophobic patterned surfaces. Such surfaces were already introduced as droplet microarrays (DMA) over the last years by the group of Prof. Dr. Pavel Levkin as a versatile tool for miniaturized biological screenings. In chapter 2.2, such microarrays were utilized for the first time for miniaturized and parallel solid phase synthesis, where every hydrophilic spot served as a microvessel, containing the reaction solutions. The use of a UV-cleavable linker allowed for a contaminant-free release of the target compounds while adding more flexibility to the screening conditions by variation of concentration via irradiation time. The biocompatibility of the photorelease was demonstrated and an exemplary 588-compound library was synthesized via the Ugi multicomponent reaction in low nanomolar scale. Several reaction types were shown to work on the DMA, such as Ugi reactions with the amine or carboxylic acid entry bound on the solid phase (chapter 2.2.1), thermally induced hydrothiolation of alkenes, copper-catalyzed azide-alkyne cycloaddition (chapter 2.2.2) and the palladium-catalysed Suzuki-Miyaura cross coupling reaction (chapter 2.2.3). With the latter one, an 800-compound library was synthesized in the sub-nanomolar range and on-chip screened for estrogenic activity. By producing the DMA directly on an ITO surface instead of glass, MALDI-ToF analysis could be performed from the polymer coated surface.

Zusammenfassung

Superhydrophobe Oberflächen stellen ein interessantes Phänomen dar und wurden in den letzten Jahrzehnten ausgiebig untersucht. Das Lotusblatt als das wohl berühmteste Beispiel inspirierte zahlreiche Wissenschaftler dazu, seine Eigenschaften auf künstliche Oberflächen zu übertragen und in verschiedenen Bereichen einzusetzen, wie z.B. dem Schutz vor Rost oder Biofilmen, der Trennung von Öl-Wasser-Gemischen oder der Kontrolle von Zelladhäsion in biomedizinischen Materialien. Wegen der steigenden Anforderungen wurden später auch schaltbare Oberflächen entwickelt, die zwischen einem hydrophilen und hydrophoben Zustand kontrolliert wechseln können. Diesen Methoden mangelt es jedoch häufig an physikalisch-chemischer Stabilität oder einem ausreichend starken Unterschied in der Benetzbarkeit, so dass im Kapitel 2.1 dieser Arbeit eine neue Methode entwickelt wurde. Diese basiert auf der Silanisierung einer intrinsisch hydrophilen und nanoporösen Polymerbeschichtung durch fluoridierte Alkylsilane, wodurch ein superhydrophober Zustand erreicht wird. Die Applikation von Fluorid-Ionen entfernt diese Modifikation selektiv, so dass die ursprüngliche, hydrophile Oberfläche wiederhergestellt wird. Beide Schritte sind innerhalb von je 2 Minuten durchführbar und komplett reversibel, wie mittels ToF-SIMS nachgewiesen wurde, sodass mehrere Zyklen hintereinander möglich waren. Die Methode war ebenfalls anwendbar für glatte Siliziumwafer als Oberfläche und andere Silane. Die Fluorid-Ionen wurden als Lösung appliziert, was durch die Verwendung von Pinsel oder automatischen Dispensiergeräten erlaubte, flexible Muster von hydrophilen-hydrophoben Bereichen zu erzeugen. Diese ähnelten der photolithografisch hergestellten Oberfläche des „droplet microarrays“, einer Plattform für miniaturisierte, biologische Screenings, die in der Arbeitsgruppe um Prof. Dr. Pavel Levkin entwickelt wurde. Solche Microarrays wurden erstmalig im Kapitel 2.2.1 dieser Arbeit für die miniaturisierte und parallele Festphasensynthese von Molekülbibliotheken verwendet. Hierbei diente jedes separierte Tröpfchen auf einem hydrophilen Spot als kleines „Reaktionsgefäß“. Ein UV-spaltbarer Linker ermöglichte es, die Reaktionsprodukte ohne das Hinzufügen von Reagenzien in die Tröpfchen zu überführen, wobei die qualitative und quantitative Kontrolle dieses Prozesses über die Variation der Belichtung erreicht wurde. Die Kompatibilität zu biologischen Systemen wurde am Beispiel von CHO-K1 Zellen gezeigt und eine Molekülbibliothek von 588 Produkten wurde mittels Ugi Reaktion im Nanomol-Maßstab synthetisiert. Eine Auswertung mittels MALDI-ToF war möglich, nachdem die abgelösten Produkte mit Matrixlösung gemischt und auf eine leitfähige ITO-Oberfläche übertragen wurden. Es wurden verschiedene Reaktionstypen auf dem „droplet microarray“ erfolgreich getestet: Die Ugi Reaktion, die thermisch initiierte Addition von Thiolen an Alkenen, eine Cu-katalysierte Azid-Alkin Cycloaddition (Kapitel 2.2.2) sowie die Pd-katalysierte Suzuki-Miyaura Kreuzkupplung (Kapitel 2.2.3). Mittels Letzterer wurde eine Bibliothek mit 800 Produkten hergestellt und auf der gleichen Oberfläche in einem hefebasierten Assay auf ihre östrogene Wirkung überprüft. Durch Verwendung von ITO-Glasträgern war es zudem möglich, MALDI-ToF Messungen direkt von der Polymeroberfläche durchzuführen.

List of Figures

| | |
|--|----|
| Figure 1. Droplets of water (10 μ l) on a superhydrophilic (A) and superhydrophobic (B) surface. Adapted with permission. ^[3] | 2 |
| Figure 2. SEM picture of a leaf from the Indian lotus shows the micropillars with hydrophobic grease and its nanostructure. Adapted with permission. ^[11] | 2 |
| Figure 3. (A) The effect of discontinuous dewetting shown with water on a DMA with 900 μ m round spots. (B) The workflow of parallel cell screening on the DMA by using the sandwiching approach. A chemical library was printed on a glass slide and dried prior to sandwiching it onto a DMA containing cells to treat the distinct volumes with the respective compounds. After incubation, the cells can be read out directly via live imaging or after live staining with CalceinAM. Staining can be performed via sandwiching with or immersion in the staining solution. Image adapted with permission. ^[25] | 7 |
| Figure 4. Overview of the solid phase-synthesis of tripeptides on DMA using a UV-cleavable linker. (A) 4 Fmoc-protected amino acids were combined column- and row-wise to achieve a exemplary library of 16 products. (B) Multi-step reaction is possible through solid phase synthesis with washing and deprotection step in between the amino acid couplings. (C) Phototriggered release of tripeptides into the distinct droplet of the DMA. Image adapted with permission. ^[2] | 9 |
| Figure 5: o-Nitrobenzyl alcohol derivates studied by Woodward et al. ^[51] Photorelease is followed by decarboxylation, yielding the amine. | 12 |
| Figure 6: Connection to the solid phase via α -substitution (left) and para-substitution (right). X = NH, O. | 13 |
| Figure 7: Photolabile linkers HEPL and FAPL , which were used in this work. | 13 |
| Figure 8. Common side products of the Ugi 4-component reaction. A Passerini product; B Product of the Ugi 3-component reaction; C Amidine byproduct | 15 |
| Figure 9. Changes of wettability of the polymer surface during silanization (A) and desilanization (B). For each given time point, the slide was immersed in the respective solution, washed extensively and analyzed via goniometry. Every data point is the average of 3 measurements at different positions on the surface. Error bars represent standard deviation. (C,D) ToF-SIMS analysis of | |

| | |
|--|----|
| the TCPS silanized surface shows the presence of fluorinated alkylsilanes indicated by the detection of Si^+ (C) and CF_3^+ (D) ion signals..... | 24 |
| Figure 10. Depth profile of a silanized polymer film via ToF-SIMS analysis. Si^+ and CF_3^+ ions are fragments from the fluorinated alkylsilane and $C_2H_3O^+$ is a fragment of the polymer coating. The silane modification is only present on the top and does not penetrate through the whole polymer layer. | 25 |
| Figure 11. General overview of cyclic wettability as a reaction scheme (A) and images of water droplets on hydrophilic (B/D) and superhydrophobic (C/E) polymer surfaces. (A) The nanoporous HEMA-co-EDMA polymer on a glass support is hydrophilic due to its hydroxyl groups and can be rapidly modified with 1H,1H,2H,2H-trichloroperfluorooctylsilane (TCPS) to exhibit superhydrophobicity. This process is completely reversible by treatment with tetra-n-butylammonium fluoride (TBAF). Each step can be performed in 2 minutes at room temperature. Structure of siloxane layer is simplified for better visualization. (B/C) Screen captures of water droplets from the water contact angle analysis. (D/E) Photographs of pipetted aqueous food dye solutions. | 27 |
| Figure 12. Static water contact angles for reversible surface modification cycles. Silanization and desilanization processes were alternated and the static water contact angles were measured after every conversion. The achieved WCA remained stable even after 16 steps..... | 28 |
| Figure 13. Surface topography of nanoporous HEMA-co-EDMA coated surfaces as measured by atomic force microscopy (small artefacts visible). (A) pristine polymer coating (B) TCPS modified surface (C) TCPS modification was removed via TBAF in 2 minutes (D) TCPS modified surface after immersion in THF for 24 h (E) prolonged immersion in 0.1 M TBAF solution for 2 h. The pictures demonstrate the dominating porous structure of the polymer coating, which is not affected by silanization or desilanization. The coating therefore shows stability against THF and TBAF..... | 29 |
| Figure 14. Depth integrated SIMS data of polymer layers: (A) non-treated, (B) TCPS-silanized, and (C) desilanized. The polymer was thoroughly eroded during measurement and the intensities of the CF^+ and CH_3O^+ ions were summarized for the whole layer. No residual CF^+ was detected after the TBAF treatment, indicating complete conversion..... | 30 |

Figure 15. A TCPS-modified slide after manual application of each 5 μ l desilanization solution (0.1 M TBAF in 10% (v/v) THF in GBL) and washing via ethanol flow. Short contact time of TBAF during washing leads to partial desilanization.31

Figure 16. Two-dimensional mapping of ToF-SIMS analysis of a spatially desilanized surface (**A–C**) and photographs of aqueous food dyes in this microarray (**D/E**). The TCPS-modified surface was printed with 8 nl of 0.1 M TBAF in 10% (v/v) THF in GBL by the automatic liquid dispensing system (iDot); the reaction time was 2 minutes. Top panels show the lateral distribution of the signal intensity of the CF+ (**A**), H+ (**B**) and C2F3+ (**C**) ions where the difference in surface chemistry is visible. **D/E** Images of the droplet microarray with a spot diameter of 1 mm and a spot-to-spot distance of 1.5 mm (500 nl of aqueous solutions of food dyes per spot were used for better visualization).32

Figure 17. Photographs of the brush writing method (**A**) and the resulting patterns (**C–D**). The desilanization solution can be applied using a brush dipped into the liquid. (**A**) Image shows the simple process of designing a fluid channel on a hydrophobic background. (**B**) After a 2-minute reaction, the liquid is washed off and the channel is filled with aqueous food dye for better visualization. (**C**) and (**D**) Images show examples of hand-made hydrophilic patterns in which aqueous dye solutions are held.33

Figure 18. Developed water contact angles of each 10 μ l deionized water on pristine, silanized and desilanized HEMA-co-EDMA (**A/B**) and silicon surfaces (**C**). First column shows the plain surfaces with static WCA of 6° (**A/B**) and 30° (**C**). Modification of the respective surfaces with either trichlorododecylsilane, trimethylchlorosilane or TCPS yielded contact angles of 110°, 102° and 107°. Treatment with the TBAF desilanization solution for 2 minutes changed the contact angles to 7° for the polymer surfaces and 55° for the silicon wafer. Prolonged treatment of the wafer for 24 h in the desilanization solution further decreased the static WCA to 35° (not presented).34

Figure 19. Surface topography of silicon wafers as measured by atomic force microscopy. (**A**) plain silicon surface (**B**) TCPS modified surface with increased surface roughness (please note the adapted color scale) (**C**) TCPS modification was removed via TBAF in 2 minutes (**D**) prolonged immersion of the silicon wafer in TBAF solution for 24 h.35

Figure 20. Droplet microarray platform combining high-throughput solid-phase synthesis and cell-based screenings. **(A)** Porous polymethacrylate thin film (12 μm thin) is functionalized with fluoroalkyl and cysteamine moieties to generate superhydrophobic and reactive hydrophilic regions, respectively. UV cleavable linker is covalently bound to the amine in the hydrophilic spots, forming the basis for the following solid-phase combinatorial synthesis. **(B)** Scheme showing a possible cell-based screening sequence: **(i)** synthesized compounds are still attached on the solid support and a cell suspension is filled into the distinct nanodroplets formed in the hydrophilic spots prior to UV irradiation to release the compounds into the solution **(ii)**. Readout can be done by fluorescence microscopy due to the transparency of the substrate. 38

Figure 21. **(A)** Attachment of chlorambucil (**CHL**) onto the hydroxyethyl photolinker (**HEPL**) with subsequent release upon UV-irradiation, leaving the cleaved photolinker (**c-HEPL**) on the surface. **(B)** Kinetics of the UV triggered release of chlorambucil as a model drug from the surface into the 5 μl droplets, determined by the spectroscopic analysis of the solution after different irradiation times. Each data point is the average of 3 experiments. Error bars represent standard deviation. **(C)** Spatial control of cleavage from **HEPL** via UV light. During cleavage of the linker, a yellow color is developed. Droplet microarrays were prepared and modified with **HEPL** in all hydrophilic spots prior to irradiation through photomasks. Top pattern: 2688 square spots with 500 μm edge length and 250 μm borders. "KIT Levkin Lab" logo was used as inverted photomask. The pictures contrast was slightly adjusted digitally to improve visibility of the logo. Bottom pattern: 80 round spots with 3 mm in diameter were irradiated in a checker-board pattern. UV linker gives full control over spatial release of compounds. 41

Figure 22. Raman analysis of a round hydrophilic spot on the DMA with the diameter of 3 mm. **(A)** The free amine groups of the cysteamine are present in the hydrophilic spots after DMA production and before modification with **HEPL**. Strong bands of C-H (2931 cm^{-1}) and alkyne groups (2120 cm^{-1} , remaining from production) are visible from the polymer support. **(B)** Attachment of **HEPL** is detectable by the increased band intensity at 1333 cm^{-1} referring to its nitro group and 1579 cm^{-1} for the aromatic system. **(C)** UV irradiation (365 nm, 2.5 mW/cm^2 , 15 min) of the surface reduces the nitro group of **HEPL** to nitroso and decreases this bands intensity. Additionally, the band at 1276 cm^{-1} of the

benzylic alcohol is reduced due to its oxidation to the ketone. **(D)** Raman microscopy mapping of the edge of a spot modified with **HEPL**. Colors show the intensity distribution of the band at $1250\text{ cm}^{-1} - 1370\text{ cm}^{-1}$ corresponding to the C-(NO₂) vibration of the linker.....43

Figure 23. Proof of principle cell experiment with CHO-K1 cells seeded on different droplet microarrays. Cells were added by pipetting 5 μl of CHO-K1 cell suspension with a concentration of 1×10^5 cells/ml in a round 3 mm spot followed by incubation for 24 h at 37 °C before staining with CalceinAM and propidium iodide. Pictures show brightfield and fluorescence microscopy pictures at 10x magnification. Samples **(A)** and **(B)** offer solely hydroxyl groups on the surface (coming from 2-mercaptoethanol) in the hydrophilic spots. While **(A)** served as negative control, sample **(B)** was irradiated with UV light (365 nm, 2.5 mW/cm², 20 minutes) directly after cell seeding. Samples **(C)** and **(D)** were modified with **HEPL** and chlorambucil; **(D)** was irradiated under same conditions as sample **(B)** to trigger the photorelease of the model drug.....45

Figure 24. CHO-K1 cells were seeded on the DMA and their viability was determined via CalceinAM/PI staining for differently treated surfaces after incubation time of 24 h. Viability was not affected either by UV light or by the presence of the immobilized chlorambucil. The cell viability was decreased only after irradiation of the surface with attached chlorambucil, which led to the release of the drug into the droplets. Every bar represents an average of 3 repetitions of the same experiment. Error bars represent the standard deviation.....47

Figure 25. Scheme of the Ugi-4-component-reaction with variable entries for surface anchored amine (**1 – 5**), carboxylic acid (**9 – 15**), aldehyde or ketone (**16 – 23**) and isocyanide (**6 – 8**) and the formed bisamide (products **24 – 36**). Bottom: detailed representation of the solid phase chemistry. Each 4-pentynoic acid tethered to the polymer layer acts as a branching point and bears two linker molecules and thus doubles the overall number of reaction sites.....48

Figure 26. Microscopic pictures of vacuum-dried MALDI matrix mixtures (CHCA/DHB, 5 mM HCl) on an ITO slide deposited via sandwiching from a HEMA-co-EDMA polymer DMA with 2x **(A, C)** and 10x **(B, D)** magnification. Top row: 10% (v/v) acetonitrile in water was used as solvent. Bottom row: 10% (v/v) DMF in water.....54

Figure 27. Process of copying the droplet microarray onto an ITO slide for MALDI-TOF MS measurements. **(A)** The sandwiching device helps to align both slides onto each other. Left side is the bottom part with the irradiated droplet microarray while on the right is the top part with the ITO slide (already stamped with matrix). **(B)** Closed sandwiching device. The two connectors on the sides pull the two halves together while the distance is controlled by four screws. Top part is lowered until all droplets touch the ITO slide. **(C)** Merged photograph of a dry DMA (14x14 1 mm hydrophilic spots, top), the DMA with 100 nl water in each spot (middle) and the dry array after UV irradiation (bottom). **(D)** ITO slide after copying the droplet microarray which contained matrix mixture (CHCA/DHB) in the droplets and drying in vacuum. **(E)** MALDI-TOF spectra of compound **37** as sodium adduct ($[M+Na]^+$, detected: 717.55 m/z, calc.: 717.38 u) and matrix background **(F)**. The compound was first cleaved into distinct droplets via UV irradiation, followed by addition of 100 nl of a saturated solution of CHCA and DHB matrix in 10 % ACN/water (containing 5 mM HCl) into each spot and sandwiching the DMA slide onto an ITO slide to copy the array. The ITO slide was dried in vacuum and analyzed by MALDI-MS. 55

Figure 28. Schematic sequence of alternating Ugi and thiol-ene reaction for the protecting group free synthesis of sequence defined oligomers. After the Ugi reaction has introduced two variable side groups and the 4-pentenal, the available olefin is coupled with 3-mercaptopropionic acid in a thiol-ene reaction to obtain again a carboxylic acid functionality for a new Ugi cycle. 58

Figure 29. Obtained negative mode mass spectra of LC-MS runs at a retention time of 5.40 minutes. **A** Ugi product **A₁I₂** after UV-triggered cleavage ($[M-H]^+$, calculated: 455.23 m/z, detected: 455.20 m/z). **B** Product after conversion of surface-bound **A₁I₂** via immersion of the DMA in 3-mercaptopropionic acid and 1% (w/w) AIBN for 18 h at 75°C under nitrogen atmosphere ($[M-H]^+$, calculated: 561.24 m/z, detected: 561.30 m/z, smaller signal of Na-adduct also visible). 62

Figure 30. Structures of exemplary approved drugs containing the biphenyl motif: Losartan (**43**), flurbiprofen (**44**) and telmisartan (**45**). 67

Figure 31. Schematic overview of the on-chip synthesis and screening approach on the droplet microarray (DMA). DMA consists of a porous polymer coating with a thickness of around 12 μm on a microscopic glass slide (h = 1 mm) **(A)** Hydrophilic spots

(d = 900 μm), surrounded by superhydrophobic borders, serve as microcompartments for the palladium-catalyzed solid phase synthesis of biphenyls via the Suzuki-Miyaura crosscoupling reaction. The use of a photocleavable linker allows for a controlled release of the products into distinct droplets via irradiation with UV-light. Catalyst and excess starting material can be washed off beforehand and fresh solvent is applied. Hormonal activity of the products is screened in a yeast based assay, which gives a fluorescent signal according to the estrogen potential of the compound. **(B)** Structure of 17 β -estradiol (**46**).68

Figure 32. **(A)** Scheme of the first SMR reaction performed on the DMA. a) Et₃N, Pd(OAc)₂, phenylboronic acid in NMP/H₂O b) 365 nm, 2.5 mW/cm², 20 minutes in H₂O **(B)** During the reaction, Pd-black precipitation occurs, leading to a total inhibition of UV-triggered release. Different washing solutions were applied at room temperature for 4 h, yielding KCN as the best performing. Diameter of the hydrophilic spots is 3 mm.69

Figure 33. EDX spectra of a 3 mm round hydrophilic spot after the SMR before **(A)** and after **(B)** removal of the precipitated palladium via washing with a 0.1 M solution of KCN in DMSO/water (1:1, v/v). Signals representing carbon, oxygen and sulphur come from the polymer backbone, while platinum comes from the pretreatment of the sample.70

Figure 34. Preliminary test of the YES-assay on DMA with 17 β -estradiol as positive control. 100 μl of sample and 50 μl of yeast suspension were dispensed in every spot and incubated for 48 h at 37°C. **(A)** Fluorescence microscopy picture of the DMA featuring 900 μm round spots. 4 blocks with each 3 repetitions of a calibration curve and a checkerboard pattern are visible. **(B)** Concentrations of the positive controls. **(C)** Detected fluorescence intensity and standard deviation of all calibration spots plotted against the sample concentration of 17 β -estradiol. Red line shows an exponential fit. Black dotted line represents the average of all background spots with deionized water as sample.79

Figure 35. **(A)** Experimental design of the DMA for the library synthesis on 900 μm spots. The 16 x 25 = 400 compound library was released once as carboxylic acid (from and once as carboxamide (from **FAPL**), leading to 800 different compounds. **(B)** Fluorescent microscopy image of the YES assay with no found active compounds.80

Figure 36. Mass spectrum of matrix background (**A**) and doxorubicin (**B**), obtained by MALDI-ToF from a 900 μm sized hydrophilic spot from a conductive droplet microarray (cDMA). Doxorubicin solution was mixed with matrix solution (CHCA/DHB) on-chip and dried in vacuum. Mass signal corresponds to the sodium adduct ($[M+\text{Na}^+]$, calculated: 566.16 m/z, detected: 566.07 m/z). 82

Table Directory

| | |
|--|----|
| Table 1. Static, advancing, receding and sliding water contact angles for polymer coating on glass made with different contents of 1-decanol as porogene. After polymerization, the slides were modified with TCPS before analysis. Each data point is the average of 3 measurements at different positions on the surface. Standard deviation is shown in parentheses. | 23 |
| Table 2. Overview of the starting molecules for the Ugi reaction. Amines (1 - 5) are attached to the surface via the photolinker, while isocyanides (6 - 8), carboxylic acids (9 - 15) and carbonyls (16 - 23) are added as 0.5 M solutions in GBL. These 23 compounds can lead to 840 different products of the Ugi reaction..... | 50 |
| Table 3. Purity of 13 exemplary compounds synthesized through the on-chip Ugi-reaction as determined by LC-MS. | 51 |
| Table 4. Structure of amines (A_x) and Isocyanides (I_y) used in this chapter. | 59 |
| Table 5. Purity of most Ugi products using amines (A_x) and isocyanides (I_y) as determined by LC-MS. I₁ and I₂ were calculated via the absorbance at 254 nm and for I₄ and I₅ the total ion count (TIC) chromatogram was integrated. Rows and columns labelled with \emptyset show the calculated average purity..... | 60 |
| Table 6. Overview of the tested reaction conditions for the SMR between surface-bound 4-iodobenzoic acid and 4-hydroxyphenylboronic acid. | 73 |
| Table 7. Structures of the carboxylic acid aryl halide (C_x) and the boronic acid (B_x) entries..... | 75 |
| Table 8. Purity of exemplary compounds synthesized in 3 mm spots to monitor synthetic success via LC-MS analysis. Product was identified via mass detector, while purity was calculated as the proportion of the product's peak integral from the summarized peaks integrals at 280 nm absorbance. | 77 |

List of Abbreviations

| | |
|----------|---|
| WCA | water contact angle |
| SEM | scanning electron microscopy |
| HEMA | hydroxyethyl methacrylate |
| EDMA | ethylene glycol dimethacrylate |
| KIT | Karlsruhe Institute of Technology |
| PFDT | <i>1H,1H,2H,2H</i> -perfluorodecanthiol |
| DMA | droplet microarray |
| DCM | dichloromethane |
| DMF | <i>N,N</i> -dimethylformamide |
| DMSO | dimethylsulfoxide |
| GBL | gamma-butyrolactone |
| NMP | <i>N</i> -methyl-2-pyrrolidone |
| THF | tetrahydrofuran |
| MALDI | matrix assisted laser desorption ionization |
| MS | mass spectrometry |
| IR | infrared |
| UV/VIS | ultraviolet / visible light |
| SMR | Suzuki-Miyaura-Reaction |
| DMPAP | 2,2-dimethoxy-2-phenylacetophenone |
| TCPS | trichloro-(<i>1,1H,2H,2H</i> -perfluorooctyl)-silane |
| ToF-SIMS | Time-of-Flight Secondary Ion Mass Spectrometry |
| TBAF | tetrabutylammoniumfluoride |

| | |
|--------|-------------------------------|
| DIC | diisopropyl carbodiimide |
| 4-DMAP | 4-(dimethylamino)-pyridine |
| SMR | Suzuki-Miyaura reaction |
| ITO | indium tin oxide |
| AIBN | azobisisobutyronitrile |
| cDMA | conductive droplet microarray |

Vorwort

Die vorliegende Arbeit entstand im Zeitraum von November 2017 bis März 2021 in der Arbeitsgruppe von Prof. Dr. Pavel Levkin am Institut für Biologische und Chemische Systeme (ehemals Institut für Toxikologie und Genetik) am Karlsruher Institut für Technologie. Sie führt die Ergebnisse meiner Masterarbeit fort, die im Sommersemester 2017 unter Prof. Dr. Pavel Levkin mit dem Titel „Establishing Combinatorial Solid Phase Synthesis on Droplet Microarrays“ von mir angefertigt wurde.^[1] Teile dieser Masterarbeit wurden in der Zeitschrift *Materials Today Bio* veröffentlicht und trugen zur Einreichung eines Patentantrages bei. („Process for treatment of at least one cell with a chemical synthesis product in a microarray“, WO2019197122A1).^[2]

Auszüge der hier vorliegenden Arbeit wurden ebenfalls bereits veröffentlicht. Kapitel 2.1 beschreibt Ergebnisse, die zu einer Veröffentlichung in *Advanced Materials Interfaces* führten,^[3] während Teile aus Kapitel 2.2 in der Zeitschrift *Small* veröffentlicht wurden.^[4] Der Anteil der Co-Autoren beschränkte sich in beiden Publikationen auf die Bedienung der jeweiligen Analysegeräte sowie die Angabe der exakten Methodik und Geräteeigenschaften.

Zwischenergebnisse wurden weiterhin auf folgenden Konferenzen als Poster präsentiert:

- *Society of Laboratory Automation and Screening Europe* – Annual Conference & Exhibition 2018
27.6. – 29.6.2018 in Brüssel, BEL
- *Society of Laboratory Automation and Screening* – International Conference & Exhibition 2019
2.2. – 6.2.2019 in Washington, D.C., USA
- *European Laboratory Research & Innovation Group* – Drug Discovery 2019
5.11. – 6.11.2019 in Liverpool, UK
- *Society of Laboratory Automation and Screening* – International Conference & Exhibition 2020
25.2. – 29.2.2020 in San Diego, CA, USA

An dieser Stelle möchte ich einigen Menschen danken:

- Pavel Levkin für die Möglichkeit, diese Dissertation in seiner Arbeitsgruppe anfertigen zu dürfen. Für sein Vertrauen in mich und meine Fähigkeiten sowie seine strukturierte Arbeitsweise, die ich von ihm lernen durfte.
- Meiner Familie und Freunde für die Unterstützung auf meinem bisherigen Lebensweg, insbesondere meiner Freundin Ella Wipfler.

- Der Arbeitsgruppe Levkin für eine freundliche, kollegiale und kreative Arbeitsatmosphäre. Allen voran Johannes Scheiger, Janne Wiedmann, Jonathan Elton, Maria Kuzina und Anna Popova für unterhaltsame, ideenreiche, problemlösende und lustige Gespräche.
- Sergiy Afonin für die Unterstützung bei den MALDI-ToF Messungen
- Stefan Heissler für seine Hilfe bei der Raman-Spektroskopie
- Alexander Welle für die Analyse meiner Proben mittels ToF-SIMS
- Der Arbeitsgruppe ComPlat, insbesondere Patrick Hodapp, für den Zugang zur LC-MS
- Prof. Dr. Andrew Cato für hilfreiche Diskussionen über hefebasierte Screenings

1 Theoretical Introduction

1.1 Wettability of Surfaces

The wettability of a surface with water can be described as hydrophilic or hydrophobic. For a hydrophilic surface, the same volume will spread over a larger area than compared to a more hydrophobic one, which yields in different water contact angles (WCA) and a more hydrophobic surface will show a higher water contact angle as a hydrophilic one. This behavior is determined by several interactions, such as the energies of the liquid-liquid, liquid-solid and liquid-vapor interfaces and was described by T. Young in 1805 with the following equation for an ideal smooth surface with the contact angle θ and the respective energies of the interfaces for solid-vapor (γ_{sv}), solid-liquid (γ_{sl}) and liquid-vapor (γ_{lv}):^[5]

$$\cos(\theta) = \frac{\gamma_{sv} - \gamma_{sl}}{\gamma_{lv}}$$

However, nearly no surfaces in reality are perfectly smooth, which motivated R. Wenzel in 1936 to add the roughness factor r , which describes the fraction of the actually wetted area from the projected area. The corrected water contact angle (θ') is calculated as:^[6]

$$\cos(\theta') = r * \cos(\theta)$$

While this model describes a situation with the highest possible surface-liquid interface, it does not apply for cases with air trapped between the liquid and the surface. This was described by A. Cassie and S. Baxter in 1944 in their equation

$$\cos(\theta') = \phi_s [\cos(\theta) + 1] - 1$$

with ϕ_s as the fraction of the surface area which is actually in contact with the liquid.^[7]

If a surface shows a static WCA above 150° and a small contact angle hysteresis, it is defined as superhydrophobic,^[8] while a contact angle close to 0° is defined as superhydrophilic.^[9] Figure 1 shows these two situations on a nanorough polymer surface with either free hydroxyl groups or perfluorinated alkyl chains present.

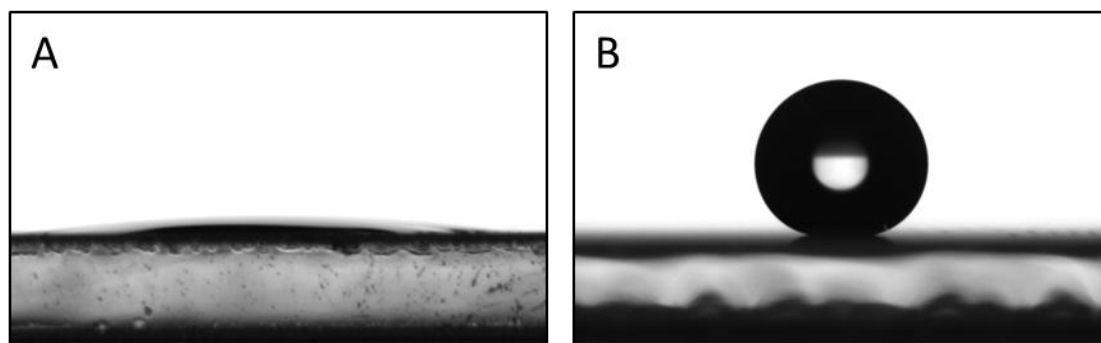


Figure 1. Droplets of water ($10\ \mu\text{l}$) on a superhydrophilic (A) and superhydrophobic (B) surface. Adapted with permission.^[3]

As the formulas above show, two main characteristics are important to control wettability and achieve a superhydrophobic surface: structure and chemistry (correlated to interface energies).^[10] A famous example of such a combination is the leaf of the lotus plant, which presents small pillars with hydrophobic grease on top^[11]. Figure 2 shows a SEM picture of a leaf from the Indian lotus to demonstrate its structuring in the micro- and nanoscale.

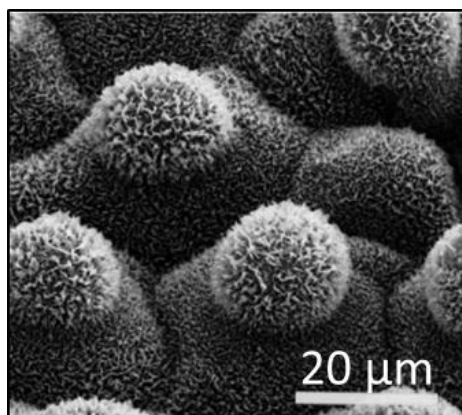


Figure 2. SEM picture of a leaf from the Indian lotus shows the micropillars with hydrophobic grease and its nanostructure. Adapted with permission.^[11]

The water-repellency and self-cleaning behaviour motivated many scientist to copy this characteristics in artificial materials. While the chemistry of the surfaces is mostly defined by hydrocarbon or fluorocarbon moieties, many different ways were introduced to structure the surface: lithography or laser structuring of silicon wafers,^[12, 13] deposition of carbon nanotubes,^[14] reactive-ion etching,^[15] electrospinning^[16] and more.^[17] As the possibilities are so manifold, the focus here should lay on the surface material which was used in this work: a nanoporous HEMA-co-EDMA copolymer (hydroxethyl methacrylate, ethyleneglycol

dimethacrylate). When hydroxyethyl methacrylate and ethylene glycol methacrylate are copolymerized in a free radical polymerization, they form a smooth polymer surface.^[10] However, in presence of porogenes such as cyclohexanol and 1-decanol, the resulting polymer has pores which induce roughness in the micro- and nanoscale. The size of the pores can be controlled by the ratio or content of both porogenes and is typically in the range of 100-500 nm for the coatings used in this work when prepared with a ratio of cyclohexanol:1-decanol 4:1 (w/w).^[18] During the polymerization reaction, the crosslinked chains of the polymer reach a decisive length and cannot be held in solution anymore by the porogenes, yielding to phase separation and globuli formation.^[10, 19] This porosity is not only inducing the hierarchical roughness needed for superhydrophobicity (after further chemical modification), but also influences how light is scattered when passing through the coating. Bigger feature size decreases the transparency of visible light, while smaller pores and globuli increase it.

1.2 The Droplet Microarray

1.2.1 Manufacturing

The droplet microarray (DMA) was developed in the group of Prof. Dr. Pavel Levkin at the KIT in 2011 and consists of a glass slide covered with nanoporous HEMA-co-EDMA copolymer, which is esterified with 4-pentynoic acid and modified via photolithography to yield an array of hydrophilic spots on a superhydrophobic background.^[18, 20]

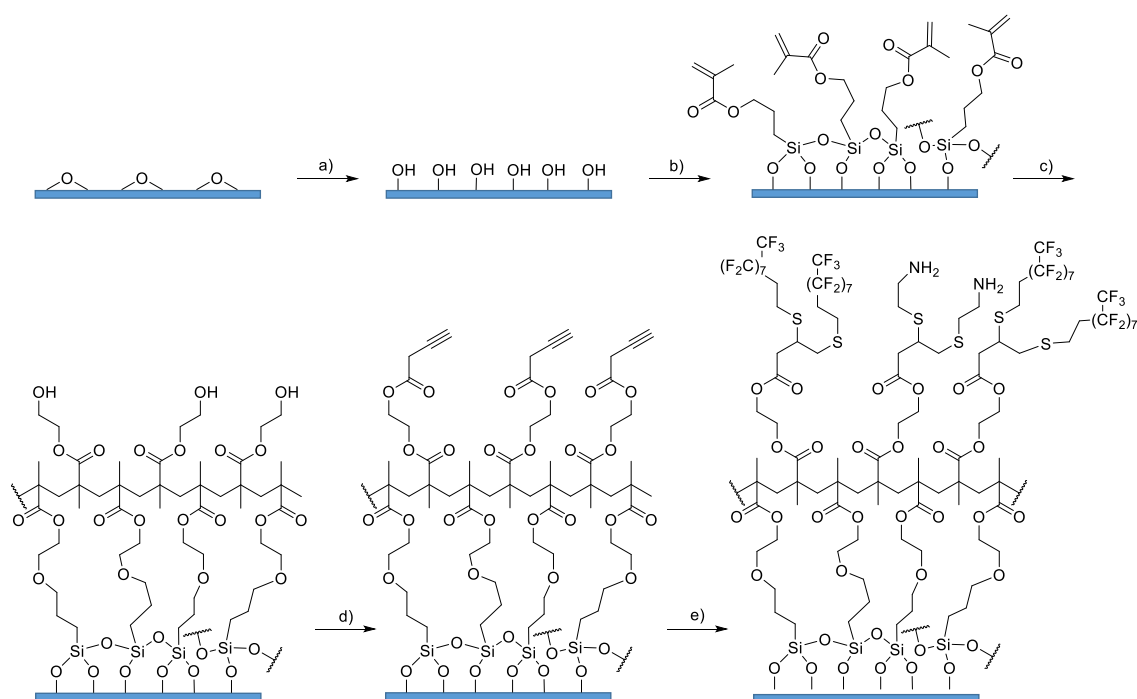
The manufacturing of the DMA on molecular level is presented in Scheme 1. First, standard microscopy glass slides in the size of 25 mm x 75 mm are treated with aqueous solutions of 1 M NaOH and 1 M HCl for 1 h each to activate the glass surface. In this step, the terminal silyl ethers are cleaved to free hydroxyl groups, which serve as reactive sites for the following silanization step. After washing the slides with water and ethanol, a solution of 3-(trimethoxysilyl)propyl methacrylate in ethanol is spread onto the surface and covered with another activated glass slide. In this step the silane crosslinks and binds covalently to the surface's hydroxyl groups while forming silyl ethers.^[21] The slides are washed again with ethanol and their surface now presents methacryl groups from the silane. Following to the modification, a polymerization mixture containing HEMA, EDMA, porogenes (*vide supra*) and photoinitiator is applied and covered with a fluorinated glass slide. This fluorinated glass slide is made by treating an activated slide with 1*H*,1*H*,2*H*,2*H*-perfluorooctyl trichlorosilane in gas phase. The sandwiched glass slides with the polymerization mixture in between are now irradiated with UV light at 254 nm to induce the polymerization. The methacrylate group on the surface acts as an anchor point for the polymer coating and accounts for its

robust attachment onto the glass slide. Sandwiching with a second glass slide stops air oxygen from interfering with the radical polymerization. After detaching the fluorinated glass slide, the topmost layer of polymer is as smooth as its glass counterpart and has to be removed. This is achieved by attaching a stripe of adhesive tape to the polymer coating and ripping it off. Afterwards, the nanoporous structure is accessible. The polymer layer after polymerization has a thickness of around 12 μm ,^[4] is hydrophilic due to the hydroxyl groups from HEMA and shows a static WCA of 6°.^[3] It should be added that the determination of a WCA on porous hydrophilic surfaces differs from non-porous hydrophilic surfaces. When water is applied on a porous hydrophilic surface, the pores will first be filled with the water by capillary forces and the droplet is then standing on the liquid-infused surface.

In the next step the hydroxyl groups are modified via Steglich esterification with 4-pentynoic acid by immersion of the whole slide in the reaction solution.^[22] The now present alkyne groups on the polymer render the surface hydrophobic and non-wettable with a static WCA of 115°.^[1] The difference between wettable and non-wettable is clearly visible for the polymer coating, as it is opaque when dry and transparent when wetted. The last step of manufacturing is based on a UV-induced thiol-yne click reaction with 1*H*,1*H*,2*H*,2*H*-perfluorodecanthiol (PFDT) and cysteaminium chloride or β -mercaptoethanol. A solution of PFDT is spread over the whole surface and areas which should be hydrophilic in the end are covered with a photomask. By irradiation with UV light at 254 nm, the PFDT binds covalently to the 4-pentynoic acid through formation of a thioether. After washing, a solution of the hydrophilic thiol is spread and the slide is covered with a non-patterned quartz glass before being irradiated in the same way as before. This photolithographic process precisely controls the spacial attachment of the different thiols and gives a strong difference in wettability: Areas modified with PFDT are non-wettable and show a static WCA of 170° (advancing contact angle: 173°, receding contact angle: 164°) while areas with cysteaminium chloride are wettable and show a static WCA of 4°.^[2]

The great mechanical and chemical stability of the DMA comes from the inherent material properties and covalent attachment of every layer and modification.^[23] Therefore, the DMA resists all common solvents such as DCM, DMSO, DMF, GBL, NMP, THF, toluene, pyridine, methanol, ethanol, acetone, isopropanol, acetic acetate or water, even when fully immersed for days. Mildly basic or acidic conditions as well as temperatures up to 70°C are tolerated. After those treatments, it can still be dried by direct blowing with an air gun without losing parts of the coating or pattern. This is especially important for multi-step experiments with several washing steps or various reactions.

Droplet formation is possible with various polar solvents such as water, DMSO, DMF, NMP, GBL, glycerine, decanol or THF, however the effect of discontinuous dewetting is only present with water and to some extent with DMSO depending on the pattern. Also ethanol-water or acetonitrile-water mixtures with at least 50% water are still held into the hydrophilic spots, but show an increased risk of droplet merging on dense patterns with small hydrophobic borders.



Scheme 1. The manufacturing sequence of the droplet microarray on molecular level. Structures of crosslinked siloxane and HEMA-co-EDMA copolymer are simplified for better overview. The process includes activation (a), modification/silanization (b), polymerization (c), esterification (d) and photolithographic patterning (e).

1.2.2 Applications

Since its introduction in 2011, the droplet microarray was applied in many different projects ranging from biology and chemistry to material science. The hydrophilic spots, surrounded by superhydrophobic borders, allow for the effect of discontinuous dewetting, where a water droplet can be rolled over the surface and will form free standing droplets in the range of nano- and microliters, depending on the spot size (see Figure 3A) This droplets serve as distinct microreservoirs and can individually be addressed via manual pipetting or dispensing robotics. Typical spot sizes and shapes are 900 μm or 3 mm for round spots and 1 mm or 500 μm for square spots, but patterning can be easily controlled by the use of different photo-masks, depending on the needs for a certain project. Typical working volumes for the 900 μm and 1 mm spots are 150-200 nL, 5-10 μL for the 3 mm spots and 20-40 nL for the 500 μm spots. While these volumes allow for a significant miniaturization of experiments, the number of spots per DMA slide (75x25 mm) can be as high as 2187 for 500 μm spot size or 4608 for 350 μm , which makes high throughput experimentation possible on this platform. This is a big step forward compared to the widely used 1536-well plate with working volumes of around 10 μL and a size of 128 mm x 86 mm.

In the beginning, the biocompatibility of the substrate for different biological systems was validated. HEK 293 cells were reverse transfected on chip with mCherry and GFP plasmids and cultured for 2 days prior to readout via fluorescence microscopy.^[18] MLTy cells expressing mCherry could be cultured next to HeLa cells expressing GFP for 72 h without crosscontamination and Spots with zebrafish pac-2 fibroblasts were acting as a reporter for TOPFLASH when they were connected with spots of cultured Wnt8 expressing cells.^[24]

The application for high throughput screening was demonstrated first in 2015 by using the sandwiching approach as shown in Figure 3B:^[25] A chemical library was printed by an automatic liquid dispenser on a glass slide and dried. The arrayed library was then sandwiched onto a DMA with cells in the droplets to treat every distinct volume with the respective compound. After 24 h of further incubation, the read-out was conducted by either direct live imaging or live staining with CalceinAM. In case of live staining, two procedures were executed: CalceinAM could be printed on a new glass slide, dried and sandwiched onto the cell droplets or the whole DMA could be immersed in the staining solution. Again, fluorescence microscopy was used as final readout. This workflow was later refined for suspension cells and by the use of a “sandwiching device” which simplifies the challenging alignment of the two slides.^[26]

In the following years, the scope of biological applications was more and more broadened.^[27] High throughput screening of pluripotent mouse embryonic stem cells was achieved by the advantageous surface chemistry and structure of the DMA which inhibited the spontaneous differentiation during culturing for 72 h.^[28] Furthermore, by turning the droplet microarray upside down in a slide holder, embryoid bodies were formed in the “hanging droplets” and were subsequently screened with a 774 compound FDA-approved drug library for toxicity and embryoid body formation.^[29] This work demonstrated that the DMA is not only suitable for 2D cell culture, but can also support cell culture in 3D, while still maintaining the arrayed format and separated, miniaturized droplets which are needed for high throughput screening. One goal of 3D cell culture is the screening of complex tissue models or organoids to be as close to the whole living system as possible, since using an entire animal is expensive and laborious, hence low throughput. However, it was shown that zebrafish larvae can be cultured on the DMA and screened for toxicity in a high-throughput approach.^[30]

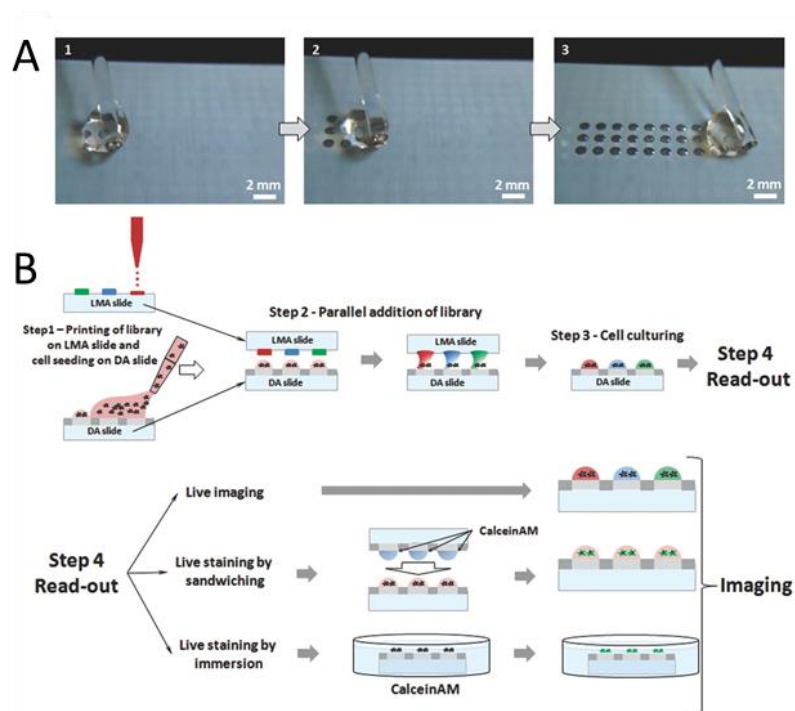


Figure 3. (A) The effect of discontinuous dewetting shown with water on a DMA with 900 μm round spots. (B) The workflow of parallel cell screening on the DMA by using the sandwiching approach. A chemical library was printed on a glass slide and dried prior to sandwiching it onto a DMA containing cells to treat the distinct volumes with the respective compounds. After incubation, the cells can be read out directly via live imaging or after live staining with CalceinAM. Staining can be performed via sandwiching with or immersion in the staining solution. Image adapted with permission.^[25]

Especially for rare materials such as patient derived cancer cells, miniaturization encouraged personalized medicine and was crucial for testing diverse drugs and drug combinations with the scarce amount of cells taken by biopsy.^[31]

Aside from the biological applications, the DMA was also adopted for material research. The shape of the hydrophilic spots served as a 2-dimensional mold for an alginate solution, which formed hydrogel particles when a CaCl_2 solution was sandwiched onto it.^[32] By changing the position of the two slides, it was possible to control the adhesion of the formed hydrogel particles and let them either sit on the DMA or detach them by immersion in medium. When present in the alginate solution prior to curing, magnetic particles and living cells could be incorporated, while maintaining good viability over 7 days as compared to 2D cell culture.

Adding the high-throughput approach to material research of hydrogels led to the screening of responsive hydrogels in nanoliter compartments.^[33] The prepolymerization mixtures were printed on the DMA with

various amounts of crosslinker and polymerized by irradiation with 365 nm UV light. Subsequent irradiation with 254 nm UV light induced degradation of the distinct hydrogel particles depending on their inherent stability.

Conducting chemical reactions in a miniaturized and parallelized way on the droplet microarray is one of the more recent applications and offers the possibility to use the obtained products directly afterwards for a biological screening. The hyphenation of synthesis and screening on the same chip accelerates the process of drug discovery while simultaneously diminishing the amount of invested materials such as chemicals, solvents or biological material. A library of 25 lipidoids was on-chip synthesized, transformed to lipoplexes and screened for transfection efficiency, demonstrating the ease of compound handling and modification in the arrayed format.^[34] Even though on-chip extraction via sandwiching was demonstrated as a possible purification step in this work, still more options were needed, especially to allow multi-step reactions for more complex chemistries. With the solid phase synthesis approach, many impurities and excess starting material could be washed off simultaneously by rinsing the DMA with a proper solvent such as acetone or ethanol.^[2] The nanoporous HEMA-co-EDMA polymer of the hydrophilic spots was utilized as solid phase and modified with a photocleavable linker, which allowed for a stable attachment of the starting material and release of the product via irradiation at 365 nm for less than 20 minutes without the need for additives such as acids. The platform was then demonstrated to be suitable for tripeptide synthesis (Figure 4) and not influencing the viability of HEK293T cells during UV cleavage conditions.^[2]

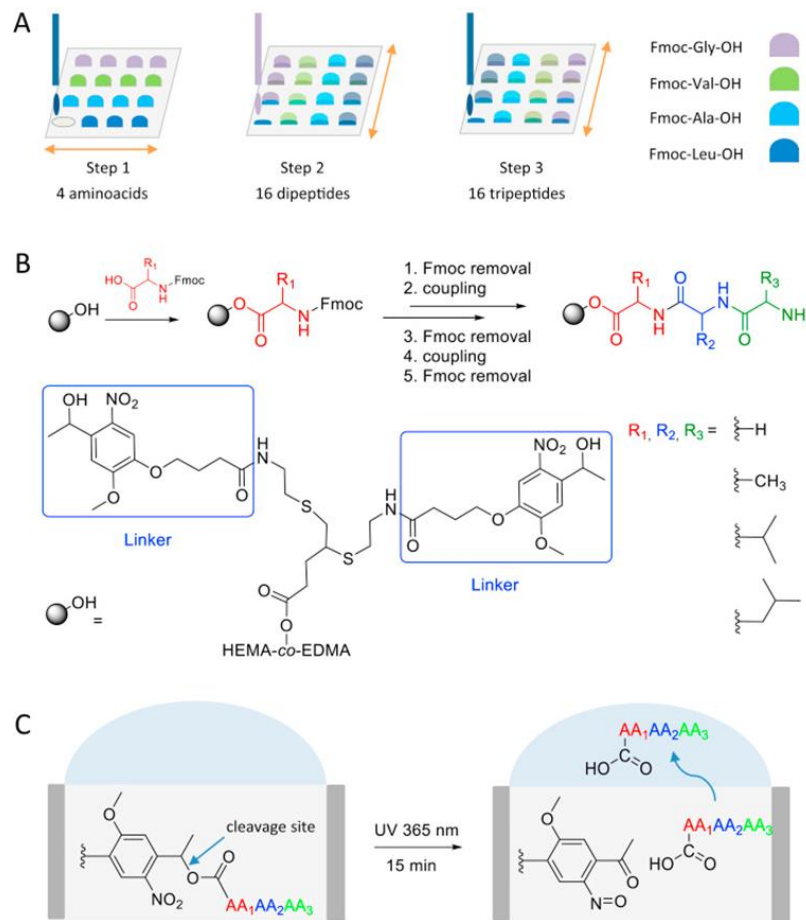


Figure 4. Overview of the solid phase-synthesis of tripeptides on DMA using a UV-cleavable linker. (A) 4 Fmoc-protected amino acids were combined column- and row-wise to achieve an exemplary library of 16 products. (B) Multi-step reaction is possible through solid phase synthesis with washing and deprotection step in between the amino acid couplings. (C) Phototriggered release of tripeptides into the distinct droplet of the DMA. Image adapted with permission.^[2]

1.3 Solid Phase Synthesis

Solid phase synthesis (SPS) was introduced by Robert B. Merrifield in 1963 and was a strong influence to synthetic chemistry, leading to a Nobel prize in 1984.^[35, 36] While it was first used for synthesizing various peptides (e.g. bradykinin,^[37] ribonuclease A,^[38] or insulin^[39]) the scope of this method was later extended to oligonucleotides^[40] and organic synthesis overall.^[1, 41]

In many cases, the solid phase consists of spherical polystyrene beads in the size of 50 – 500 µm. For greater stability, 1-2% of crosslinker (divinylbenzene, DVB) is added during polymerization in the production process.^[42] Such resins offer loadings between 0.2 and 4.0 mmol/g, depending on the requirements of the synthesis. A crucial factor for successful solid phase chemistry is proper swelling of the resin. Only if the solvent can access all reactive sides in the polymer structure, the reaction (or washing) will proceed satisfyingly. Therefore, the choice of solvents is limited and a suitable combination of resin material and solvent is needed.

The starting molecules are attached to this solid phase via different linkers, which allow for a controlled cleavage of the products after synthesis. Various linkers are known and offering a broad range of cleavage conditions, since the release should be orthogonal to the reactions used in the synthesis. Typical triggers are acids, bases, nucleophiles, metal catalysts or light.^[43] As two UV-cleavable linkers were used in this work, the following chapter will highlight their development and properties.

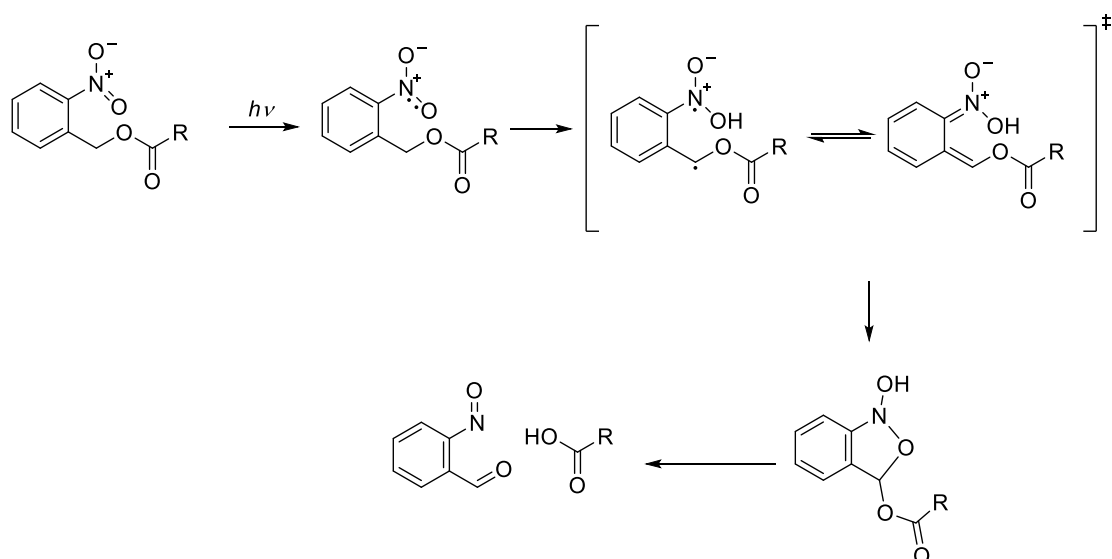
Only a suitable combination of resin, solvent and linker strategy allows for a positive synthetic outcome and therefore gives more variables to the chemist for possible troubleshooting.

However, SPS has several advantages. One is the ease of handling: After addition of reagents and the reaction time, the resin beads can be filtered off the reaction mix and washed several times to remove residual reactants. This straightforward purification simplifies syntheses with multiple steps (such as peptide synthesis) and allows for automation of the process. Also high concentrations of reactants can be employed which improves conversion to the product.^[43]

1.4 Photolabile Linkers

Photocleavable groups hold a big advantage over other linker or protection groups (e.g. Fmoc, Boc, Alloc), because they do not require the addition of cleaving agents such as bases, acids, metal catalysts or nucleophiles.^[44] Thus, there is no further purification needed and it's even possible to release molecules which are sensitive to other cleaving conditions. There are several different photolabile groups known so far, e.g. benzyl alcohols,^[45] phenacyl esters,^[46] or o-nitrobenzyl alcohols.^[47] As this work is utilizing a photocleavable linker from the latter group, its class will be presented here.

The ortho-nitrobenzyl alcohol group is widely used as linker and protecting group,^[47] since it offers in general good stability against acids, bases, higher temperatures and nucleophiles. Since Bamford and Norrish investigated the mechanism of photocleavage in those systems back in 1935,^[48] o-nitrobenzyl alcohol derivatives have been studied and used as protecting groups for carboxylic acids, amides, alcohols, thiols, phosphates and carbonates.^[49] Because of their work and suggested mechanism, the reaction of the photocleavage is called *Norrish-type II* (see Scheme 2). First, the π -bond between nitrogen and oxygen reacts with a photon of a suitable wavelength (200 nm - 400 nm, depending on the exact structure) to form the excited state of a diradical. On the benzylic position, a hydrogen is abstracted by the nitrogen radical and forms the *aci*-nitro compound. Due to the resonance of the π -electrons, a five membered ring is formed intermediately, which cleaves off the carboxylic acid during reopening and formation of a 2-nitroso benzaldehyde. In comparison to the original molecule, the benzylic carbon is oxidized and the o-nitro group is reduced after the cleavage.



Scheme 2: Mechanism of Norrish-type II deprotection of a carboxylic acid. The aromatic nitro-group is reduced to nitroso and the benzylic carbon is oxidized to an aldehyde.^[50]

Patchornik *et al.*^[51] later described the 6-nitroveratroyloxycarbonyl group (NVOC) and compared it to the 2-nitrobenzyloxycarbonyl (NBOC) and 2,2'-dinitrodiphenylmethyloxycarbonyl (DNBOC) group for the protection of amino acids (see Figure 5). In this case, photodeprotection of the carbamate is followed by a spontaneous decarboxylation, leading to the free amine.

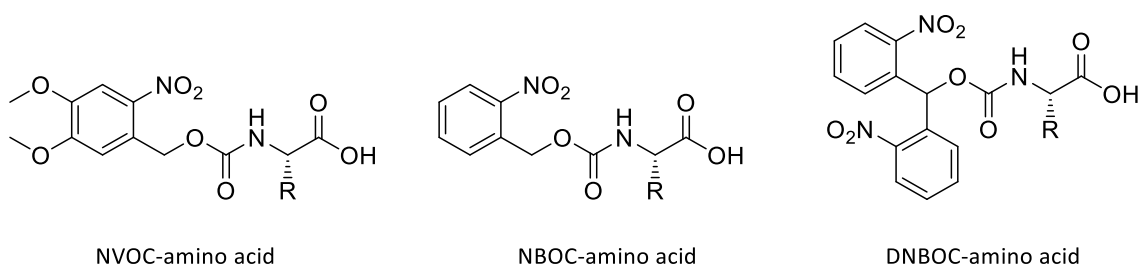


Figure 5: *o*-Nitrobenzyl alcohol derivatives studied by Woodward *et al.*^[51] Photorelease is followed by decarboxylation, yielding the amine.

The two methoxy substituents of the NVOC group introduce a bathochromic shift which increases the absorbance at higher wavelengths than 320 nm and makes deprotection of UV-sensitive molecules such as tryptophan possible. A common side-reaction following the deprotection is the imine formation from the released amine and the new aldehyde of the linker, which can be avoided by adding a carbonyl scavenger such as semicarbazide to the solution or introducing a substituent in the benzylic position and thus forming a less reactive ketone after deprotection.^[51]

Cameron and Fréchet did a more detailed investigation of the α -substitution and showed that a α -methyl group, which was expected to stabilize the intermediate radical, did even decrease the quantum yield from $\phi = 0.13$ of the unsubstituted NBOC to $\phi = 0.11$.^[52] This is explained by statistics, since there is only one hydrogen left to be abstracted. In the other way, adding a second nitro group in the ortho-position of NBOC promotes the quantum yield significantly to $\phi = 0.62$, which is explained by the doubled amount of hydrogen abstracting groups compared to NBOC. As a combination of both, DNBOC offers an α -substituted variant with two reactive nitro groups to compensate for the statistical handicap, leading to a quantum yield of $\phi = 0.26$.

To be used as linker, an interconnection of the solid phase and the photolabile group has to be incorporated. The connection point could either be the α -position,^[53] or – more common – the *para*-position of the aromatic system (see Figure 6).^[54]

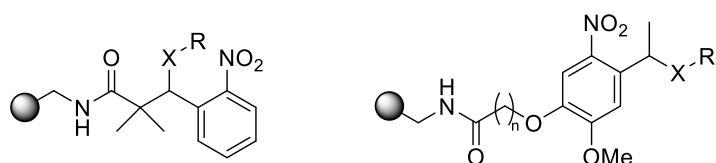


Figure 6: Connection to the solid phase via α -substitution (left) and *para*-substitution (right). $X = NH, O$.

As linkers for this work, 4-[4-(1-Hydroxyethyl)-2-methoxy-5-nitrophenoxy]butanoic acid (also called “Hydroxyethyl-Photolinker”, **HEPL**) and 4-[4-[1-(Fmoc)ethyl]-2-methoxy-5-nitrophenoxy]butanoic acid (“Fmoc-amine Photolinker”, **FAPL**) were used because of their fast cleavage at 365 nm in aqueous conditions and purchasability.^[55, 56]

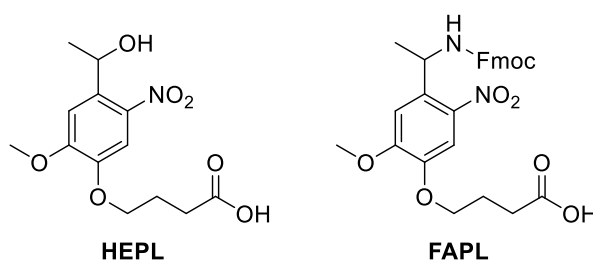


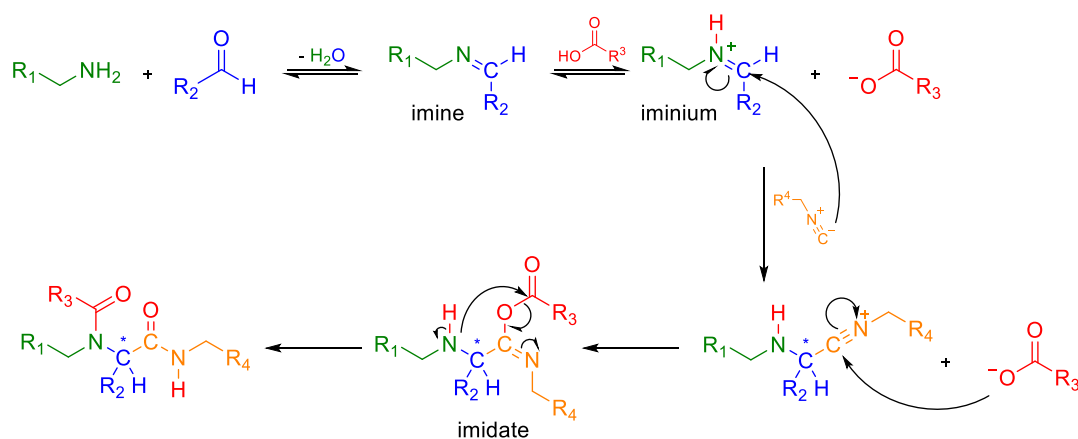
Figure 7: Photolabile linkers **HEPL** and **FAPL**, which were used in this work.

1.5 Chemical Reactions

1.5.1 Ugi-Reaction

The Ugi reaction was first demonstrated by Ivar Ugi in the early 1960s and is similar to the older Passerini reaction.^[57, 58] As a one-pot multi-component reaction, it fuses an aldehyde/ketone, a carboxylic acid, an amine and an isocyanide into a bisamide structure. This gives the possibility to rapidly achieve a high number of different products by varying the starting materials. For example, if every building block has 5 different variants, it can already produce $5*5*5*5=625$ combinations out of the 20 single starting materials. As comparison, a two-component reaction could only produce $10*10=100$ products out of the same amount of building blocks. In addition to this, simple handling of starting materials and the mild conditions of the reaction like room temperature, ambient atmosphere, good atom economy and tolerance against many functional groups motivated many scientists to employ the Ugi reaction in the parallel synthesis of compound libraries, leading ultimately to various pharmaceutical active compounds, which have the Ugi reaction in their synthetic sequence.^[59, 60] Water is also tolerated as additive or solvent and can even accelerate the reaction in some cases.^[61] However, most attempts work with methanol as a solvent and high concentrations of the starting materials.^[62]

A proposed mechanism is presented in Scheme 3,^[63] starting with the condensation of an amine and aldehyde (which can be replaced by a ketone) to an imine. It has been shown that the preformation of this imine prior to addition of acid and isocyanide can increase the yield of the reaction by suppressing side reactions such as the Passerini reaction.^[64] The formed imine intermediate can be protonated by the carboxylic acid to an iminium and subsequent addition of the isocyanide forms a nitrilium ion with a new stereocentre. Under common conditions, the Ugi reaction is not stereoselective, which was a significant drawback until the introduction of asymmetric catalysts in 2018.^[65] As a second intermediate, an imidate is formed through addition of the carboxylate to the nitrilium, which undergoes a Mumm rearrangement to the final bisamide product. Driving force of the overall reaction sequence is the oxidation of isocyanide carbon from +II to +IV.^[66] The reaction can be accelerated by addition of Lewis acids such as scandium or titanium.^[67, 68]



Scheme 3. Mechanism of the Ugi reaction. The preformed imine is protonated to an iminium by the carboxylic acid before the addition of isocyanide. Further addition of the carboxylic acid leads to an imidate, which undergoes Mumm rearrangement to yield the final racemic bisamide product. ^[63]

Common side reactions are the Passerini reaction, the Ugi 3-component reaction and the formation of an amidine (Figure 8).^[63, 66, 69] In case of the Passerini reaction, the amine is not taking part in the reaction and the carbonyl, carboxylic acid and isocyanide form an α -acyloxyamide. This can be suppressed by pre-formation of the imine intermediate from the carbonyl and amine entry prior to the addition of the acid and isocyanide. In the Ugi 3-component reaction, water reacts as the acid component and forms α -aminoamides, leaving out the carboxylic acid entry. Formation of amidines occurs through addition of the amine to the isocyanide and subsequent nucleophilic substitution at the isocyanide-carbon from a second starting molecule. General structures of this 3 possible byproducts are shown in in Figure 8.

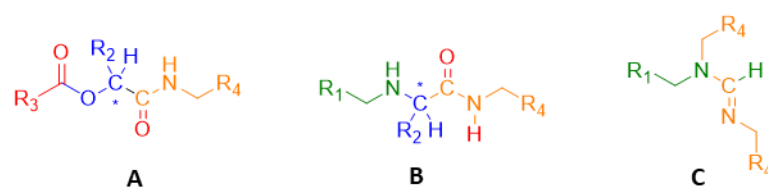


Figure 8. Common side products of the Ugi 4-component reaction. A Passerini product; B Product of the Ugi 3-component reaction; C Amidine byproduct

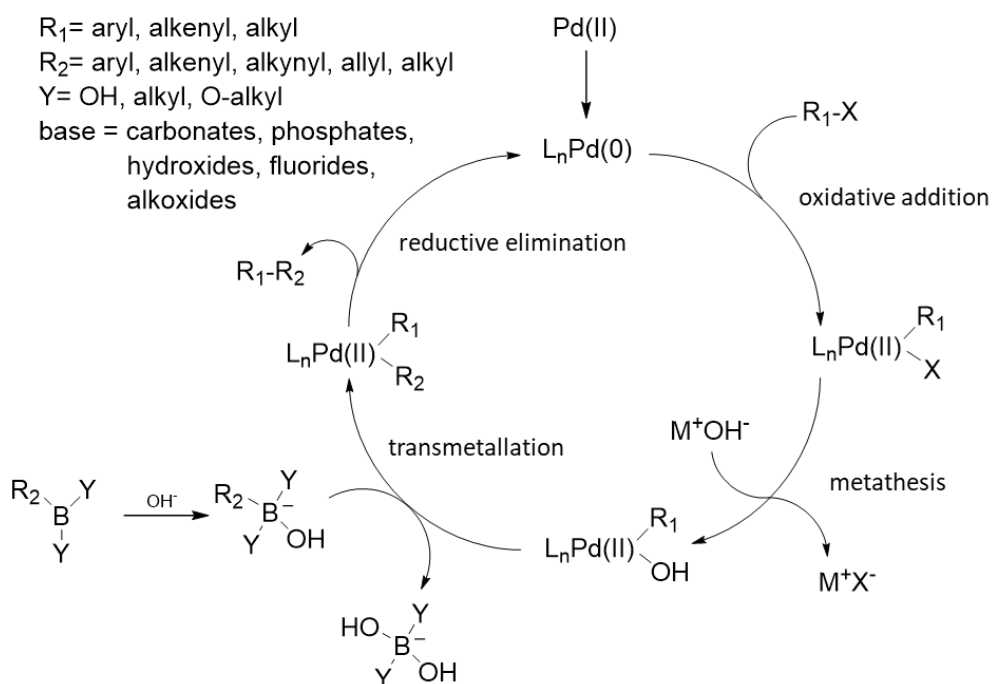
To increase the variability of core structures, several modifications of this reaction were introduced, mostly by coupling orthogonal reactions to the Ugi reaction, such as an intramolecular Diels-Alder,^[70] Pd-catalyzed arylation,^[71] Heck-coupling,^[72] or thiol-ene reaction.^[73] Especially the latter one offered the possibility to synthesize sequence defined oligomers through cycles of alternating Ugi and thiol-ene reactions, incorporating two variable side groups in each cycle. A similar approach was also demonstrated by performing alternating Ugi and Fmoc-deprotection steps to yield peptide-peptoid hybrid structures.^[74]

1.5.2 Suzuki-Miyaura-Reaction

The Suzuki-Miyaura-Reaction (SMR) was introduced in 1979 by Akira Suzuki and Norio Miyaura and is a palladium-catalyzed cross-coupling reaction between a boronic acid and an organohalide, which typically forms a new C(sp²)-C(sp²) bond,^[75, 76] but C(sp²)-C(sp³) couplings using alkyboranes were also demonstrated.^[77] It was quickly adapted by synthetic chemists and awarded with a Nobel prize in 2010.^[78]

Among the other famous transition-metal-catalyzed cross-coupling reactions such as the Negishi-, Heck-, Kumada-, or Stille-coupling, the SMR has several advantages: The reaction conditions are mild and tolerate many functional groups, since it is commonly employed below 80°C with a broad scope of bases, depending on the sensitivity and needs of the substrate.^[79] Additionally, the boronic acid derivatives are easily prepared from widely available reagents, show a high stability and considerable less toxicity as compared to organozinc or organotin compounds.^[80] Water is tolerated as additive or pure solvent, but oxygen is excluded in most protocols.^[81] However, SMR under ambient atmosphere was shown to work in few cases.^[82, 83] Cross-coupling reactions can be performed homogeneous or heterogeneous, depending on how the catalyst is present.

The homogeneous catalytic cycle of the SMR is presented in Scheme 4, starting with a palladium catalyst precursor.^[84, 85] While the catalytically active species is a Pd(0) complex and can be directly added as (for example) tetrakis(triphenylphosphine)palladium(0) (Pd(PPh₃)₄), the handling and storage of this air-sensitive compound is inconvenient and less flexible compared to the *in situ* formation of catalyst from Pd(II) precursors and various ligands. Common Pd(II) sources are Pd(OAc)₂, Na₂PdCl₄ or PdCl₂, where the Pd(II) can be reduced to Pd(0) by an excess of the phosphine ligand, boronic acid or base in the reaction mix.^[84] Some protocols do not add ligands to the reaction mixture and are therefore called “ligandless”,^[86] however the palladium is then coordinated to base or solvent molecules.^[87] For example, triethylamine can act as solvent, base and ligand in simple systems.^[88] Nevertheless, the use of sophisticated ligands can drastically improve the reaction outcome under disadvantageous conditions such as room temperature, low catalyst loading or less reactive reactants.^[84] Such ligands are typically phosphines or N-heterocyclic carbenes (NHC) and can precisely control the catalytic activity via rational design of the substituents due to modulation of electronic and steric properties of the catalyst.^[89] The first step of the SMR (Scheme 4) is the oxidative addition of the L_nPd(0) catalyst to the aryl halide and formation of an arylpalladium(II) halide intermediate. This is facilitated by a high electron density at the palladium center, which can be increased by electron donating ligands like trialkylphosphines. The reactivity of the aryl (pseudo)halide also differs in the sequence Ar-I > Ar-OTf > Ar-Br >> Ar-Cl as well as with different substituents.^[90] In contrast to the catalyst, electron withdrawing groups support the oxidative addition and electron donating groups deactivate the substrate. Therefore, difficult reaction partners need highly active catalysts in well adjusted conditions for a sufficient coupling.^[91]



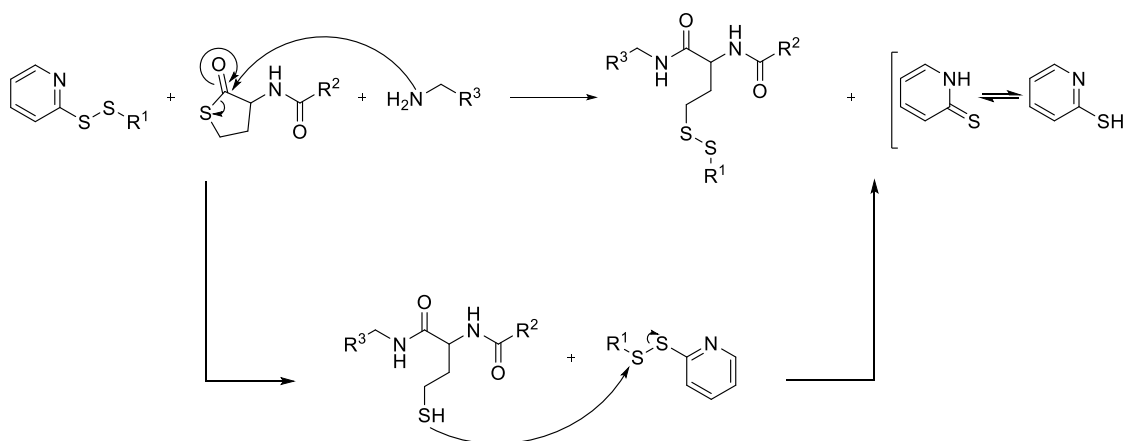
Scheme 4. Catalytic cycle of the Suzuki-Miyaura-Reaction. After being reduced to Pd(0), liganded catalyst inserts to the arylhalide via oxidative addition. Metathesis exchanges halide with the base anion prior to a transmetalation with a preactivated boronic acid. Via reductive elimination, the two carbons are coupled and catalyst is regenerated.^[84, 89]

In the next step, the (pseudo)halide is exchanged with the anion from the base (most commonly OH⁻) in a metathesis reaction, followed by the transmetalation, where the organic rest of the preactivated boron species is exchanged with the base anion from Pd(II). Preactivation occurs by addition of a base anion to the boron substrate and formation of a borate. Subsequent reductive elimination of the Pd(II) regenerates Pd(0) for the next cycle and forms the new C-C bond. This elimination is facilitated by sterically demanding ligands at the palladium center, such as P(^tBu)₃ or dialkybiaryl phosphines.^[92]

1.5.3 Thiolactone Aminolysis & Disulfide Exchange

The thiolactone aminolysis and disulfide exchange reaction (TADE) combines the two orthogonal reactions into a three-component one-pot reaction without the need of additives and was first introduced by Molla *et al.* in 2018.^[93] As a first step, an amine opens the ring of the thiolactone derivate via an addition-elimination reaction on the carbonyl and therefore releasing the thiol. The free thiol can then rapidly undergo a disulfide exchange with a 2-pyridyl-disulfide to yield the disulfide product and 2-thiopyridone as byproduct (Scheme 5). The byproduct shows a strong absorbance at 343 nm and can be used for yield determination as it is formed parallel to the product.^[94]

The TADE has several advantages: While many interesting amine derivatives can be purchased, the 2-pyridyl-disulfides and thiolactone derivatives can be easily prepared from thiols and activated carboxylic acids in a one-step synthesis. The one-pot reaction proceeds fast at room temperature without additives and can be monitored via quantification of the byproduct. It was used to conveniently synthesize a 288 compound library of lipidoids to be tested for their transfection efficiency, where the yield was quantitative and purification could be done via precipitation in methanol.^[93]



Scheme 5. Schematic overview of the thiolactone aminolysis and disulfide exchange reaction (TADE). First, an amine opens the thiolactone via nucleophilic addition-elimination and sets free the thiol, which rapidly reacts with a 2-pyridyl disulfide derivate. By this, 3 variable components are fused into a disulfide-containing molecule.

2 Experimental Part

2.1 Reversible Wettability by Silanization

Over recent decades, controlling surface wettability has received a great deal of attention^[95] due to its potential applications in processes such as oil-water separation,^[96] self-cleaning surfaces,^[97] corrosion inhibition,^[98] or anti-biofouling.^[99] Spatial control of surface wettability also allows for discontinuous dewetting and microfluidic applications.^[100]

As already presented in chapter 1.1, the key to achieving superhydrophobicity is a suitable combination of surface topography and chemistry. While alkylated or fluorinated materials are the most common chemical constituents of artificial superhydrophobic (SH) surfaces, diverse and sophisticated methods of surface structuring have been developed including lithography,^[12] laser structuring,^[13] polymer phase separation,^[10] silicon nanograss,^[101] and carbon nanotubes.^[14] Furthermore, strategies to induce the transition of a surface between the hydrophilic and hydrophobic states have been developed and extensively studied.^[102] For example, the wetting behavior of oxides of tin,^[103] zinc,^[104] and tungsten^[105] are altered by UV irradiation due to a photoinduced radical rearrangement process. While the metal oxides are superhydrophobic after manufacturing, they rapidly become hydrophilic after irradiation. However, this transition is temporary and the metals slowly return to the thermodynamically more stable superhydrophobic state when placed in darkness. Another method that achieves a more stable transition is UV-triggered azobenzene isomerization, which is based on the change in polarity induced by a *cis/trans* transition of surface-bound azobenzene compounds.^[106] Although the transition is rapid and easily reversible by irradiation with different wavelengths, the surface will not reach a superhydrophilic state due to the non-polar aromatic systems.^[107]

To achieve complete conversion between the superhydrophilic and superhydrophobic states on the same structured surface requires significant changes in the chemistry of the surface, which must remain stimuli-responsive for reversibility. The Levkin group recently published a UV-triggered disulfide exchange reaction on a surface, which complies with these specifications.^[108] The disulfide bond formed is not only more stable than the bonds formed by imines,^[109] but also allows for a versatile reversible patterning as a result of the spatially controlled and rapid interchange of surface chemistry. However, one can conceive of a surface that demands stable, yet switchable wettability without the need for UV irradiation. Thus, the concept of the reversible modification of surfaces by silanization is proposed. While the silanization process is not new and somewhat standard in surface chemistry, it is regarded as permanent (except for

unselective laser ablation^[110]), although the fast and specific cleavage of the silicon-oxygen bond by fluoride ions is also a well-established method in organic chemistry.^[111]

In this chapter, the influence of the simple and rapid process of silanization and desilanization on wettability of a nanorough polymer coating or silicon wafer was investigated. It was demonstrated that the transition from the hydrophilic to the superhydrophobic state and *vice versa* can be accomplished in 2 minutes or less and can also be spatially controlled by automated liquid dispensing or manual “drawing”.

2.1.1 Materials and Methods

2.1.1.1 HEMA-co-EDMA Polymer Coating of Glass Slides^[25]

A microscopy glass slide was activated by sequential immersion in 1 M aqueous NaOH and 1 M aqueous HCl (1 h each). The hydroxyl groups formed on the surface were then modified by applying a 20% (v/v) solution of 3-(trimethoxysilyl)propyl methacrylate in ethanol for 30 min twice. After washing with ethanol and drying under air flow, 30 μ l polymerization mixture was spread on the surface of the slide, which was then placed face down on a fluorinated glass slide. Polymerization mixture consisted of 24% (w/v) 2-hydroxyethyl methacrylate (HEMA), 16% (w/v) ethylene glycol dimethacrylate (EDMA), 0.4% (w/v) 2,2-dimethoxy-2-phenylacetophenone (DMPAP) and 59.6% (w/v) porogenes with various content of 1-decanol and cyclohexanol (see chapter 1.1). Fluorination of glass slides was carried out by treating an activated slide with 1H,1H,2H,2H-Trichloroperfluorooctylsilane in the gas phase for 16 h and subsequent washing with acetone. The coating was polymerized by UV irradiation at 254 nm (4 mW/cm², BioLink 254, Vilber Lourmat, Eberhardzell, Germany) for 15 min.

2.1.1.2 Surface Modification via Silanization

A polymer-coated glass slide or silicon wafer was immersed in 2% (v/v) trichloro-(1H,1H,2H,2H-perfluorocetyl)-silane (TCPS) solution in dry toluene for 2 minutes and washed extensively with acetone and ethanol before drying with an air gun. For the kinetic investigation, the immersion time was varied. Trichlorododecylsilane and chlorotrimethylsilane were used accordingly.

2.1.1.3 Surface Desilanization by Immersion

To regain the hydrophilic polymer or silicon surface, the silane-modified surface was immersed in a solution of 0.1 M TBAF in THF for 2 minutes, washed with ethanol and dried with an air gun. For the kinetic investigations, the concentration and immersion time were varied.

2.1.1.4 Water Contact Angle Measurements

For determination of water contact angles (WCA), the droplet shape of 10 μl of deionized water was analyzed using a DSA25 drop shape analyzer by Krüss (Hamburg, Germany) and the manufacturer's software. The static WCA was determined for a droplet at equilibrium after placement on the surface. Advancing and receding angles were measured by slowly (0.1 $\mu\text{l/s}$) adding and removing water from the droplet at the same speed. Sliding angles were determined for a free-standing droplet placed on a table tilted at a speed of $1^\circ/\text{s}$.

2.1.1.5 Wettability Cycles

For reversible modification of the polymer surface, silanization (2% (v/v) TCPS in dry toluene) and desilanization (0.1 M TBAF in THF) via immersion were performed with a measurement of the static WCA between each step. The surfaces were washed extensively with acetone and ethanol and carefully dried to avoid contamination of the solutions or disturbance of the measurements.

2.1.1.6 Superhydrophobic-Hydrophilic Pattern Printed by Liquid Dispenser

iDot by Dispensix (Stuttgart, Germany) was used for contactless liquid dispensing. The array of spots was generated with a center-to-center distance of 1.5 mm using the programmed printing pattern in the manufacturer's software. Subsequently, various volumes of a 0.1 M solution of TBAF in 10% (v/v) THF in GBL were printed onto each spot. The reaction was incubated at room temperature for 2 minutes before immersion in ethanol to wash off the reaction liquid.

2.1.1.7 Time-of-Flight Secondary Ion Mass Spectrometry (ToF-SIMS)^[3]

ToF-SIMS was performed on a TOF.SIMS5 instrument (IONTOF GmbH, Münster, Germany). Measurement and fragment identification was done by Alexander Welle. This spectrometer is equipped with a Bi cluster primary ion source and a reflectron type time-of-flight analyzer. UHV base pressure was below 5×10^{-8}

mbar. For high mass resolution, the Bi source was operated in a bunched mode providing short Bi^{3+} primary ion pulses at 25 keV energy, a lateral resolution of approx. 4 μm , a target current of 0.35 pA. The short pulse length of 0.95 ns allowed for high mass resolution. For large fields of view, both, the sample stage and the primary ion beam were rastered. For static SIMS images primary ion doses were kept below 10^{11} ions/cm². For charge compensation an electron flood gun providing electrons of 21 eV was applied and the secondary ion reflectron tuned accordingly. Spectra were calibrated on the omnipresent C^- , C_2^- , C_3^- , or on the C^+ , CH^+ , CH_2^+ and CH_3^+ peaks. Based on these datasets the chemical assignments for characteristic fragments were determined. As the thickness of the polymer layer exceeds the probing depth of static SIMS (a few nm) depth integrated spectra were obtained with full erosion of the polymer layer by an argon cluster ion beam, 20 keV, Ar_{1300} . This erosion beam was rastered across 800x800 μm and with a non-interlaced timing scheme data were recorded from a concentric 500x500 μm field of view.

2.1.1.8 Atomic Force Microscopy (AFM)^[3]

Atomic force microscopy measurements were conducted on a Dimension Icon AFM from Bruker (Billerica, USA) using micro cantilevers from Olympus (Tokio, Japan) with a resonance frequency of ca. 300 kHz. Data analysis was done with Nanoscope Analysis from Bruker (Billerica, USA). Measurement was done by Johannes Scheiger, while data analysis and interpretation was done by me.

2.1.2 Results and Discussion

2.1.2.1 Investigation of Different Polymer Porosities

First, the ideal porosity for the polymer coating was investigated. As already explained in chapter 1.1, this can be controlled by varying the content of the porogenes cyclohexanol and 1-decanol. Increased porosity gives a higher surface roughness and achievable hydrophobicity after chemical modification of the initially hydrophilic HEMA-co-EDMA polymer, but decreases its mechanical stability. Polymerization mixtures with a 1-decanol content of 12, 15, 20 and 25 % (w/v) were prepared and used for sample manufacturing. Each sample was then modified with trichloro-(1H,1H,2H,2H-perfluorooctyl)-silane (TCPS) in toluene for 2 minutes and analyzed via contact angle goniometry. The results are shown in Table 1. As expected, the static WCA is increasing from 147° for the sample with 12 % (w/v) 1-decanol to 160° for the sample made with 25 % (w/v) 1-decanol. While advancing contact angles do not show a significant change, receding contact angles increase from 118° to 153° between the same two samples. The decrease of sliding angles from 30° to 9° indicates that the surface made with 25% (w/v) 1-decanol is much less sticky and more slippery.^[112] Higher amounts of 1-decanol yielded polymer coatings which were too brittle to be handled

without damaging of the surface and were not investigated. As a result, polymerization mixture with 25% (w/v) 1-decanol and 34.6% (w/v) cyclohexanol was used to prepare polymer coatings for all further experiments.

Table 1. Static, advancing, receding and sliding water contact angles for polymer coating on glass made with different contents of 1-decanol as porogene. After polymerization, the slides were modified with TCPS before analysis. Each data point is the average of 3 measurements at different positions on the surface. Standard deviation is shown in parentheses.

| % (w/v) 1-decanol | static WCA (°) | advancing WCA(°) | receding WCA (°) | sliding angle(°) |
|--------------------------|-----------------------|-------------------------|-------------------------|-------------------------|
| 12 | 147 (± 1) | 164 (± 3) | 118 (± 3) | 30 (± 8) |
| 15 | 162 (± 1) | 166 (± 2) | 145 (± 5) | 18 (± 6) |
| 20 | 161 (± 3) | 166 (± 2) | 147 (± 1) | 13 (± 6) |
| 25 | 160 (± 1) | 162 (± 1) | 153 (± 3) | 9 (± 4) |

For the pristine surface prior to silanization, a static WCA of 6° (± 1) was observed. It should be noted that this value does not represent the classic water–solid contact angle, but is the contact angle between the water droplet and the liquid-infused surface of the porous polymer. This effect is visible in Figure 11D, where some of the water first enters the pores by capillary action followed by gradual formation of a droplet on the wetted surface. Advancing and receding contact angles could not be determined due to the capillary effect. Nevertheless, the very low static water contact angle confirms the highly hydrophilic state of the surface and as expected, a sliding angle was not observed.

2.1.2.2 Process of Silanization

The kinetic of silanization was investigated by measuring water contact angles after different immersion times of the slide in a solution of 2% (v/v) TCPS in dry toluene. The data as presented in Figure 9A shows a rapid conversion from hydrophilic to superhydrophobic in less than 2 minutes. Similar to the change of surface roughness, the static water contact angle was influenced faster than the advancing, receding and sliding contact angle. The contact angle hysteresis as an additional parameter for “stickiness” was calculated as the difference of advancing and receding contact angle and it decreases simultaneously with the sliding angle. The decline of the contact angle hysteresis was dominated by the kinetics of the receding WCA, as the advancing WCA reached its endpoint already after 15 s, while the receding WCA needed 45–60 s to reach the endpoint.

A ToF-SIMS analysis of the silanized surface after 2 minutes of immersion was performed to investigate the lateral distribution of the silane layer. Figure 9C/D shows the plotted intensity of Si⁺ and CF₃⁺ ions. These ions were identified by their m/z value and are fragments from the fluorosilane layer on the surface.

They were not present prior to the silanization and indicate that the silane forms a coherent layer on the whole surface.

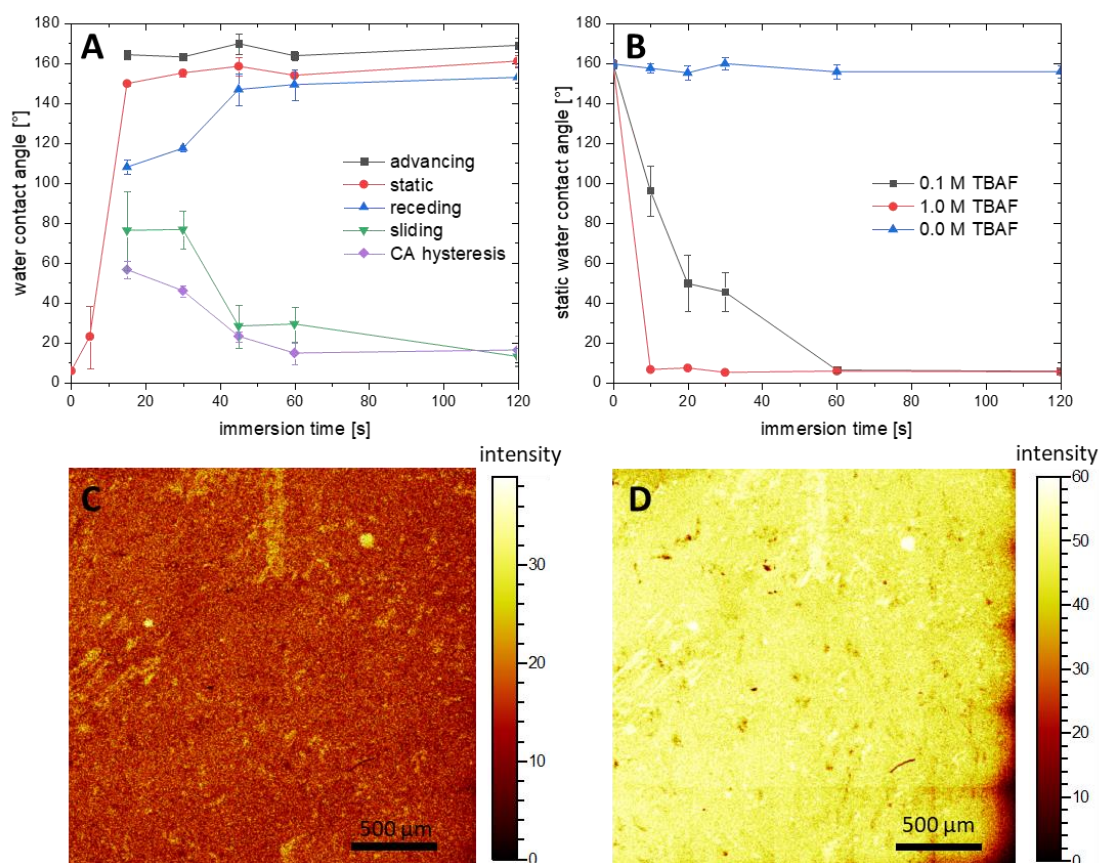


Figure 9. Changes of wettability of the polymer surface during silanization (A) and desilanization (B). For each given time point, the slide was immersed in the respective solution, washed extensively and analyzed via goniometry. Every data point is the average of 3 measurements at different positions on the surface. Error bars represent standard deviation. (C,D) ToF-SIMS analysis of the TCPS silanized surface shows the presence of fluorinated alkylsilanes indicated by the detection of Si^+ (C) and CF_3^+ (D) ion signals.

Further analysis of the modified surface was conducted via ToF-SIMS. The polymer was eroded with Argon clusters and the obtained depth profiles of Si^+ (27.98 m/z), $C_2H_3O^+$ (43.02 m/z) and CF_3^+ (68.99 m/z) are plotted in Figure 10. Fluence is shown on the x-axis and is the value of all detected ions per cm^2 summarized and roughly represents the “depth”. It can be seen that the intensity of a fragment ion from the polymer coating ($C_2H_3O^+$) stays mostly stable with a small overall increase, most probably because of different ionization tendencies in deeper areas of the coating. In contrast, the fragment ions for the silane modification (CF_3^+ and Si^+) are strongly present in the beginning, but rapidly decrease during erosion. This indicates that the silane modification does not penetrate the whole polymer layer and is only present on the top.

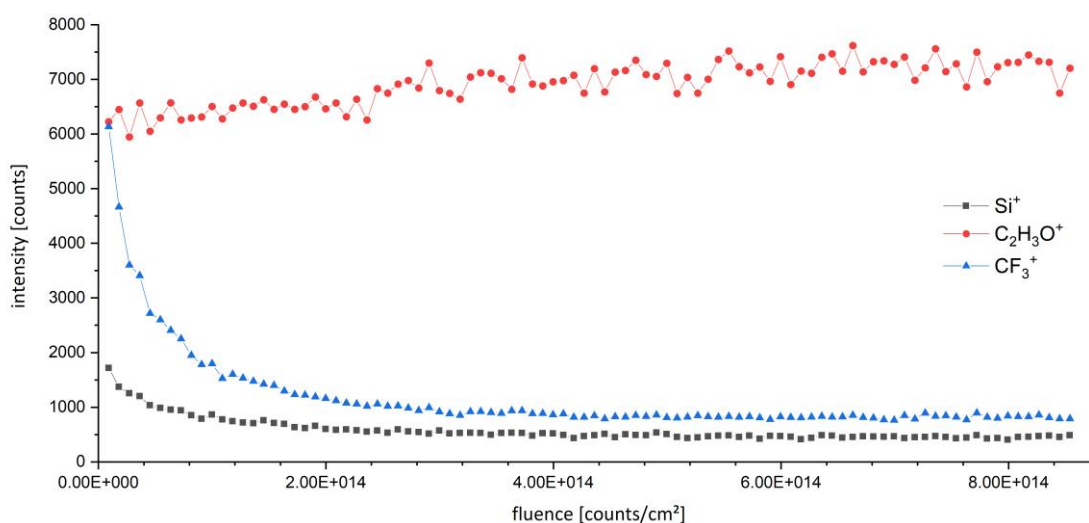
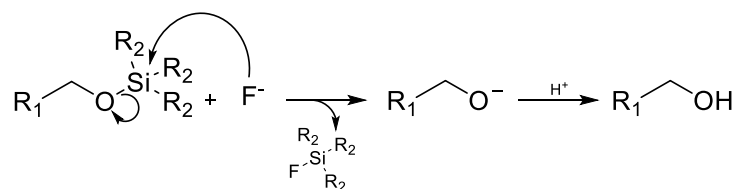


Figure 10. Depth profile of a silanized polymer film via ToF-SIMS analysis. Si^+ and CF_3^+ ions are fragments from the fluorinated alkylsilane and $\text{C}_2\text{H}_3\text{O}^+$ is a fragment of the polymer coating. The silane modification is only present on the top and does not penetrate through the whole polymer layer.

2.1.2.3 Desilanzation Process

The modification of a surface via silanization is based on the formation of a silyl ether from a silane and hydroxyl group, where the latter one is present in pristine HEMA-co-EDMA polymer. By cleaving this Si-O bond, the free hydroxyl groups can be restored to drastically change the surface chemistry and wettability. Traditionally in organic synthesis, this is performed by treatment with fluoride anions added as tetrabutyl ammonium fluoride (TBAF), HF or NaF.^[113] TBAF was chosen for this project since it is a common chemical in synthetic laboratories, can be conveniently handled as a solution in THF and mixed with water or organic solvents. Scheme 6 shows the reaction of silyl ether cleavage.^[111] The driving force of this reaction is the formation of the very stable Si-F bond whose bond energy is around 172 kJ/mol higher than the energy of the Si-O bond (369 and 541 kJ/mol).^[114]



Scheme 6. Mechanism of a silyl ether cleavage by fluoride anions followed by protonation of the alkoxide.^[111] Driving force is the high Si-F bond energy.

The kinetic of desilanization was investigated by measuring water contact angles after different immersion times of a TCPS modified slide in a solution of TBAF in THF. Concentrations were 1 M, 0.1 M, and 0 M where pure THF served as a negative control to show that the desilanization occurs only with the TBAF and not just by the solvent. Figure 9B shows a rapid decrease in the static WCA for both TBAF concentrations, however a faster conversion is achieved by the 1 M solution which restores the WCA of the unmodified polymer surface after just 10 seconds. In 0.1 M TBAF solution, the same endpoint is reached slower, but still in under 1 minute. In pure THF, no change of the static WCA is seen, even after 2 minutes of immersion, indicating a stable modification of the surface.

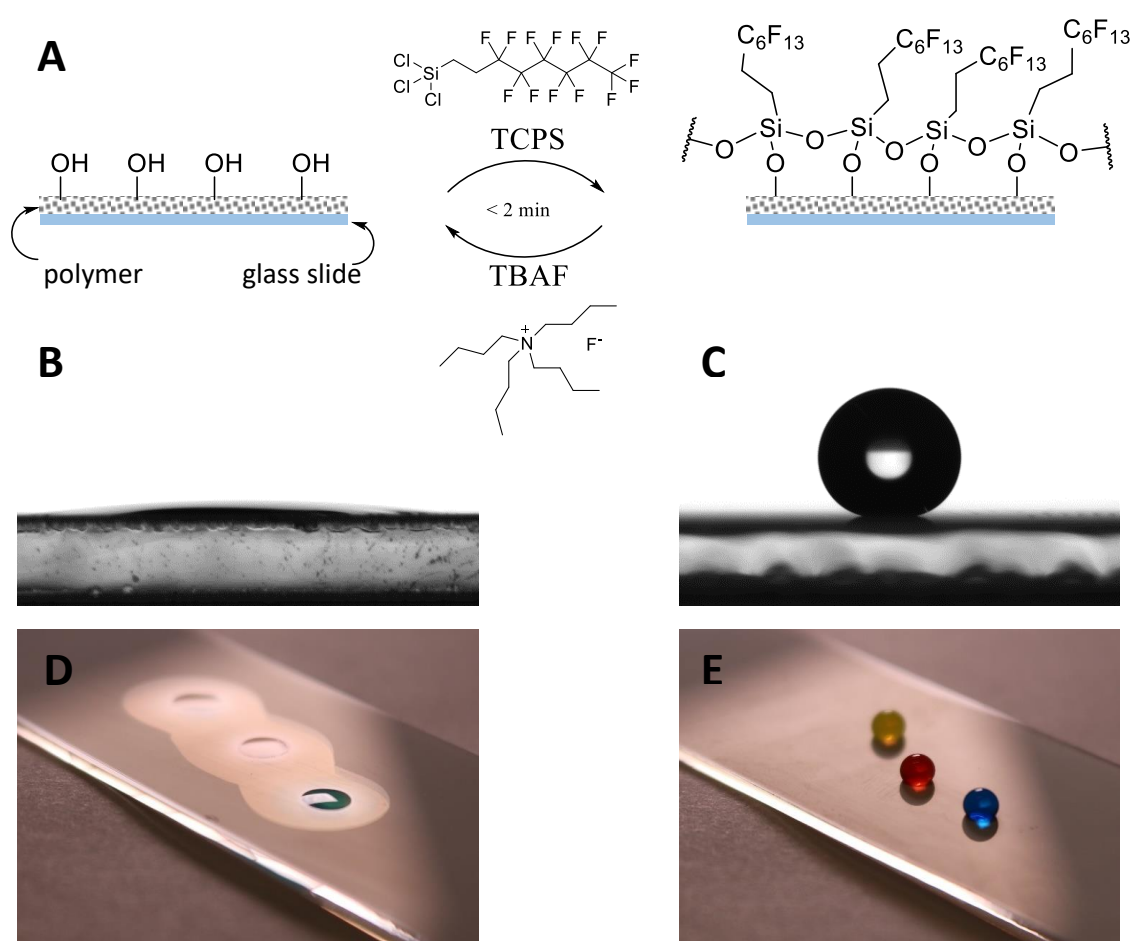


Figure 11. General overview of cyclic wettability as a reaction scheme (A) and images of water droplets on hydrophilic (B/D) and superhydrophobic (C/E) polymer surfaces. (A) The nanoporous HEMA-co-EDMA polymer on a glass support is hydrophilic due to its hydroxyl groups and can be rapidly modified with 1H,1H,2H,2H-trichloroperfluorocetyl silane (TCPS) to exhibit superhydrophobicity. This process is completely reversible by treatment with tetra-*n*-butylammonium fluoride (TBAF). Each step can be performed in 2 minutes at room temperature. Structure of siloxane layer is simplified for better visualization. (B/C) Screen captures of water droplets from the water contact angle analysis. (D/E) Photographs of pipetted aqueous food dye solutions.

2.1.2.4 Reversible Wettability

Since it was now shown that the hydrophilic, hydroxyl group containing surface of the polymer can be modified via silanization and restored by desilanzation, it was now tested if it is possible to make multiple cycles of silanization and desilanzation. Figure 11A shows the process on the surface as a reaction scheme and the two states of wettability, each as pictures made during goniometry and as photograph. For the photographs, aqueous food dyes were used for better visualization.

To show the total reversible wettability, a cycle of several silanization and desilanzation steps was performed and the static WCA was measured after every step. Figure 12 shows the progressive changes in the static WCA after each step, starting with a non-modified nanoporous HEMA-co-EDMA polymer coating.

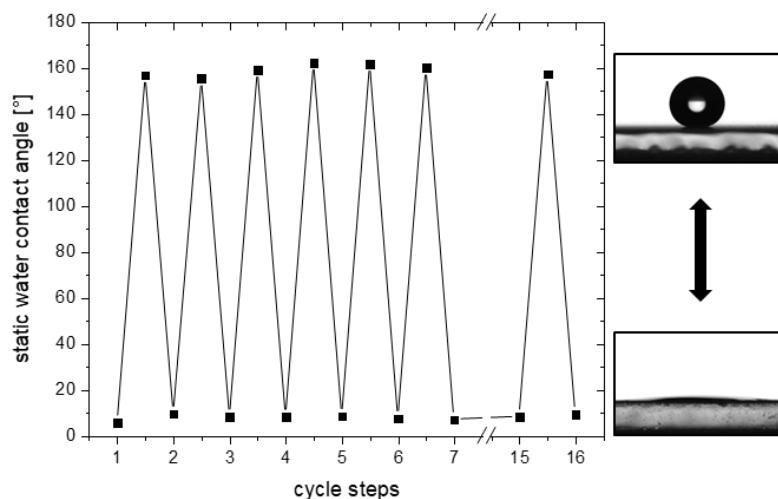


Figure 12. Static water contact angles for reversible surface modification cycles. Silanization and desilanzation processes were alternated and the static water contact angles were measured after every conversion. The achieved WCA remained stable even after 16 steps.

The immersion time for every silanization and desilanzation step was 2 min and the TBAF concentration was 0.1 M. The average static WCA for the hydrophilic states was measured as 7° with a standard deviation of 1°. In the hydrophobic states, the surface showed an average static WCA of 159° with a standard deviation of 3°. These results demonstrate that the achieved static WCA endpoints remained stable over 30 steps representing 15 full cycles. Summarized after this experiment, the polymer substrate has been immersed in the TBAF solution for 30 min (15 × 2 min) and was still mechanically stable against blow drying with an air gun. Further stability studies of the topography via AFM were conducted and are presented in Figure 13. First, a pristine HEMA-co-EDMA polymer coating was analyzed. The porous structure made by agglomeration of globuli is clearly visible (Figure 13A) and is not changed through several treatments. Samples after silanization (Figure 13B) and desilanzation (Figure 13C) according to the standard procedure showed no change in surface topography, indicating that the increase of WCA is achieved mostly by the chemical modification rather than a structural transformation. Additionally, the stability of the polymer against prolonged immersion in THF (24 h, Figure 13D) or 0.1 M TBAF in THF (2 h, Figure 13E) was tested and again, no damage or difference of the topography can be seen in AFM.

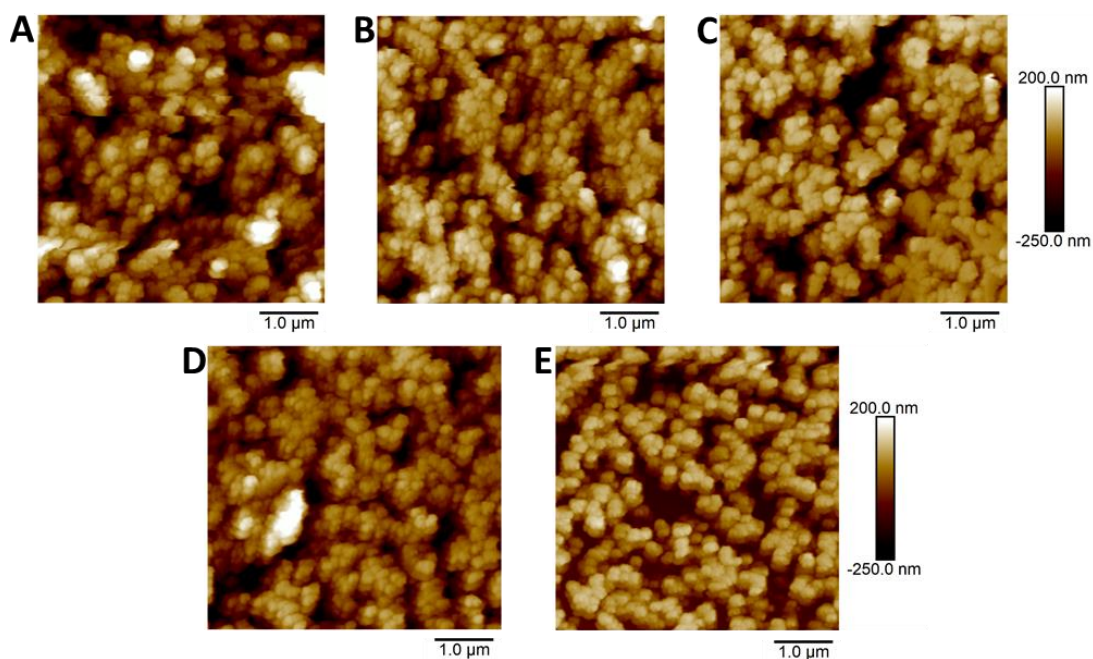


Figure 13. Surface topography of nanoporous HEMA-co-EDMA coated surfaces as measured by atomic force microscopy (small artefacts visible). (A) pristine polymer coating (B) TCPS modified surface (C) TCPS modification was removed via TBAF in 2 minutes (D) TCPS modified surface after immersion in THF for 24 h (E) prolonged immersion in 0.1 M TBAF solution for 2 h. The pictures demonstrate the dominating porous structure of the polymer coating, which is not affected by silanization or desilanization. The coating therefore shows stability against THF and TBAF.

Parallel to the surface topography, its chemistry was investigated via ToF-SIMS during the reversible silanization. Three samples were prepared: a freshly produced non-modified polymer-coated slide (Figure 14A), a TCPS-modified polymer-coated slide (Figure 14B) and a desilanized sample of the latter (Figure 14C).

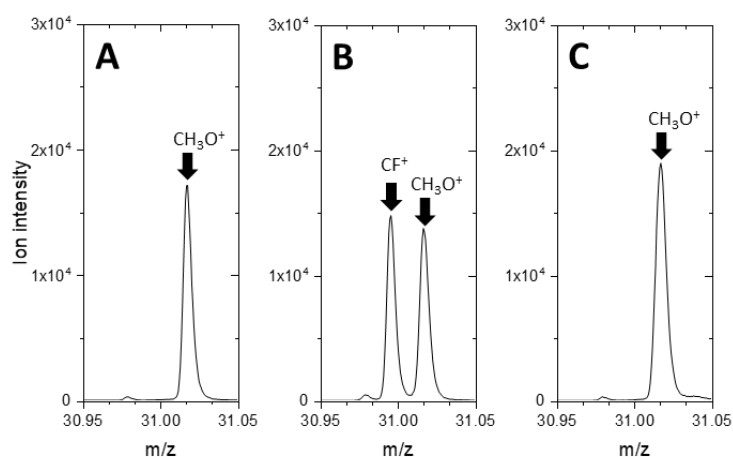


Figure 14. Depth integrated SIMS data of polymer layers: (A) non-treated, (B) TCPS-silanized, and (C) desilanized. The polymer was thoroughly eroded during measurement and the intensities of the CF^+ and CH_3O^+ ions were summarized for the whole layer. No residual CF^+ was detected after the TBAF treatment, indicating complete conversion.

By argon cluster bombardment during the ToF-SIMS measurement, the entire polymer layers of all three samples were eroded and sampled. The ion intensity of CF^+ at 30.997 m/z and a signal corresponding to the polymer fragment CH_3O^+ at 31.017 m/z were summed as a reference. As expected, there was no ion signal corresponding to the TCPS modification at the start of the cycle prior to exposure to the silanization solution. After the modification was completed and the polymer coating was converted to the superhydrophobic state, the emergence of the CF^+ signal (and others) indicated the presence of the fluoroalkylsilane. Following desilanization of the sample, the peak correlating to the modification was lost, thus demonstrating the total reversibility of the modification of the functional groups on the surface.

2.1.2.5 Spatial Control of Desilanization

To evaluate the potential for an additional application of this method, the reversible modification was performed spatially on the surface. Using an automatic contactless liquid dispensing system (iDOT), the desilanization solution was applied to distinct points on the surface. Starting with a TCPS-modified superhydrophobic polymer surface and applying the desilanization solution in a spatial configuration, an array of wettable spots surrounded by a superhydrophobic background should be generated. However, due to the rapid evaporation of the organic solvent THF, which was used for the desilanization process, a more suitable solvent system for this application needed to be chosen. The main requirement was a low vapor pressure, so that even small volumes (in the nanoliter range) would be non-volatile and remain on the surface long enough to allow the reaction to occur. On the other hand, highly polar solvents with a high

surface tension (e.g. water) would neither wet the superhydrophobic surface, nor react with it. To accomplish this, 10% (v/v) of THF in γ -butyrolactone (GBL) as a solvent was selected with a TBAF concentration of 0.1 M.

The non-contact liquid dispensing system (iDOT) was programmed to print 8 nl of the TBAF solution in an array of spots with a spot-to-spot distance of 1.5 mm. After dispensing and 2 minutes of reaction time, the slide was washed with ethanol. Interestingly, for the first attempts of this experiment, the printed spots were indeed wettable with water and turned transparent, but the remained TCPS-modified borders were not superhydrophobic anymore and inhibited discontinued dewetting and formation of distinct droplets. For a better investigation of this effect, several droplets (each 5 μ l) of the desilanzation solution for printing were manually applied on a TCPS-modified slide and washed off after reaction time. When water was then spread over the slide, it formed droplets as shown in Figure 15: On the right side from each thoroughly wettable spot, parts of the surface are less hydrophobic. In a miniaturized array, this effect yields to merging of the droplets.



Figure 15. A TCPS-modified slide after manual application of each 5 μ l desilanzation solution (0.1 M TBAF in 10% (v/v) THF in GBL) and washing via ethanol flow. Short contact time of TBAF during washing leads to partial desilanzation.

Since the washing process was carried out by holding the slide with a tweezer slightly tilted over a waste beaker and rinsing it with ethanol from a squeezing bottle, the flow of solvent over the surface was from left to right. When the ethanol flow reached a droplet of desilanzation solution, it mixed with it and transported the diluted TBAF away over the surface. This short contact time with a in the beginning only slightly diluted TBAF solution is already enough for the desilanzation to occur. As only some fluoroalkyl silane groups are removed, the surface is still not completely wettable, but more “sticky”.

This effect was avoided by exchanging the washing step via flow with immersion in the solvent. A 0.5 L beaker was filled with 300 ml ethanol and the slide was horizontally immersed in the solvent for 1 minute. By this, the TBAF from the dispensed spots was removed and diluted without being transported over the surface.

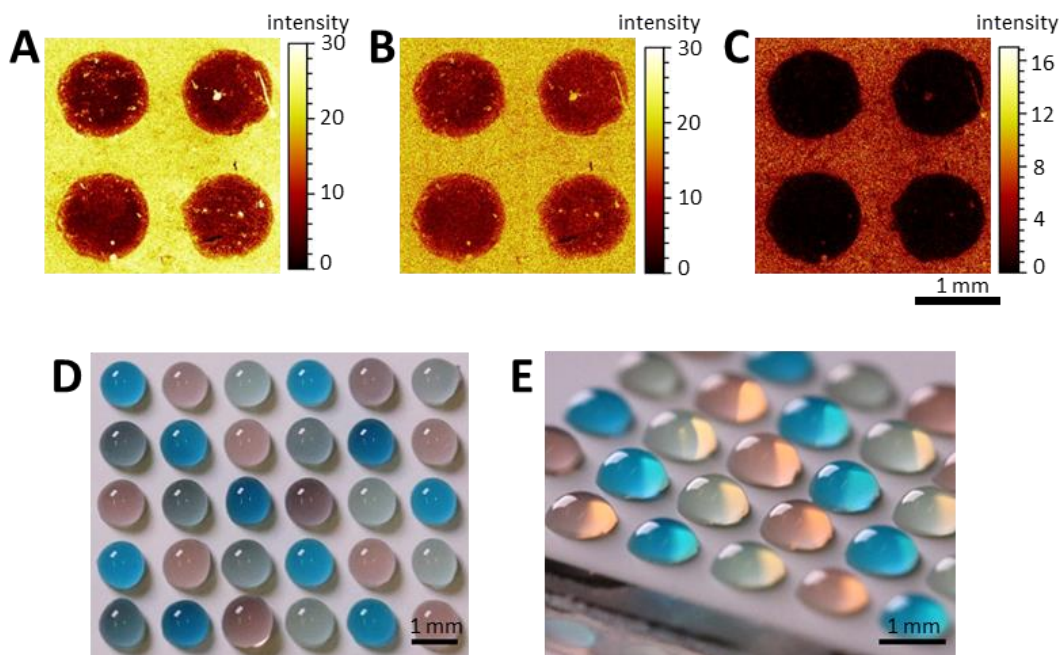


Figure 16. Two-dimensional mapping of ToF-SIMS analysis of a spatially desilanized surface (A–C) and photographs of aqueous food dyes in this microarray (D/E). The TCPS-modified surface was printed with 8 nl of 0.1 M TBAF in 10% (v/v) THF in GBL by the automatic liquid dispensing system (iDot); the reaction time was 2 minutes. Top panels show the lateral distribution of the signal intensity of the CF^+ (A), H^+ (B) and $C_2F_3^+$ (C) ions where the difference in surface chemistry is visible. D/E Images of the droplet microarray with a spot diameter of 1 mm and a spot-to-spot distance of 1.5 mm (500 nl of aqueous solutions of food dyes per spot were used for better visualization).

With this improved washing method, an array of wettable spots could be created via liquid dispensing of the desilanzation solution. After washing and drying the polymer with an air gun, the surface was rinsed with deionized water and discontinuous dewetting occurred, yielding a self-forming array of distinct droplets due to the wettability contrast of the superhydrophobic background and the hydrophilic spots (see Figure 16).

A sample of the spatially desilanized sample was analysed via ToF-SIMS to investigate the removal of silane and the shape of the edges. The top panels in Figure 16 show the lateral distribution of CF^+ , H^+ and $C_2F_3^+$ ions. It can be seen that removal of the silane is not as quantitative as compared to the immersion method and leaves some small parts of the modification on the surface, which is not detectable via wettability. A possible explanation is the high polarity of the solvent system, which can not penetrate the hydrophobic polymer as easily as pure THF. However, all ion signals showed distinct round spots with a diameter of

around 1 mm and differing chemistry compared to the surrounding background. The edges of the spots were clearly defined since the reaction occurs only in the areas wetted with the desilanization solution. The signals at 68.99 m/z and 80.98 m/z, which represent fragments of the fluorinated alkyl silanes CF^+ and C_2F_3^+ , were significantly decreased in the hydrophilic areas indicating the chemical conversion of fluorinated silyl ether to free hydroxyl groups by the cleavage of the silyl ether. Additionally, as the chemical environment in the spots changed, the ionization tendency of hydrogen ions was also altered (Figure 16B), which was detectable as a lower ion intensity for H^+ in the spots.

Greater flexibility in the design and creation of hydrophilic areas on the hydrophobic background can be achieved by using an artist's brush to spread the desilanization solution on the polymer coating. A solution of 0.1 M TBAF in 10% (v/v) THF in GBL was prepared for use in the same way as an ink or dye. The brush was dipped into this solution and used to draw a channel on a TCPS-modified surface as shown in Figure 17B. After a reaction time of 2 minutes, the solution was washed off via immersion in ethanol and the surface was dried under an air flow. Once dry, no pattern was visible on the polymer coating; however, by applying a stream of water on the slightly tilted slide, the different wettability conditions caused a channel to form spontaneously as the water flowed off the surface. The hydrophobic background stabilized the stream even at higher flow rates. The method is not just limited to simple channels, and various shapes can be drawn (Figure 17 C/D) showing the simplicity and versatility of this method.

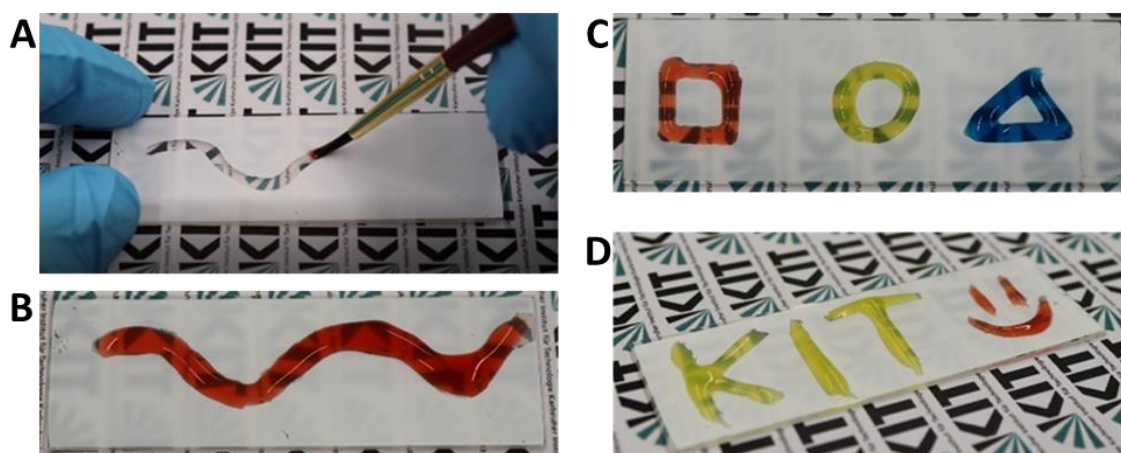


Figure 17. Photographs of the brush writing method (A) and the resulting patterns (C–D). The desilanization solution can be applied using a brush dipped into the liquid. (A) Image shows the simple process of designing a fluid channel on a hydrophobic background. (B) After a 2-minute reaction, the liquid is washed off and the channel is filled with aqueous food dye for better visualization. (C) and (D) Images show examples of hand-made hydrophilic patterns in which aqueous dye solutions are held.

2.1.2.6 Application of Other Substrates

To test the flexibility of the introduced method, modified samples of the polymer coating with trichlorododecylsilane and trimethylchlorosilane were prepared. Both silanes changed the prior hydrophilic polymer (static WCA $6^\circ \pm 1$) to hydrophobic surfaces with static water contact angles of $110^\circ (\pm 2)$ for trichlorododecylsilane and $102^\circ (\pm 1)$ for trimethylchlorosilane (Figure 18 A/B). By immersion in the TBAF solution for 2 minutes, the WCAs decreased again to $7^\circ (\pm 2)$ for both surfaces, indicating the removal of the silanes.

Additionally, the reversibility on silicon wafers as substrate (Figure 18C) was tested. Plain Si wafers show a water contact angle of $30^\circ (\pm 1)$, which increased to $107^\circ (\pm 3)$ after the modification with TCPS. In contrast to the polymer film, treatment under standard conditions with TBAF for 2 minutes did not completely restore the initial surface, which was observed by a contact angle of $55^\circ (\pm 1)$. However, after a prolonged treatment for 24 h, the water contact angle further decreased to $35^\circ (\pm 3)$, indicating reversibility for silicon substrates under longer reaction times.

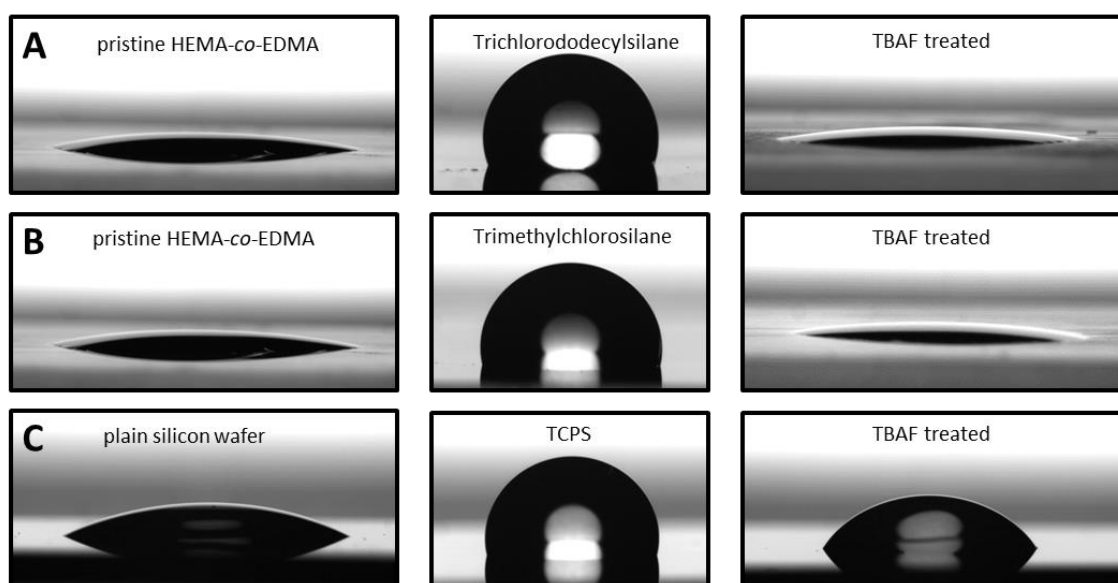


Figure 18. Developed water contact angles of each $10 \mu\text{l}$ deionized water on pristine, silanized and desilanized HEMA-co-EDMA (A/B) and silicon surfaces (C). First column shows the plain surfaces with static WCA of 6° (A/B) and 30° (C). Modification of the respective surfaces with either trichlorododecylsilane, trimethylchlorosilane or TCPS yielded contact angles of 110° , 102° and 107° . Treatment with the TBAF desilanization solution for 2 minutes changed the contact angles to 7° for the polymer surfaces and 55° for the silicon wafer. Prolonged treatment of the wafer for 24 h in the desilanization solution further decreased the static WCA to 35° (not presented).

Similar to the process on polymer coatings, the topography was investigated by AFM analysis of the silicon wafer surface (Figure 19). The plain silicon surface is flat with small irregularities, most probably from the production process or handling. Upon silanization with TCPS, the surface develops a noticeable rough struc-

ture from the three dimensional network of siloxane on the surface. This roughness is completely removed by treatment with the desilanization solution for 2 min. While prolonged incubation in TBAF solution for 24 h had further changes in wettability, no significant changes in the topography could be detected via AFM except for small inconsistencies, which are assumed to be precipitations from the desilanization solution.

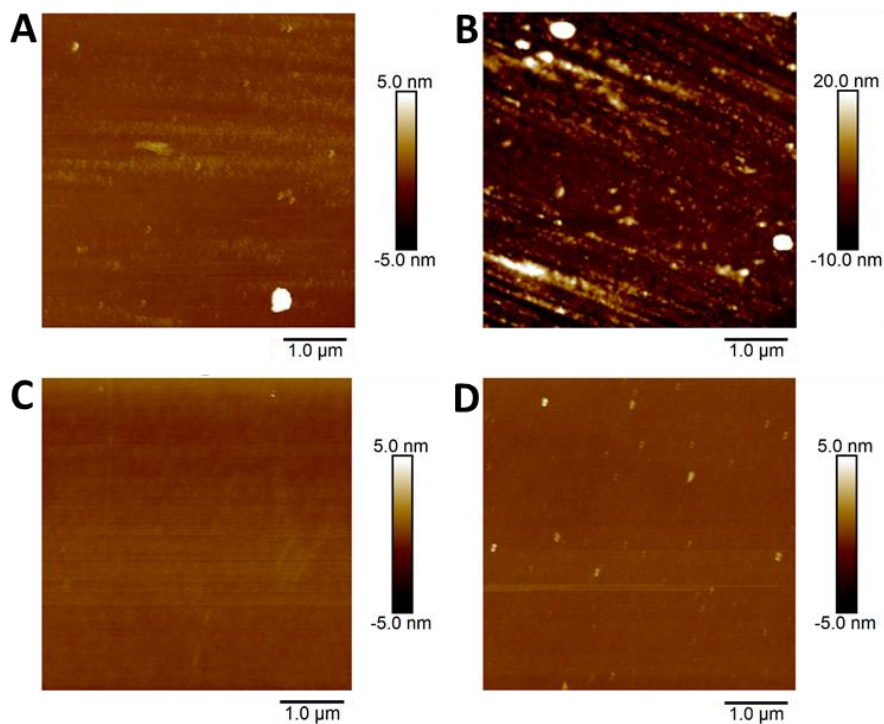


Figure 19. Surface topography of silicon wafers as measured by atomic force microscopy. (A) plain silicon surface (B) TCPS modified surface with increased surface roughness (please note the adapted color scale) (C) TCPS modification was removed via TBAF in 2 minutes (D) prolonged immersion of the silicon wafer in TBAF solution for 24 h.

2.1.3 Conclusion

The rapid and versatile modification of suitable materials via silanization to change its chemical and physical properties is a basic procedure in surface science. Furthermore, the conversion of a hydroxyl group to a silyl ether – for example via trimethyl silyl chloride (TMS-Cl) – is a well-known method used by synthetic chemists to protect free hydroxyl groups during multi-step synthesis. For the latter methods, the fast and selective cleavage of the Si-O bond via fluoride anions is important and makes this strategy so convenient. In this study, knowledge of synthetic and surface chemistry was combined to achieve variable control of surface wettability by either coupling a fluorinated alkyl silane (TCPS) to the naturally hydrophilic surface of a HEMA-co-EDMA nanoporous polymer coating or silicon wafer to achieve superhydrophobicity or by removing it from the surface by application of fluoride anions to regain hydrophilicity. The changes in WCA and ToF-SIMS analysis showed that this process is completely reversible in either direction in 2 minutes. Moreover, the spatial application of fluoride anions in a TBAF solution allowed formation of various and flexible patterns, for example via automated liquid dispensing. For greater flexibility, the solution can also be applied manually using an artist's brush. Using this method, hydrophilic channels were formed allowing rapid flow of the water over the surface following the manually drawn path. In conclusion, a rapid, reversible and versatile control of surface wettability was achieved by modification of hydrophilic surfaces with fluorinated alkyl silane and its spatial cleavage by fluoride anions.

2.2 Application of Droplet Microarrays for Solid Phase Synthesis

2.2.1 Nanomolar Synthesis in Droplet Microarrays for UV-Triggered On-Chip Cell Screening

Discovering new drugs is a major challenge and can take more than 20 years of work producing costs of over 2 billion dollars per drug.^[115] These expenses do not include the costs of the synthesis of compound libraries, which are critical for the drug discovery process. In order to solve this important problem, the process of the synthesis of compound libraries and their biological screenings have to be drastically changed. The new process should be compatible with (a) highly parallel synthesis; (b) miniaturization, synthesis in submicroliter volumes; and (c) the same platform should be compatible with both library synthesis and biological screenings. Such platform may significantly reduce the amounts of used chemicals, solvents and biological material and accelerate the whole process via parallelization of synthesis and integration of chemistry and biology. For example, the simple switch from a 96-well plate to a 384-well format decreases the sample volume by a third and increases experimental density by four.

Various platforms addressing miniaturized high-throughput synthesis and screenings have been developed. The group of Frank introduced the *SPOT* technique, where a cellulose membrane served as the solid support for a stepwise, combinatorial and parallel peptide synthesis.^[116] Over the years, the scope has also been expanded to other chemistries such as small molecules.^[117] The low price of the cellulose and the easy handling are important advantages of this platform. However, the size of the spots is determined by the pipetted volume of the reaction solution, which leads to the risk of cross contamination or incomplete reaction if too much or too little solution is applied.^[118] Also the use of the synthesized compounds in a solution-based assay after cleavage from the support is laborious and difficult to miniaturize.^[119] With standard liquid handling robotics, an array of peptides with density of up to 14 peptides per cm² was achieved.^[120, 121] To overcome the problems of liquid handling, the group of Breitling developed solvent-free laser printer-based peptide array synthesis,^[122, 123] increasing peptide densities to 40,000 cm⁻² and applying them to study protein-antibody interactions.^[122] The limitation of this method is that produced peptides stay bound to the surface, making solution-based biochemical or cell-based assays difficult without cross-contamination.

The Droplet Microarray (DMA) has been exploited as a platform for miniaturized high-throughput cell screening in diverse biological applications with volumes down to several nanoliters (see chapter 1.2). It was recently reported to use of the DMA platform for liquid phase chemistry, where the droplets served as microvessels to synthesize a library of lipidoids, which were screened for transfection efficiency.^[34]

Introducing a photocleavable linker to couple the starting material to the polymer layer of the DMA allowed for the synthesis of tripeptides via solid phase peptide synthesis as the first multistep synthesis performed on this platform.^[124] However, the attachment of the compound to the solid support of the hydrophilic spot has more advantages such as simple purification by washing off the reaction solution or the possibility to immerse the whole DMA in reaction mixtures or sterilization solutions without cross-contamination. An overview of the workflow is presented in Figure 20.

In the following chapters, the scope of the platform will be expanded to more complex chemistry and further investigate the possibility of on-chip screenings of the synthesized libraries.

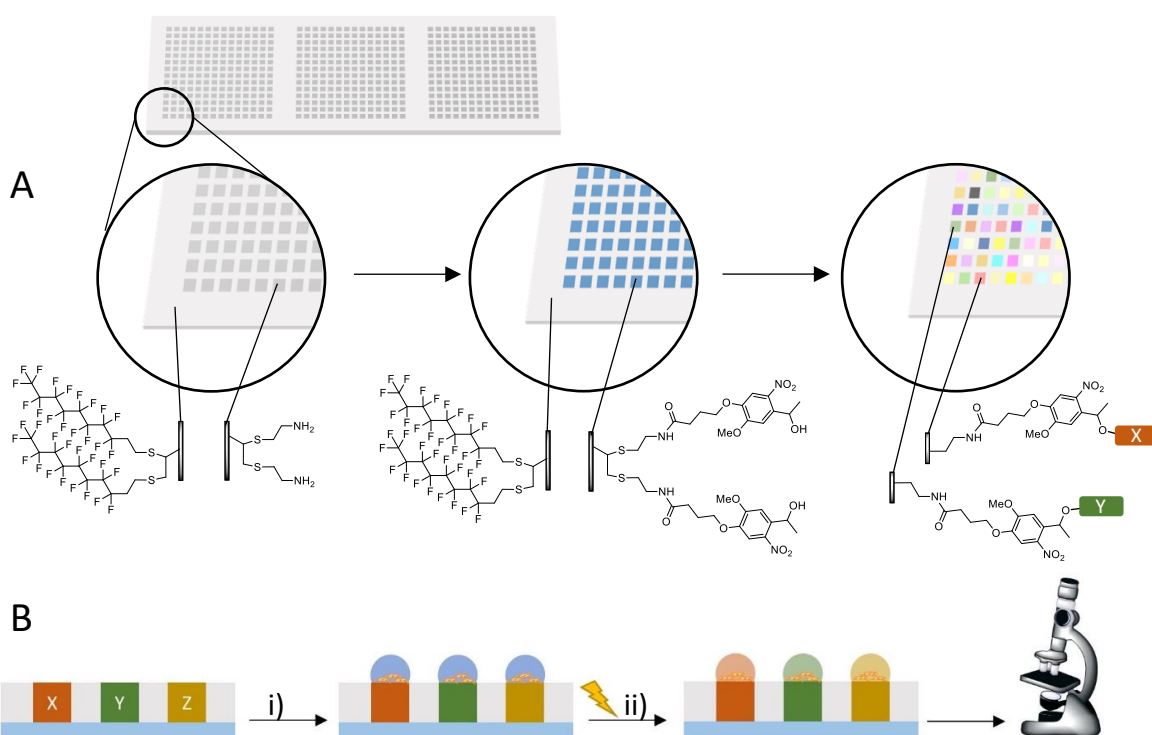


Figure 20. Droplet microarray platform combining high-throughput solid-phase synthesis and cell-based screenings. **(A)** Porous polymethacrylate thin film (12 μm thin) is functionalized with fluoroalkyl and cysteamine moieties to generate superhydrophobic and reactive hydrophilic regions, respectively. UV cleavable linker is covalently bound to the amine in the hydrophilic spots, forming the basis for the following solid-phase combinatorial synthesis. **(B)** Scheme showing a possible cell-based screening sequence: (i) synthesized compounds are still attached on the solid support and a cell suspension is filled into the distinct nanodroplets formed in the hydrophilic spots prior to UV irradiation to release the compounds into the solution (ii). Readout can be done by fluorescence microscopy due to the transparency of the substrate.

2.2.1.1 Materials and Methods

2.2.1.1.1 Patterning and Functionalization of the Polymer with Photolinker

The droplet microarrays were prepared according to the already published procedure (see also chapter 1.2.1).^[25, 27] Briefly, a microscope glass slide (76 x 26 x 1 mm) was coated with a layer of nanoporous poly(2-hydroxyethyl methacrylate-*co*-ethylene dimethacrylate) (HEMA-*co*-EDMA) followed by a Steglich esterification of the polymer using 4-pentynoic acid. Next, the surface was wetted with a solution of 1*H*,1*H*,2*H*,2*H*-perfluorodecanethiole in isopropanol and covered with a quartz photomask of the desired pattern. After UV irradiation at 254 nm (4 mW/cm²) for 2 minutes, the slide was washed, a solution of cysteaminium chloride in 1:1 (v/v) EtOH/water was spread and it was covered with a clear quartz glass slide before irradiating it again with UV light. After washing, the surface can show the effect of discontinuous dewetting.

To immobilize the linker onto the surface of the hydrophilic spots, linker (**HEPL** or **FAPL**, see chapter 1.3), diisopropyl carbodiimide (DIC) and 1-hydroxybenzotriazol were dissolved in *N*-methyl-2-pyrrolidone (NMP) to a final concentration of 0.1 M per compound. In a round spot in the size of 3 mm, 5 µl of this solution were pipetted and incubated in the dark at room temperature for 18 h (overnight). Respective volume for the smaller spots (1 mm square or 900 µm round) was 150 nl. The DMA was then washed with acetone and dried in air flow. In case of FAPL, the Fmoc group was removed by addition of 5 µl or 150 nl of 20 % (v/v) piperidine in NMP for 4 h and washing with acetone.

2.2.1.1.2 Photorelease and LC-MS Analysis of Products

If not stated otherwise, the UV-induced cleavage from the surface for LC-MS analysis was performed by pipetting 5 µl of deionized water into each round spot (d = 3 mm) and irradiating the DMA in a Biolink BLX UV chamber (Vilber Lourmat, Eberhardzell, Germany) with 2.5 mW/cm² at 365 nm for 15 minutes. The aqueous solutions were then pipetted off into glass vials and 5 µl DMF were applied into each spot to dissolve potential hydrophobic compounds. The DMF was then combined with the aqueous phases of the corresponding spots and injected to the LC-MS via autosampler (15 µl sample volume).

A HP 1100 (Hewlett-Packard, Palo Alto, USA) system with a C18 column (XB-C18, 100 Å, 100 x 4.60 mm, Phenomenex, Torrance, USA) was used for LC-MS analysis of products. Mobile phase contained acetonitrile (0.1 % formic acid) as A and deionized water (0.1 % formic acid) as B with a gradient of A from 10 % to 99 % over 10 minutes, remaining for 5 minutes and decreasing back to 10 % over 5 minutes. Mass detector was used in negative mode for samples synthesized with **HEPL** and positive mode for samples synthesized with **FAPL** (if not stated otherwise). Spectra were analysed via "Spectrus Processor" software (Advanced Chemistry Development Inc., Toronto, Canada) and target masses were calculated with ChemDraw (PerkinElmer, Waltham, USA).

2.2.1.2 Results and Discussion

2.2.1.2.1 Loading and Photorelease

The kinetic of the UV-cleavage was investigated by coupling chlorambucil (CHL, see Figure 21A) as model drug to the hydroxyethyl photolinker (HEPL) and determine its concentration in the droplet after different irradiation times. **CHL** was linked via Steglich esterification with a solution of chlorambucil hydrochloride (50 mM), 4-DMAP (5 mM) and DIC (50 mM) in NMP (5 μ l per spot) for 8 h at room temperature. The UV-triggered release was performed according to the general method (chapter 2.2.1.1.2) with different irradiation times and the volume of 4 spots (40 μ l in total) was pipetted off the surface and diluted to 100 μ l with DMF/water (1:1 v/v). This mixture was then measured for its absorbance at 284 nm, which refers to the wavelength of the previously determined maximum extinction coefficient ($\epsilon = 1950 \text{ l}\cdot\text{mol}^{-1}\cdot\text{cm}^{-1}$).

The amount of released **CHL** per surface area was determined using the Beer-Lambert law and 7.01 mm^2 for the area of a 3 mm round spot and plotted against irradiation time in Figure 21B.

The linker's half-life (irradiation time when half of the molecules are released) under UV exposure was measured to be around 7.5 minutes. The rapid photolytic cleavage of the linker in aqueous environment is important for the application of UV-induced drug release process under biologically relevant conditions. This half-life is in a similar range as values for the UV release of acetate from the same linker in liquid phase known from literature (around 3 minutes at $10 \text{ mW}/\text{cm}^2$).^[54] A maximum loading of chlorambucil of $0.68 \text{ nm}/\text{mm}^2$ was achieved, which was completely released into the droplets after 15 minutes of UV irradiation (365 nm , $2.5 \text{ mW}/\text{cm}^2$). The area of a circle with the diameter of 3 mm (7.01 mm^2) can therefore hold 4.77 nmol of chlorambucil. When the spot is filled with 5 μ l of solvent, this leads to a maximum accessible concentration of $954 \text{ }\mu\text{M}$. According to literature, the recommended concentration for primary screens in high throughput hit discovery is in the range of $1 - 10 \text{ }\mu\text{M}$,^[125, 126, 127] showing that the amount of compound in each spot is enough for biological screenings even in cases of non-quantitative conversions. By thickening the polymer layer, the loading can be increased with the drawback of a higher background signal during fluorescence microscopy. The coatings in this work were around $12 \text{ }\mu\text{m}$ thick as measured by optical profilometry (see chapter 5.1.1) and offer a suitable balance between loading capacity and microscopic read-out.

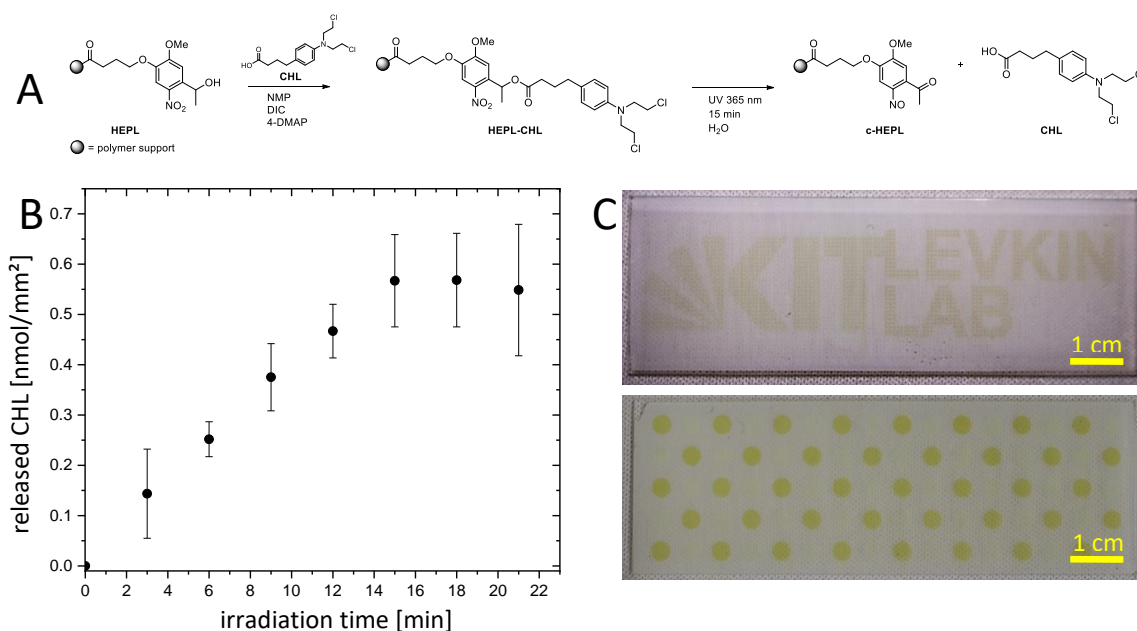


Figure 21. (A) Attachment of chlorambucil (CHL) onto the hydroxyethyl photolinker (HEPL) with subsequent release upon UV-irradiation, leaving the cleaved photolinker (c-HEPL) on the surface. (B) Kinetics of the UV triggered release of chlorambucil as a model drug from the surface into the 5 μ l droplets, determined by the spectroscopic analysis of the solution after different irradiation times. Each data point is the average of 3 experiments. Error bars represent standard deviation. (C) Spatial control of cleavage from HEPL via UV light. During cleavage of the linker, a yellow color is developed. Droplet microarrays were prepared and modified with HEPL in all hydrophilic spots prior to irradiation through photomasks. Top pattern: 2688 square spots with 500 μ m edge length and 250 μ m borders. "KIT Levkin Lab" logo was used as inverted photomask. The pictures contrast was slightly adjusted digitally to improve visibility of the logo. Bottom pattern: 80 round spots with 3 mm in diameter were irradiated in a checker-board pattern. UV linker gives full control over spatial release of compounds.

The nanoporous HEMA-co-EDMA polymer is opaque when dry, but turns transparent when wetted in the hydrophilic spots due to the reduction of light scattering. Because of this transparency and the thin coating, the UV light can access the whole reactive areas on the polymer without getting blocked. When compared to non-transparent cellulose-based platforms such as SPOT and their ammonia- or photo-triggered release,^[128, 129] the photorelease on the DMA is 20 times or 6 times faster, respectively. Besides, dry cleavage is essential in the case of other arrayed synthetic platforms to keep the format intact, since there are usually no self-separating and predefined droplet patterns like on the DMA.

Light can easily be controlled by focused beams or photomasks to spatially irradiate the surface, thus inducing cleavage only on the desired spots of the DMA. To demonstrate this, a droplet microarray was prepared with the format of $28 \times 96 = 2688$ square spots in the size of 500 μ m and 250 μ m borders and all the hydrophilic spots were modified with HEPL. A quartz glass photomask with the logos of KIT and the Levkin group was put on top and the surface was irradiated at 365 nm for 15 minutes with the intensity of 2.5 mW/cm². During the UV triggered cleavage process, the nitro substituent of the linker HEPL is reduced to a nitroso group (c-HEPL, see chapter 1.3 or Figure 21A), which leads to a bathochromic shift and

an occurring yellow color. The irradiated areas show the respective yellow logo, however minor adjustments of the pictures contrast were made to gain better visibility (Figure 21C, top). When a DMA with $5 \times 16 = 80$ round spots with a diameter of 3 mm was irradiated in the same way but with a chess pattern photomask instead, the developed color is clearly seen without any adjustments (Figure 21C, bottom). The controlled irradiation and cleavage gives an additional dimension for variation of screening conditions on the droplet microarray. This results show that the release of compounds can not only be controlled quantitatively via irradiation time, but also spatially via selected irradiation of the hydrophilic spots

2.2.1.2.2 Raman Microscopy of Linker-Modified DMA

The surface chemistry was analysed via Raman microscopy (Hyperion 3000 by Bruker, Ettlingen, Germany; operated by Stefan Heissler from IFG, KIT; Illumination was executed by a laser beam at 532 nm and 2 mW intensity). For this, three samples were prepared according to the standard protocol: a DMA slide with free amino groups of the immobilized cysteamine (Figure 22A) and **HEPL** modified slides before (Figure 22B) and after UV-irradiation (Figure 22C). The pictures show a part of the spectra with subtracted baseline (raw spectra are presented in the appendix). For the first sample (Figure 22A), the spectrum shows bands at 2931 cm^{-1} and 1440 cm^{-1} for the C-H bonds of the polymethacrylate substrate, 1732 cm^{-1} for the C=O stretching vibration and at 3221 cm^{-1} for the polymers hydroxyl groups and 2120 cm^{-1} for alkyne groups which remained in the polymer from the production process. Since alkyne groups give a very strong signal in Raman spectroscopy, even small residual amounts are detected and visible in the spectra. When the DMA is then modified with the aromatic nitro group containing linker (**HEPL**, Figure 22B), bands at 1333 cm^{-1} and 1579 cm^{-1} are evolving. These bands correlate to the vibrations of C-(NO₂) and C-C (aromatic) and indicate the presence of the linker on the surface. Additionally, the band at 1276 cm^{-1} can be assigned to the linker's hydroxyl group. After irradiating this spot with UV light (365 nm, 2.5 mW/cm^2 , 15 min, Figure 22C), the intensities of the bands representing the nitro group and the benzylic alcohol decrease again, indicating the reductive transformation of the nitro group to a nitroso group and the oxidation of alcohol to carbonyl during the UV induced cleavage. The bands of the polymer background are not affected by this transition.

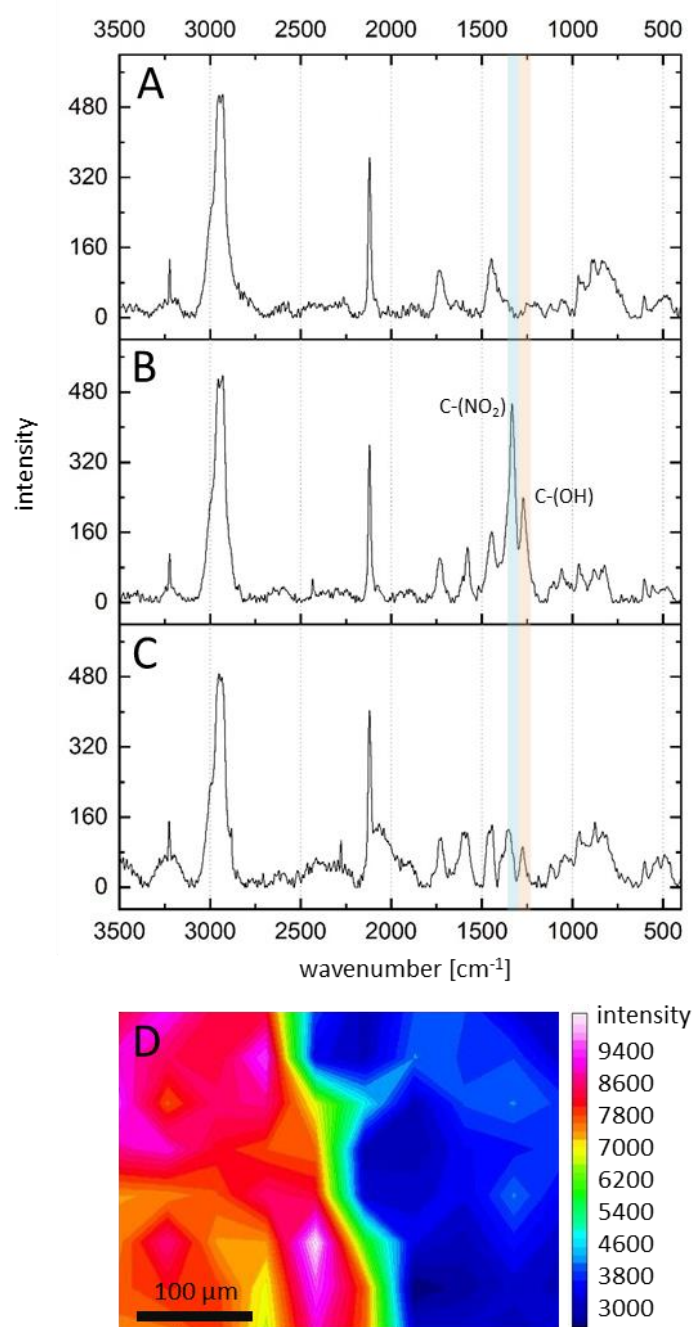


Figure 22. Raman analysis of a round hydrophilic spot on the DMA with the diameter of 3 mm. (A) The free amine groups of the cysteamine are present in the hydrophilic spots after DMA production and before modification with HEPL. Strong bands of C-H (2931 cm^{-1}) and alkyne groups (2120 cm^{-1} , remaining from production) are visible from the polymer support. (B) Attachment of HEPL is detectable by the increased band intensity at 1333 cm^{-1} referring to its nitro group and 1579 cm^{-1} for the aromatic system. (C) UV irradiation (365 nm , 2.5 mW/cm^2 , 15 min) of the surface reduces the nitro group of HEPL to nitroso and decreases this bands intensity. Additionally, the band at 1276 cm^{-1} of the benzylic alcohol is reduced due to its oxidation to the ketone. (D) Raman microscopy mapping of the edge of a spot modified with HEPL. Colors show the intensity distribution of the band at $1250\text{ cm}^{-1} - 1370\text{ cm}^{-1}$ corresponding to the C-(NO₂) vibration of the linker.

Next, the band between 1250 cm^{-1} and 1370 cm^{-1} was assigned to the nitro group of **HEPL** and a 2D mapping was achieved by measuring 81 single spectra on a field of $400 \times 400\ \mu\text{m}$ (focusing on the edge of a hydrophilic spot). The resulting band intensities were plotted as a function of position (Figure 22D). As expected, the linker is only found in the hydrophilic spots, owing to the precision of the photolithographic patterning process.^[130]

The results show that Raman microscopy can be used to obtain chemical information about the surface of the DMA. However, due to the very small amount of sample being present, the acquisition time for each spectra was around 2 hours, so the throughput of this method was too low to be used as a standard analytical method.

2.2.1.2.3 Biocompatibility and Selectivity of UV-Release

To demonstrate the performance of the DMA as a platform for solid-phase synthesis that can be directly followed by a biological read-out or cell screening, chlorambucil (CHL, see chapter 2.2.1.2.1) was used as a model drug. The drug was attached to the linker in the round 3 mm hydrophilic spots via Steglich esterification (*vide supra*) and the slides were subsequently washed and sterilized in 70 v% ethanol/water. Chinese hamster ovary cells (CHO-K1) were used as the biological reporter. This cell line is sensitive to the model drug and undergoes apoptosis when it comes in contact with nanomolar concentrations of **CHL**.^[131]

CHO-K1 cells were provided by ScreenFect GmbH (Eggenstein-Leopoldshafen, Germany). They were cultured in Ham's F12 medium with 10% (w/v) fetal calf serum (FCS) in a humid incubator at 37°C with 5% CO_2 and passaged every 2-3 days by detachment with 0.25% (w/v) trypsin / 0.02% (w/v) EDTA solution and dilution in fresh media. All biological experiments were performed under sterile conditions in a clean bench with laminar flow.

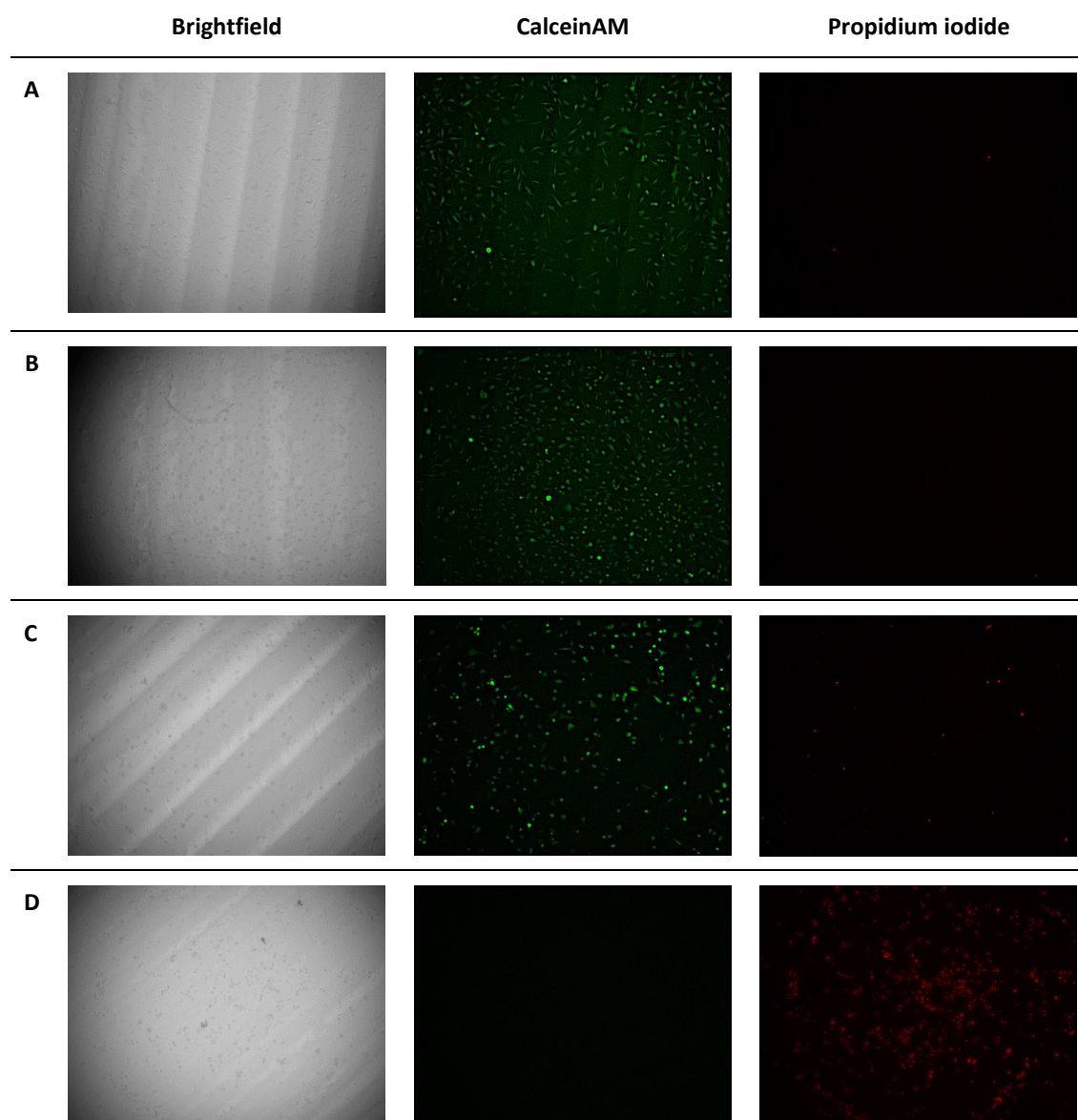


Figure 23. Proof of principle cell experiment with CHO-K1 cells seeded on different droplet microarrays. Cells were added by pipetting 5 μ l of CHO-K1 cell suspension with a concentration of 1×10^5 cells/ml in a round 3 mm spot followed by incubation for 24 h at 37 °C before staining with CalceinAM and propidium iodide. Pictures show brightfield and fluorescence microscopy pictures at 10x magnification. Samples (A) and (B) offer solely hydroxyl groups on the surface (coming from 2-mercaptoethanol) in the hydrophilic spots. While (A) served as negative control, sample (B) was irradiated with UV light (365 nm, 2.5 mW/cm², 20 minutes) directly after cell seeding. Samples (C) and (D) were modified with HEPL and chlorambucil; (D) was irradiated under same conditions as sample (B) to trigger the photorelease of the model drug.

DMA with linker-bound chlorambucil was used as a positive control, while a DMA which was functionalized with 2-mercaptoethanol (instead of cysteamine) in the hydrophilic spots served as negative control. A gelatin solution was prepared by adding 3 ml of sterile cell medium to 66 mg gelatin from bovine skin. To increase the solubility of gelatin, the solution was gently warmed in a water bath at 37°C. Once gelatin was completely dissolved, the solution was sterilized by filtering through sterile 0.22 µm filter and was then applied onto all DMA spots. The DMA was then incubated for 30 min at 37°C and 5% CO₂ atmosphere, followed by air drying of gelatin under sterile conditions. The gelatine treatment of the surface has been shown to be necessary for several types of cells.^[18, 28] Subsequently, 5 µl of CHO-K1 cell suspension were seeded onto the spots with a concentration of 1×10⁵ cells/ml, leading to around 500 cells per spot. One DMA functionalized with chlorambucil and one DMA with β-mercaptoethanol (serving as a control) were irradiated with UV-light at 365 nm for 20 minutes. Cells were incubated for 24 h at 37°C and 5% CO₂ prior to live/dead staining with CalceinAM and propidium iodide. CalceinAM stained cells were manually counted as alive and propidium iodide stained cells were considered dead as detected in fluorescence microscopy using a Keyence BZ-9000 microscope (KEYENCE, Osaka, Japan). The viability was calculated as

$$\text{Viability [\%]} = N_{\text{CalceinAM}} / (N_{\text{CalceinAM}} + N_{\text{PI}}) * 100$$

where $N_{\text{CalceinAM}}$ is the number of cells stained with CalceinAM and N_{PI} as the number of cells stained with propidium iodide.

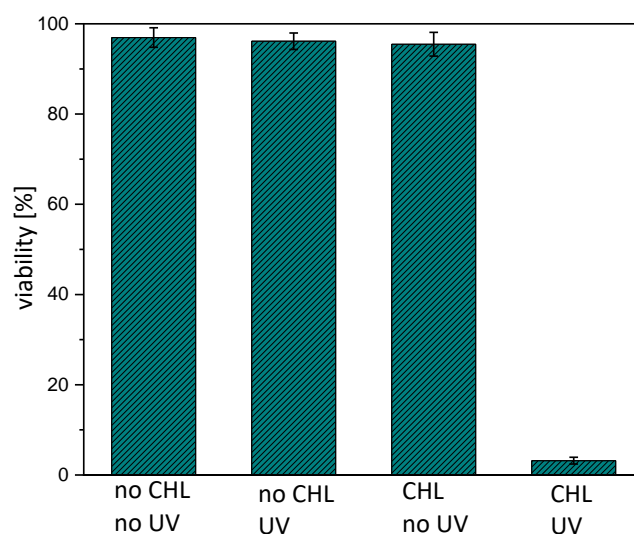
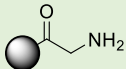
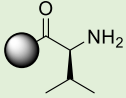
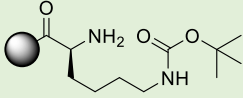
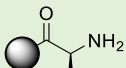
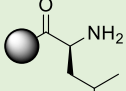
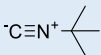
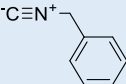
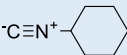
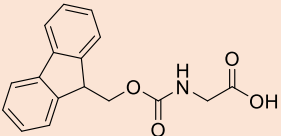
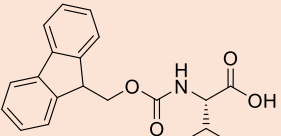
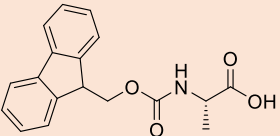
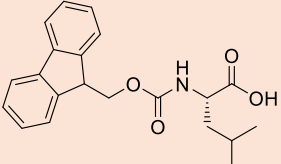
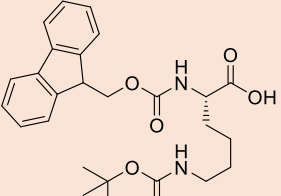
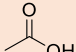
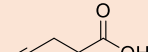
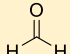
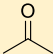
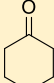
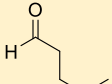
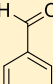
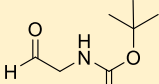
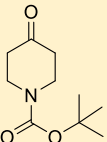
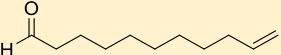


Figure 24. CHO-K1 cells were seeded on the DMA and their viability was determined via CalceinAM/PI staining for differently treated surfaces after incubation time of 24 h. Viability was not affected either by UV light or by the presence of the immobilized chlorambucil. The cell viability was decreased only after irradiation of the surface with attached chlorambucil, which led to the release of the drug into the droplets. Every bar represents an average of 3 repetitions of the same experiment. Error bars represent the standard deviation.

On the negative control slide (not chlorambucil-modified and not UV irradiated), the cell viability rate was 97% and there was no significant effect of UV irradiation on the viability (96%). Modification of DMA with chlorambucil did not reduce the viability of the cells, provided the slides were not irradiated with UV light. The combination of the chlorambucil pre-modification with UV irradiation, however, led to a significant drop of the viability to 3%, indicating the release of chlorambucil into the droplets. This experiment proves that cells' viability (as measured by staining with CalceinAM and propidium iodide and subsequent fluorescence microscopy) is neither affected by the cleavage conditions (365 nm, 20 min, 2.5 mW/cm²) for the drug release, nor by the surface-bound drug alone. This demonstrates that it is possible to "store" the drug in the polymer layer of the hydrophilic spot until it has to be released into the droplet microreservoir. By this it is possible to have a low cell-to-drug contact area while still offering enough sample compound to obtain an active concentration after photorelease.^[131]

by addition of 2 μl per spot of a solution containing 0.5 M aldehyde or ketone in γ -butyrolactone (GBL) for 15 minutes at room temperature. Subsequently, 2.5 μl of carboxylic acid (0.5 M in γ -butyrolactone) and 3 μl of isocyanide solution (0.5 M in γ -butyrolactone) were added which summed up to 7.5 μl reaction mixture per spot. The slide was incubated for 62 h at room temperature in a closed and darkened Petri dish with a GBL soaked paper tissue to minimize evaporation. Afterwards, the slide was extensively washed with acetone and dried in nitrogen flow. Cleavage from the surface and LC-MS analysis was carried out according to the standard procedure explained in chapter 2.2.1.1.2.

Table 2. Overview of the starting molecules for the Ugi reaction. Amines (**1 - 5**) are attached to the surface via the photolinker, while isocyanides (**6 - 8**), carboxylic acids (**9 - 15**) and carbonyls (**16 - 23**) are added as 0.5 M solutions in GBL. These 23 compounds can lead to 840 different products of the Ugi reaction.

| | | |
|--|--|--|
|  1 |  2 |  3 |
|  4 |  5 | |
|  6 |  7 |  8 |
|  9 |  10 |  11 |
|  12 |  13 |  14 |
| | |  15 |
|  16 |  17 |  18 |
|  19 |  20 |  21 |
|  22 |  23 | |

By collecting the solution of 5 spots after cleavage, each with the same target compound, it was possible to have enough sample volume for LC-MS analysis of 13 exemplary reactions (Table 3), which showed purities between 21% and 91% (average: 43%). These values are in the expectable range of Ugi reactions without fine tuning of the reaction conditions for every single combination of starting materials.^[66, 133, 134] The products were identified by their m/z values, mostly detected as $[M-H]^+$. For products containing an Fmoc-group, fragment ions of $[M-Fmoc-H]^+$ were found as main mass signal.

Table 3. Purity of 13 exemplary compounds synthesized through the on-chip Ugi-reaction as determined by LC-MS.

| Product | Amine | Isocyanide | Carboxylic acid | Aldehyde / Ketone | Purity ^[a] |
|---------|-------|------------|-----------------|-------------------|-----------------------|
| 24 | 1 | 7 | 9 | 16 | 91% |
| 25 | 1 | 7 | 10 | 16 | 58% |
| 26 | 1 | 7 | 11 | 16 | 57% |
| 27 | 1 | 7 | 12 | 16 | 43% |
| 28 | 1 | 7 | 13 | 16 | 29% |
| 29 | 1 | 7 | 15 | 16 | 21% |
| 30 | 4 | 7 | 9 | 19 | 65% ^[b] |
| 31 | 4 | 7 | 9 | 23 | 59% ^[b] |
| 32 | 4 | 7 | 9 | 21 | 35% ^[b] |
| 33 | 1 | 8 | 9 | 16 | 23% |
| 34 | 3 | 8 | 9 | 16 | 21% |
| 35 | 4 | 8 | 9 | 16 | 24% |
| 36 | 5 | 8 | 9 | 16 | 32% |

[a] Purity was calculated via LC-MS analysis of the cleavage solution as the product peaks ratio of summarized peak area at 254 nm absorbance.

[b] The signals of the two formed diastereomers were combined.

As described in chapter 1.5.1, the Ugi reaction can undergo side reactions that lower the yield of the desired product. The LC-MS data of the 13 representative compounds were investigated for these byproducts. Since the Passerini reaction occurs without the amine component, these byproducts should be washed away prior to the UV triggered release and not be present in the cleavage mixture and indeed, no corresponding mass signals were found. Also no mass signals were detected which could come from the formation of amidines.

Masses that could represent the products from the respective Ugi 3-component reaction were found in all 13 spectra as minor traces. Premature cleavage products of Fmoc or Boc protective groups could also

not be detected, most likely due to the mild reaction conditions. There was also no mass signal of unreacted amino acid or Fmoc-protected amino acid detectable.

Since the sample volume was very low, deeper analysis of side products via other analytical methods was not possible and their structure could not be identified. It should be noted that the Ugi reaction was just used as a model reaction here to show the general possibilities of the platform and optimizing its performance was not in the scope of this chapter.

2.2.1.2.5 Copying of the Array for MALDI-TOF Analysis

To prove the possibility of miniaturization on the platform, the pattern was switched from the round hydrophilic spots with a diameter of 3 mm, which could accommodate 5 μ l to square spots with an edge length of 1 mm and volume of around 150 nl. This enlarged the possible library on one single DMA glass slide from 80 spots to 588 and the compound density from 4 spots/cm² to 30 spots/cm². In every spot, 30 nl of the aldehyde or ketone solution were printed by a non-contact liquid dispenser (iDot by Dispendix, Stuttgart, Germany) and incubated in a closed petri dish for 15 minutes to preform the imine. Subsequently, 35 μ l of the carboxylic acid solution and 40 μ l of the isocyanide solution per spot were printed to start the reaction. Isocyanide was added at last to avoid acid induced hydrolysis. All solutions were used with a concentration of 0.5 M in GBL. The DMA was incubated for 3 days in the dark at room temperature in a closed petri dish with a GBL soaked paper tissue to avoid evaporation. To end the reaction, the reaction mixtures were washed from the DMA with acetone and the slide was dried in air flow. 100 nl of deionized water were printed into each spot and the products were released into the separated droplets by irradiating the whole DMA with UV light of 365 nm (2.5 mW/cm²) for 15 minutes. MALDI matrix addition was performed by dispensing 100 nl per spot of a saturated solution of α -cyano-4-hydroxycinnamic acid (CHCA) and 2,5-dihydroxybenzoic acid (DHB) in 10 v% acetonitrile in water (containing 5 mM HCl).^[135] Directly after dispensing, the droplet microarray was sandwiched onto an indium tin oxide (ITO) coated glass slide, which was immersed in 30% aqueous hydrogen peroxide solution for 5 minutes prior to use. Activation with hydrogen peroxide increases the hydrophilicity of the ITO surface and improves the attachment of the droplets during sandwiching. The design of the sandwiching device that helps to align two slides over each other was already published by the Levkin group.^[136] After contact of the droplets from the DMA with the ITO slide, the slides were separated again, leaving part of the droplets containing both synthesized compounds and matrix solution attached to the ITO surface in the array format mirroring the DMA slide. Due to inhomogeneity of the surface, the dispensing process and droplet evaporation, some droplets were smaller and could not come in contact with the ITO slide. Additional 20 nl of matrix mixture were added to those droplets and the sandwiching was repeated until all droplets were in contact with the ITO slide. This process copies the array of single droplets, each with a synthesized product and

matrix mixture, from the DMA to the ITO slide.

Two solvent systems were tested for transferring of product and matrix: 10% (v/v) acetonitrile in water and 10% (v/v) DMF in water. The formed product-matrix co-crystals on the ITO slide after evaporation of the solvents in vacuum are shown in Figure 26. It is commonly known that the co-crystallization of matrix and analyte is an important factor for satisfying spectra.^[137] It should form small, homogeneous crystals to offer a high surface area, where desorption can occur. When the matrix-sample mixture is crystallized from 10% (v/v) DMF in water, the amount of transferred matrix is higher due to better solubility (as described above, saturated solutions were used) and the crystals are bigger as compared to crystallization from 10% (v/v) acetonitrile in water. In the latter case, the formed crystals are overall smaller, but arrange in a ring with bigger crystals around the much smaller crystals inside. This may occur because of premature evaporation of the solution before the slide could be placed in vacuum and therefore two different drying speeds. Because of the favourable crystallization from acetonitrile in water, this solvent system was chosen.

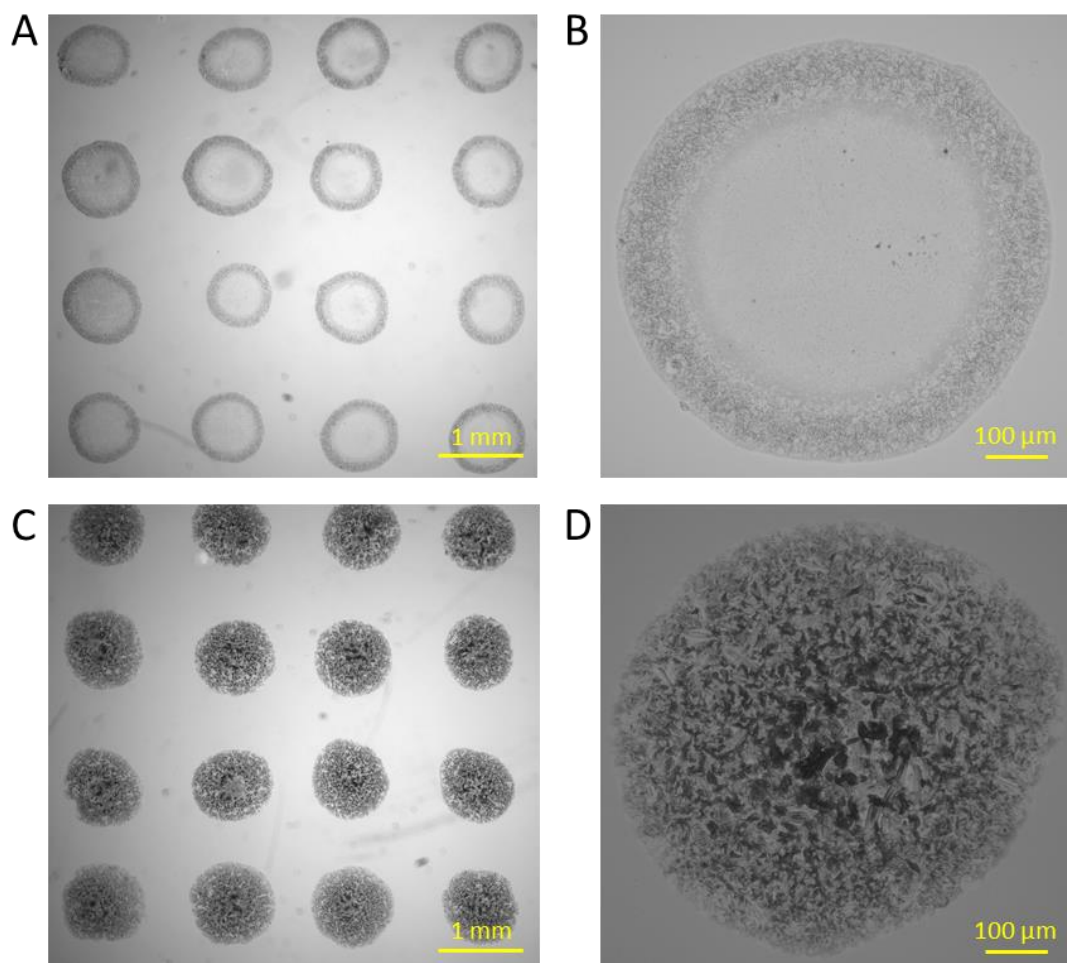


Figure 26. Microscopic pictures of vacuum-dried MALDI matrix mixtures (CHCA/DHB, 5 mM HCl) on an ITO slide deposited via sandwiching from a HEMA-co-EDMA polymer DMA with 2x (A, C) and 10x (B, D) magnification. Top row: 10% (v/v) acetonitrile in water was used as solvent. Bottom row: 10% (v/v) DMF in water.

ITO slides are conductive and are commonly used for MALDI imaging. In preliminary experiments, standard MALDI steel plates were used, which also worked. But the transparency of the ITO slides simplifies the handling during the sandwiching because it is visible when the droplets are in contact with the ITO surface. The deposited mixtures were dried in vacuum and passed to MALDI-TOF analysis. As it can be seen in Figure 27, the obtained spectrum of representative compound **37** gives the $[M+Na^+]$ adduct peak with the visible isotopic pattern.

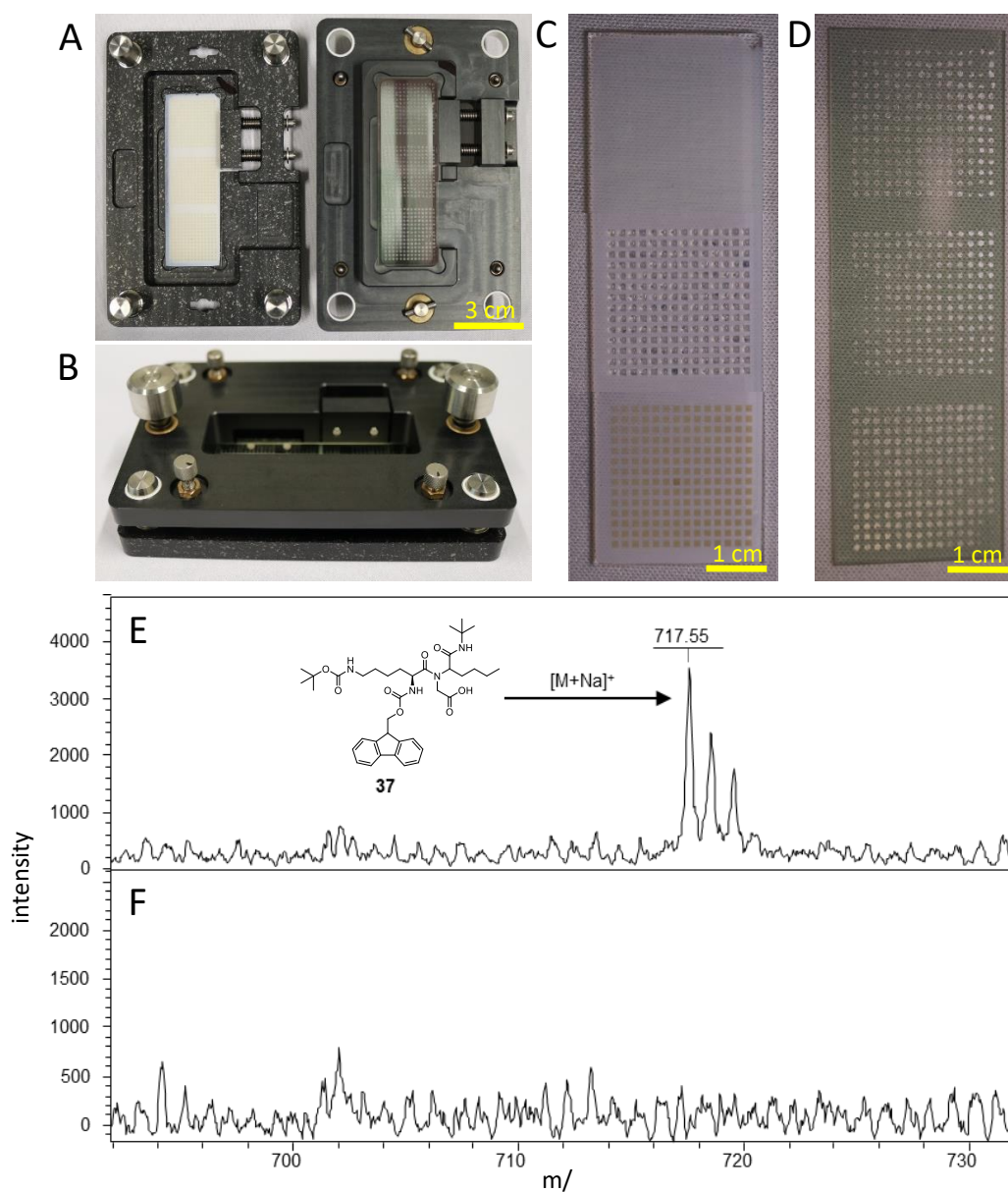


Figure 27. Process of copying the droplet microarray onto an ITO slide for MALDI-TOF MS measurements. **(A)** The sandwiching device helps to align both slides onto each other. Left side is the bottom part with the irradiated droplet microarray while on the right is the top part with the ITO slide (already stamped with matrix). **(B)** Closed sandwiching device. The two connectors on the sides pull the two halves together while the distance is controlled by four screws. Top part is lowered until all droplets touch the ITO slide. **(C)** Merged photograph of a dry DMA (14x14 1 mm hydrophilic spots, top), the DMA with 100 nl water in each spot (middle) and the dry array after UV irradiation (bottom). **(D)** ITO slide after copying the droplet microarray which contained matrix mixture (CHCA/DHB) in the droplets and drying in vacuum. **(E)** MALDI-TOF spectra of compound **37** as sodium adduct ($[M+Na]^+$, detected: 717.55 m/z, calc.: 717.38 u) and matrix background **(F)**. The compound was first cleaved into distinct droplets via UV irradiation, followed by addition of 100 nl of a saturated solution of CHCA and DHB matrix in 10 % ACN/water (containing 5 mM HCl) into each spot and sandwiching the DMA slide onto an ITO slide to copy the array. The ITO slide was dried in vacuum and analyzed by MALDI-MS.

2.2.2 Sequence-Defined Oligomers via Ugi/Thiol-ene Cycles

Over millions of years, nature was developing highly adapted molecular “workers”, which are known as enzymes or peptides. Their unique three-dimensional structure is important for the particular structure-function relationship and is based on the one-dimensional primary structure where single amino acids, coupled via amide bonds, form a macromolecule with a specific sequence of side chain functionalities. Another example is the DNA found in every living cell, which stores huge amounts of data just by the exact sequence of the same four nucleotides.^[138] This exactly defined sequence of monomers in a macromolecule, although crucial in nature, has always been a challenge for chemists to imitate.^[139] One approach are controlled radical polymerizations,^[140, 141, 142] which are simple to perform, but suffer from side product formation due to the highly reactive species.^[143, 144] Instead of a monodisperse macromolecule, one will end up with a broad distribution of products, which differ in size, mass, sequence and other properties. More control and monitoring over the designed oligomer is achieved by step-by-step iterative synthesis like it is done for peptides,^[145] oligonucleotides,^[40] peptoids,^[146, 147] and oligosaccharides,^[148] but is laborious for larger scales and sequences since there is a need for protecting groups (and deprotection steps) and/or activation agents. As the experienced reader will notice, most examples are generally carried out by solid phase synthesis techniques, because it accelerates washing and purification of the growing product after every reaction step. To minimize the effort for protection, deprotection or activation of monomers during iterative synthesis, plenty of working groups have developed different combinations of orthogonal chemical reactions,^[149] which are performed alternating to achieve simpler and upscaleable free chain growing of the sequence defined oligomers.^[150] For example, some recently introduced strategies used azide-alkyne/amide formation,^[151] iterative radical cyclization via NHS-ester and pyridyl-disulfides,^[152] aminolysis of thiolactones/Thio-Michael addition,^[153] or multicomponent reactions with isocyanides such as the Passerini 3-component reaction (P-3CR) or Ugi 4-compound reaction (U-4CR) in combination with hydrogenolysis of benzyl esters^[154] or thiol-ene click reactions.^[73] Especially the combination of the U-4CR and thiol-ene reaction offers important advantages: While two of the functional entries in the U-4CR are used for backbone structure and chain elongation, the other two can be used for parallel introduction of different side chain functionalities with defined sequence in the yielded oligomer. As a click reaction, thiol-ene reactions are fast, usually quantitative and less prone to side reactions, thus making them ideal for longer synthetic protocols with multiple repetitions of it. While a lot of interest was put in synthesis, characterization and analysis of the oligomers, less effort was taken for the biological activity of such oligomers, even though they seem promising because of their N-substituted peptidomimetic backbone structure.^[155]

In this chapter, the aim was to use the DMA platform for synthesizing miniaturized arrays of sequence defined oligomers via Ugi/thiol-ene cycles to offer them for screenings in a high-throughput approach for biological effects.

2.2.2.1 First Ugi Cycle

In chapter 2.2.1, the Ugi reaction was used to synthesize a library of various bisamides, starting with coupling of an Fmoc-protected amino acid to the linker (**HEPL**) and subsequent cleavage of the protecting group to obtain the amine as one component for the synthesis. This approach was chosen because of the wide variability of Fmoc-amino acids and their rapid deprotection. However, purities were not high, especially not enough for several repetitive steps like it would be required for the planned oligomer synthesis.

As a new approach to be tested, the carboxylic acid functionality was attached to the solid phase, while the varied preformed imine and isocyanide was added in solution. Incorporating a terminal alkene into the product by the use of 4-pentenal allowed for a subsequent thiol-ene reaction with 3-mercaptopropionic acid without the need for additional deprotection or activation. The new carboxylic acid functionality should then be used for the next Ugi reaction. This iterative synthesis is shown in Figure 28.

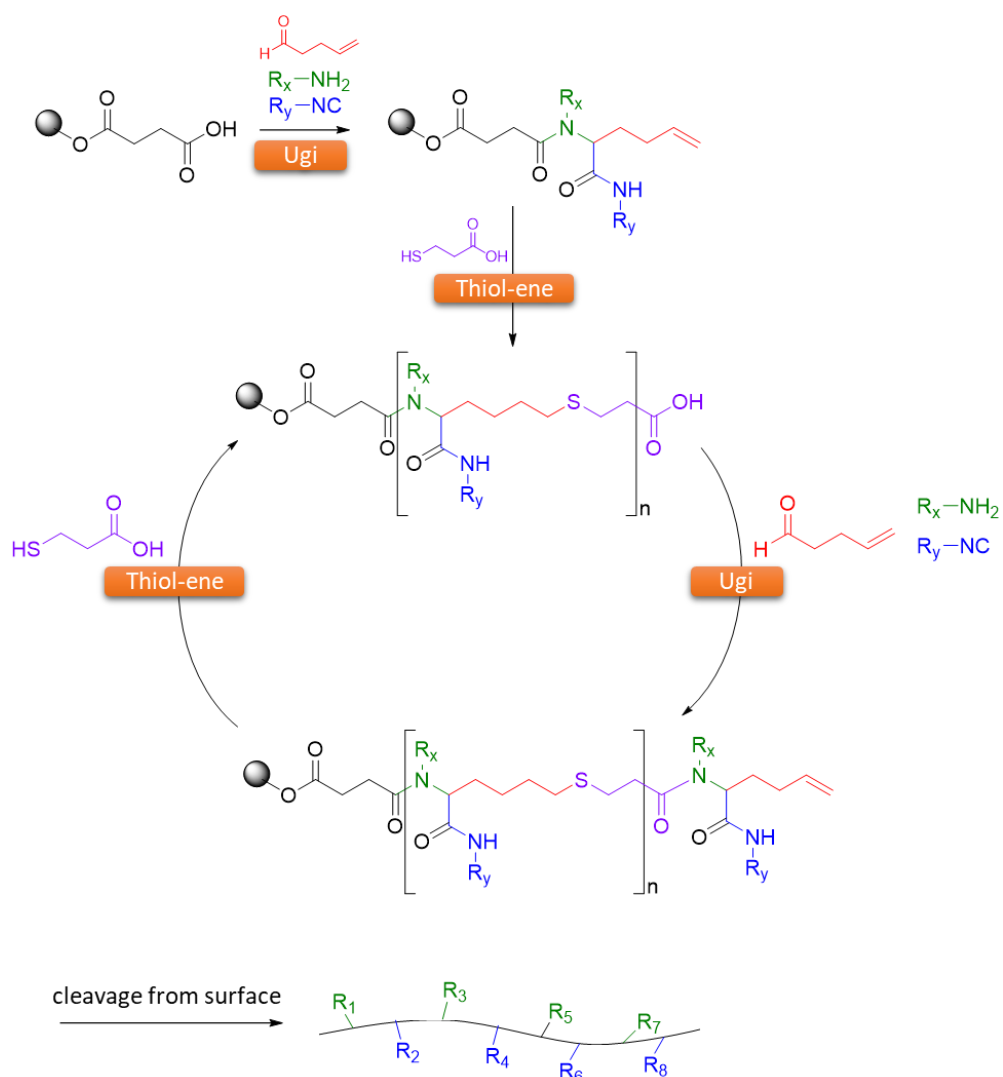
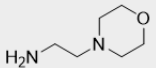
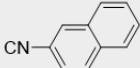
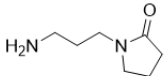
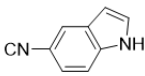
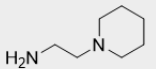
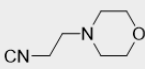
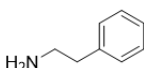
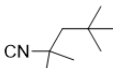
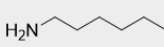

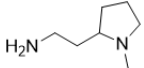
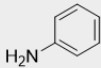
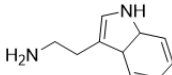


Figure 28. Schematic sequence of alternating Ugi and thiol-ene reaction for the protecting group free synthesis of sequence defined oligomers. After the Ugi reaction has introduced two variable side groups and the 4-pentenal, the available olefin is coupled with 3-mercaptopropionic acid in a thiol-ene reaction to obtain again a carboxylic acid functionality for a new Ugi cycle.

Starting from **HEPL** in the hydrophilic spots, its hydroxyl group was acylated by pipetting 5 μ l of a solution containing 0.1 M succinic acid anhydride and 0.01 M 4-DMAP in NMP in every round spot ($d = 3$ mm) and let it react in a darkened petri dish at room temperature for 18 h. After the reaction time, the slide was washed with ethanol and dried in air flow.

Table 4. Structure of amines (A_x) and Isocyanides (I_y) used in this chapter.

| # | Amine R_x | # | Isocyanide R_y |
|-------|---|-------|---|
| A_1 |  | I_1 |  |
| A_2 |  | I_2 |  |
| A_3 |  | I_3 |  |
| A_4 |  | I_4 |  |
| A_5 |  | I_5 |  |
| A_6 |  | | |
| A_7 |  | | |
| A_8 |  | | |

The following Ugi reaction was performed by mixing 4-pentenal and the corresponding amine in GBL to a final concentration of 0.5 M each and let it preform the imine for 15 minutes at room temperature. 3 μ l of this solution were then pipetted into each spot and the reaction was started by addition of 2 μ l of the isocyanide solution (0.5 M in GBL). The slide was then stored in the dark at room temperature for 3 days before being washed with acetone and ethanol. Cleavage and LC-MS analysis of the products was conducted as described in 2.2.1.1.2. Table 4 shows the structure of the different starting materials and in Table 5 the calculated purities of possible products are shown. For the products derived from the aromatic isocyanides I_1 and I_2 , the purity was calculated as product peaks ratio of summarized peak area at 254 nm absorbance. As the alkyl isocyanides I_4 and I_5 showed very low signals in the UV detector for most products, the total ion count (TIC) chromatogram was used for calculation of purity. Target molecules containing I_3 were detected as broad peaks in the chromatogram which overlapped with the injection peak in some cases, making peak integration not suitable. This can be explained by the additional possible cationic charge in the side group of I_3 and its polar character. Therefore, the whole ion chromatogram was summarized and the corresponding masses of all products were present. With an average purity of 70% and

several products with purities over 80%, the outcome of the reaction screening was satisfying. Also lower performing combinations (e.g. **A3I1** and **A8I1**) could be identified to be left out in iterative synthesis. While the possible Passerini-sideproduct should be detectable in this approach, the corresponding masses were not found in any LC-MS run, indicating a sufficient suppression by imine preformation.

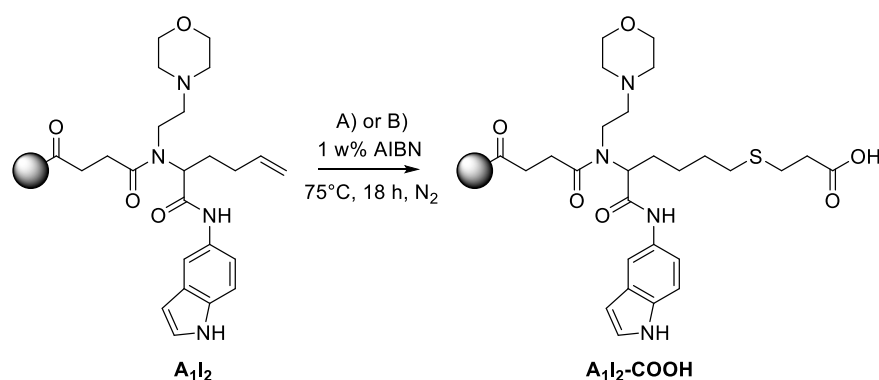
*Table 5. Purity of most Ugi products using amines (**A_x**) and isocyanides (**I_y**) as determined by LC-MS. **I₁** and **I₂** were calculated via the absorbance at 254 nm and for **I₄** and **I₅** the total ion count (TIC) chromatogram was integrated. Rows and columns labelled with \emptyset show the calculated average purity.*

| | I₁ | I₂ | I₄ | I₅ | \emptyset |
|----------------------|----------------------|----------------------|----------------------|----------------------|-------------|
| A₁ | 79% | 89% | 81% | 83% | 83% |
| A₂ | 87% | 90% | 75% | 82% | 83% |
| A₃ | 11% | 59% | 59% | 47% | 44% |
| A₄ | 67% | 80% | 83% | 84% | 79% |
| A₅ | 36% | 90% | 67% | 63% | 64% |
| A₆ | 86% | 79% | 85% | 87% | 84% |
| A₇ | 68% | 80% | 81% | 55% | 71% |
| A₈ | 26% | 46% | 65% | 52% | 47% |
| \emptyset | 58% | 77% | 75% | 69% | 70% |

In contrast to amino acids, the mass of unreacted succinic acid was detected in all attempts as part of the injection peak. When the reactions were carried out twice, there was still residual succinic acid present, indicating that the reason is more likely to be sterical hindrance from the Ugi product and not lack of reactants (because of possible side-reactions in the solution). A possible blocking procedure would have been esterification or amidation of the carboxylic acid, but it was decided to test first if a blocking step is required at all, since the residual starting material showed no reactivity.

2.2.2.2 Thiol-Ene Reaction with 3-Mercaptopropionic Acid

A new starting point for the next Ugi reaction cycle was introduced via thiol-ene reaction between the terminal alkene of the Ugi product and 3-mercaptopropionic acid. This hydrothiolation can be initiated by irradiation with UV light at 254 nm or different radical initiators. As the UV irradiation would also induce cleavage from the linker, a thermal radical initiation with azobisisobutyronitrile (AIBN) was tested.



*Scheme 7. Thiol-ene reaction of surface-bound Ugi product **A_{1I}2** was tested under two different conditions. A) 1 M 3-mercaptopropionic acid in DMF B) pure 3-mercaptopropionic acid without solvent. 1% (w/w) AIBN was added in both attempts and the samples were heated to 75°C for 18 h under nitrogen atmosphere.*

Two DMA with the formed Ugi product **A_{1I}2** still attached to the linker in the hydrophilic spots (3 mm round) were placed in 50 ml brown centrifuge tubes and sealed with rubber stoppers. Inert atmosphere was created by evacuating the tubes and flushing with nitrogen several times. Via syringe 45 ml of a solution of 3-mercaptopropionic acid and 1% (w/w) AIBN were added. Solution A contained 1 M of thiol in DMF while solution B was thiol without additional solvent (see Scheme 7). The tubes were then heated in an oil bath to 75°C for 18 h. After reaction time, slides were washed and the products were cleaved off the linker and analysed in LC-MS according to the standard procedure. For solution A, no conversion to the thioether occurred, while solution B yielded quantitative conversion. Since the thioether had a similar retention time as the Ugi product, the results are presented as the obtained mass spectra at 5.40 minutes retention time in Figure 29. When the reaction in solution B was repeated without inert atmosphere, 5% of a byproduct was formed which was identified as oxidized thioether (sulfoxide) via its mass signal.

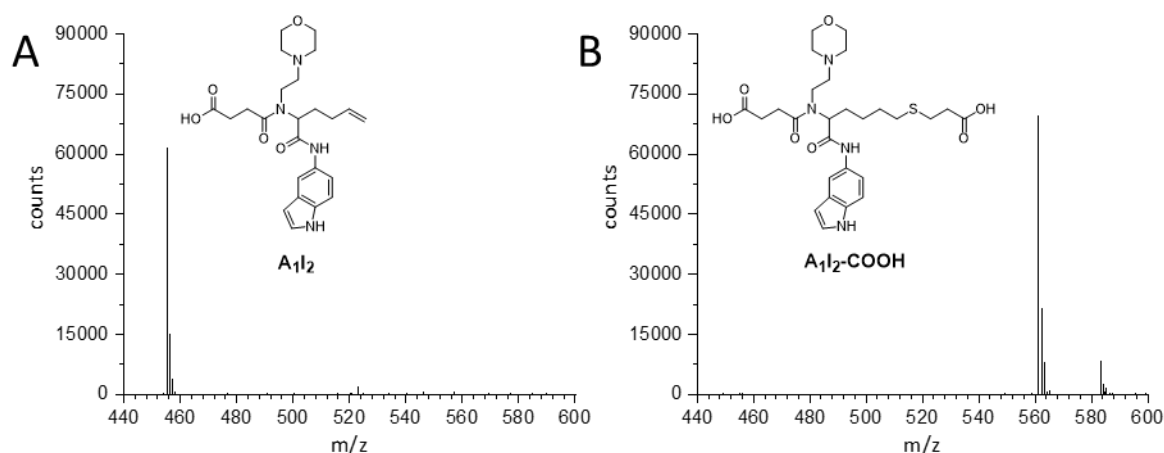


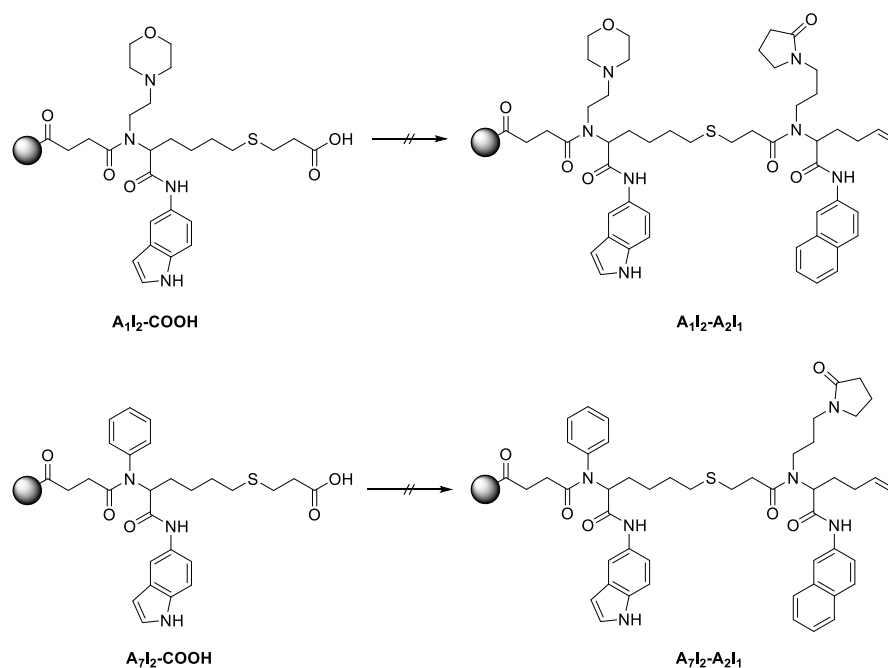
Figure 29. Obtained negative mode mass spectra of LC-MS runs at a retention time of 5.40 minutes. **A** Ugi product **A₁I₂** after UV-triggered cleavage ($[M-H]^+$, calculated: 455.23 m/z, detected: 455.20 m/z). **B** Product after conversion of surface-bound **A₁I₂** via immersion of the DMA in 3-mercaptopropionic acid and 1% (w/w) AIBN for 18 h at 75°C under nitrogen atmosphere ($[M-H]^+$, calculated: 561.24 m/z, detected: 561.30 m/z, smaller signal of Na-adduct also visible).

2.2.2.3 Second Ugi Cycle

The now available carboxylic acid in the molecule **A₁I₂-COOH** was then employed in the second Ugi reaction with amine **A₂** and isocyanide **I₁** to yield the product **A₁I₂-A₂I₁** (see Scheme 8).

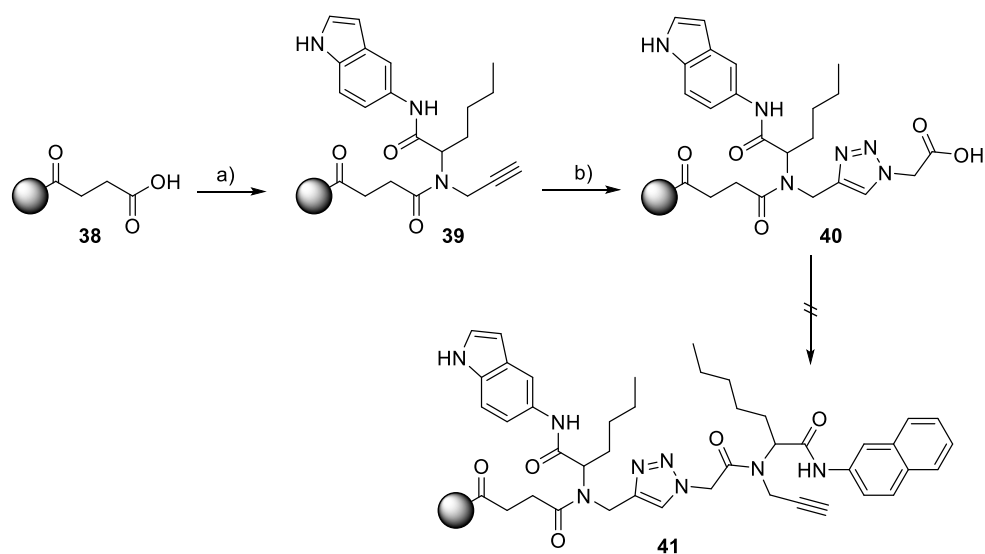
Under the same conditions as the first Ugi reaction (0.5 M reactants in GBL, imine preformation, 3 d, r.t.), no product was detected after the UV cleavage from the surface and LC-MS analysis. Also no side reaction occurred, since the chromatograms of cleaved products before and after the second Ugi reaction showed no difference. This indicates that the reactive sites on the surface are not accessible, probably because of bad solvent penetration and swelling of the polymer. However, other tested solvents such as DMSO, NMP and ethylene glycol did not change the outcome, also when 10% (v/v) methanol was added. In case of ethylene glycol, 0.1 M concentration of reactants was used due to limited solubility. The choice of solvents on DMA is generally limited by their vapor pressure and possibility to form stable droplets on the surface, but pure methanol was tested as solvent by immersion of the slide in the reaction mixture for 3 d. Again, no conversion was detected. Slightly warming the DMA to 40°C via heating plate during the reaction (with GBL as solvent) also yielded no product. Addition of 10% (v/v) of a 0.1 M aqueous solution of scandium(III) trifluoromethanesulfonate [Sc(OTf)₃] as catalyst to the reactants in GBL did not help with the reaction as well.^[67] GBL as solvent with 1% (v/v) Triton-X was also tested without success, while higher concentrations of the surfactant lowered the surface tension of the solvent to a critical point where droplet formation was negatively inflicted and merging occurred on the surface. Same results of the tested conditions were seen when the starting molecule was **A₇I₂-COOH** instead of **A₁I₂-COOH**, indicating that the tertiary amine

group of A_1 did not cause this issues.



Scheme 8. Second Ugi cycle, tested with $A_{1I_2}\text{-COOH}$ and $A_{7I_2}\text{-COOH}$ as starting molecules. Conversion to $A_{1I_2}\text{-}A_{2I_1}$ and $A_{7I_2}\text{-}A_{2I_1}$ was tested under several conditions which all yielded no product.

It was suspected that maybe the linkage between the first Ugi product and the carboxylic acid was causing the lack of reactivity via on-surface aggregation,^[156] so a different and more polar linkage was tested. Reducing the loading of the solid phase could be another possible solution, but this would drastically reduce the accessible concentration of the final product, especially after several iterative steps. The incorporated amine was therefore exchanged with propargylamine and 4-pentenal was exchanged with pentanal, offering an alkyne group in the resulting product (see Scheme 9).



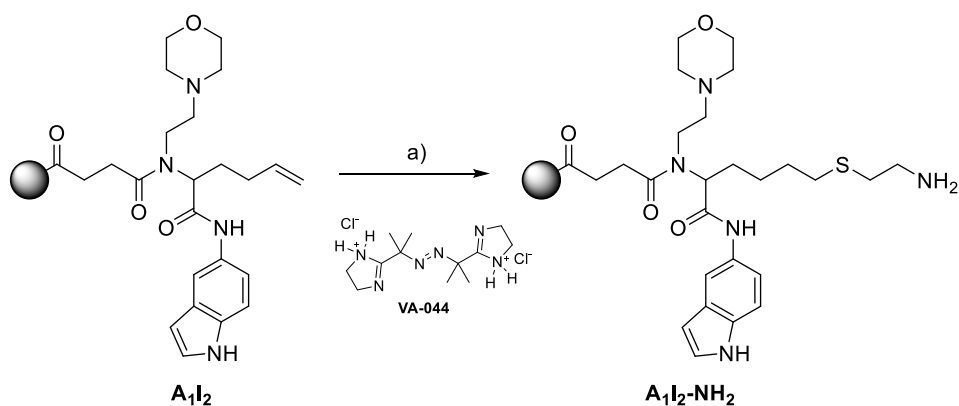
Scheme 9. Linkage to the new carboxylic acid was achieved via CuAAC reaction. Second Ugi reaction did not occur under several conditions. a) propargylamine, pentanal, 1-H-indol-5-yl isocyanide, GBL, 3 d, r.t. b) 2-azidoacetic acid, CuSO₄, sodium l-ascorbate, 18 h, r.t.

This Ugi reaction yielded **39** in 98% purity as detected via LC-MS (at 254 nm absorbance) after UV-induced cleavage. A copper catalysed azide-alkyne cycloaddition reaction (CuAAC) with 2-azido acetic acid was performed to introduce a carboxylic acid for the next Ugi reaction via a 1,2,3-triazole linkage. For this, 2.5 μ l of 0.5 M 2-azidoacetic acid in DMSO/water (1:1, v/v) were pipetted into each spot followed by 2.5 μ l of 0.05 M CuSO₄ and 0.25 M sodium l-ascorbate in DMSO/water (1:1, v/v). After the reaction time of 18 h, the slide was washed and 5 spots were used for analysis of the formed product via LC-MS after photorelease. The CuAAC reaction showed quantitative conversion to **40** with only traces of starting material present in the mass spectrum. The second Ugi reaction was then tested with propargylamine, hexanal and naphthyl isocyanide at concentrations of 0.5 M in GBL, DMSO or NMP. Each solvent had 3 variations with either no additives, 10% (v/v) of 0.1 M aqueous solution of Sc(OTf)₃ or 1% (v/v) Triton-X and was heated to 40°C. As no reaction occurred in all attempts and formation of **41** was not detectable, it was decided to exchange the carboxylic acid group to an amine group and therefore increasing the reactivity of the surface-bound material.

2.2.2.4 Thiol-Ene Reaction with Cysteaminium Chloride

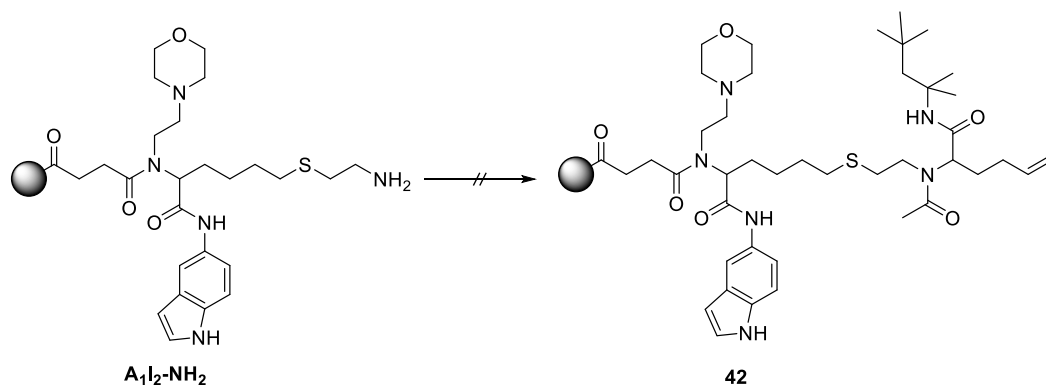
Cysteaminium chloride was chosen as reactant for the introduction of an amine group via thiol-ene addition, because it is the simplest combination of a thiol and amine and is already successfully employed in the production process of the DMA.

Since the addition 3-mercaptopropionic acid was carried out under solvent-free conditions with the liquid thiol, the procedure could not be transferred to the solid cysteaminium chloride. Therefore, a solution of 25% (w/w) cysteaminium chloride in water/ethanol (1:1, v/v) was used, where 1% (w/w) of the water-soluble thermal radical initiator VA-044 was added (see Scheme 10). After immersion of the DMA with surface-bound Ugi product **A₁I₂** in the mixture under nitrogen atmosphere, it was heated to 65°C for 18 h. Following to washing and photorelease, the conversion to **A₁I₂-NH₂** was measured as nearly quantitative with only traces of olefin detectable.



Scheme 10. Introduction of an amine group to the Ugi product **A₁I₂** to yield the product **A₁I₂-NH₂**. a) 25% (w/w) cysteaminium hydrochloride, 1% (w/w) VA-044, in water/ethanol (1:1, v/v) at 65°C for 18 h. The following Ugi reaction

was attempted according to the protocol described in chapter 2.2.1.2.4 with isocyanide **1a**, acetic acid and 4-pental to yield product **42** (see Scheme 11).



Scheme 11. Second Ugi cycle, tested with surface-bound **A₁I₂-NH₂** and 0.5 M solutions of **1a**, acetic acid and 4-pental. Conversion to **42** was attempted under several conditions which all yielded no product.

Similar conditions to the other attempts were tested. The variation of solvents included GBL, NMP, DMSO and methanol (via immersion) with 0.5 M concentration of the reactants in all cases. Each solvent was employed at room temperature and at 40°C during the usual reaction time of 3 days. Also the addition of scandium triflate or Triton-X in GBL (*vide supra*) was examined. Again, no reaction occurred with the surface-bound starting material under all these conditions, indicating again that the reaction sides are not accessible for a second Ugi cycle.

After testing three different linkages between the two desired Ugi products, each with 4 different solvents and two additives, no second Ugi reaction could be achieved and the project was canceled. HEMA-co-EDMA polymer was once chosen for the manufacturing of the DMA because of its physical and mechanical properties (stability, roughness) and not evaluated for its possible use as a solid phase for complex chemical reactions, especially while aiming for relatively large molecules. Even though the synthesis of oligomers could not be achieved, three new reactions were shown in this chapter to be compatible on the DMA: (1) Ugi-reaction starting with a carboxylic acid on the surface (2) thermally initiated radical alkene hydrothiolation (3) copper catalysed azide-alkyne cycloaddition reaction (CuAAC). Also the DMA was first used under nitrogen atmosphere and with elevated temperatures. As the use of the DMA for solid phase synthesis just started, every additional possible reaction is a new valuable tool for future projects, thus broadening its scope.

2.2.3 Pd-Catalysed Synthesis of Biphenyls and Screening for Estrogenic Activity

To improve the versatility of the DMA as a platform for synthesis, an influential reaction type needs to be added to its toolbox: Palladium-catalyzed cross-coupling reactions, and especially the palladium-catalyzed Suzuki-Miyaura reaction (SMR).^[75, 76] After being introduced in 1979, it rapidly took over medicinal chemistry and is now the most used reaction for C-C coupling^[157] and occurs in 20% of all production steps^[158]. Only one type of reaction is used even more in the production steps: the amide bond formation with an occurrence of 32%. One reason for the success of the SMR may be its great selectivity and tolerance against functional groups as well as the mild reaction conditions. It is easy to run in parallel and can be therefore expanded for a large set of analogues, if a compound showed activity in a primary screen and needs to be varied for further investigations.^[159] The resulting biphenyl structure of the SMR is a common motif in biologically active compounds and can be seen in many approved drugs such as losartan (**43**), flurbiprofen (**44**) or telmisartan (**45**, see Figure 30).^[160, 161, 162]

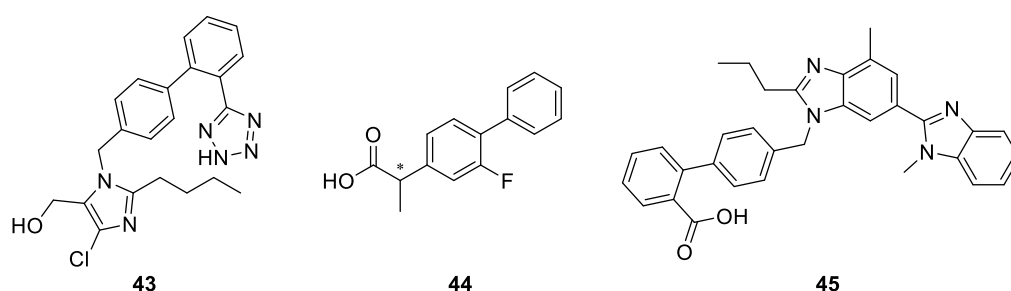


Figure 30. Structures of exemplary approved drugs containing the biphenyl motif: Losartan (**43**), flurbiprofen (**44**) and telmisartan (**45**).

A special case is the class of the hydroxylated biphenyls, which can act as nonsteroidal ligands for estrogen receptors.^[163, 164] Since this type of molecules can influence the growth and behavior of estrogen or androgen sensitive cancer cells, the ongoing discovery and research on such compounds is important. In this chapter, the droplet microarray platform will be utilized to synthesize in parallel an array of 800 carboxylic acid or amide containing biphenyls via the palladium catalyzed Suzuki-Miyaura reaction. Subsequently, the library will be screened for potential estrogenic effects on the same chip in a yeast estrogen screening (YES) assay. Figure 31 gives an overview of this approach.

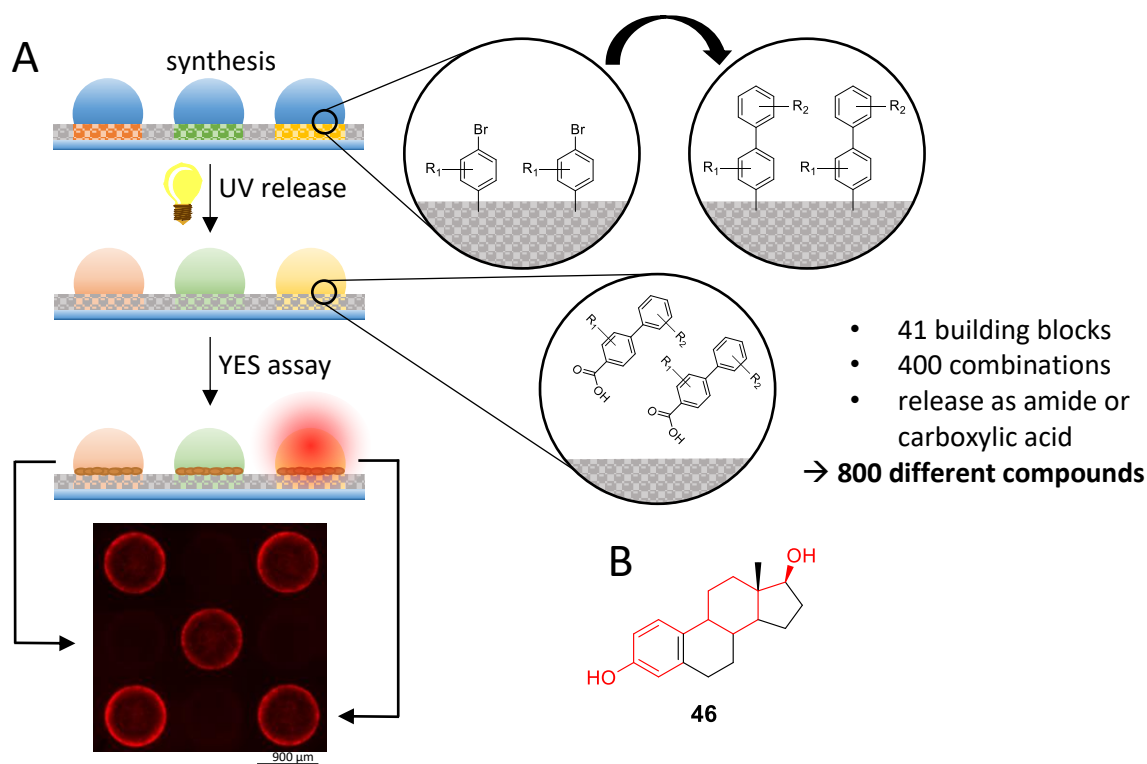


Figure 31. Schematic overview of the on-chip synthesis and screening approach on the droplet microarray (DMA). DMA consists of a porous polymer coating with a thickness of around 12 μm on a microscopic glass slide ($h = 1 \text{ mm}$) (A) Hydrophilic spots ($d = 900 \mu\text{m}$), surrounded by superhydrophobic borders, serve as microcompartments for the palladium-catalyzed solid phase synthesis of biphenyls via the Suzuki-Miyaura crosscoupling reaction. The use of a photocleavable linker allows for a controlled release of the products into distinct droplets via irradiation with UV-light. Catalyst and excess starting material can be washed off beforehand and fresh solvent is applied. Hormonal activity of the products is screened in a yeast based assay, which gives a fluorescent signal according to the estrogen potential of the compound. (B) Structure of 17β -estradiol (**46**).

2.2.3.1 Results and Discussion

In a preliminary experiment, just one combination of starting materials was tested. For this, 4-iodobenzoic acid was attached to HEPL in 3 mm round hydrophilic spots via Steglich esterification (0.1 M 4-iodobenzoic acid, 0.01 M 4-DMAP in NMP containing 5% (v/v) DIC, 18 h, r.t.). The following cross-coupling reaction was then performed by addition of 3 μl of a solution containing 80 mM palladium(II) acetate [$\text{Pd}(\text{OAc})_2$] and 3 μl of a 2 M phenyl boronic acid solution including 2 M triethylamine.^[165] Solvent for both solutions was 10% (v/v) water in NMP. A few minutes after mixing the solutions on-spot, the color of the reaction mixtures changed from brownish-reddish (coming from palladium(II) acetate) to black, indicating a formation of metallic palladium particles. After the reaction time of 18 h, the solutions were washed off with acetone and ethanol, which left precipitated palladium black on the surface (see Figure 32). Spots where only the catalyst was applied, did not show Pd black formation. Since this layer was blocking the UV light

from reaching the polymer and therefore totally inhibiting the cleavage of products from the surface, a suitable removal strategy had to be found.

The leaching of precious metals (such as palladium) from ores, electronic waste or old car catalysts is an interesting field in the recycling industry, so there is a lot of research conducted about it.^[166, 167, 168] 6 different washing solutions were applied at room temperature for 4 h with a volume of 5 μ l per spot: (1) 1 M CuSO_4 , 1 M NaCl in water (2) 1 M CuSO_4 , 1 M NH_4Cl in water (3) 3 M KSCN, 1 M CuSO_4 in 25% (w/w) aqueous ammonia (4) 2 M $\text{Na}_2\text{S}_2\text{O}_3$ + 2 M CuSO_4 in 25% (w/w) aqueous ammonia (5) 25% (w/w) aqueous ammonia (6) 0.1 M KCN in water/DMSO (1:1, v/v).

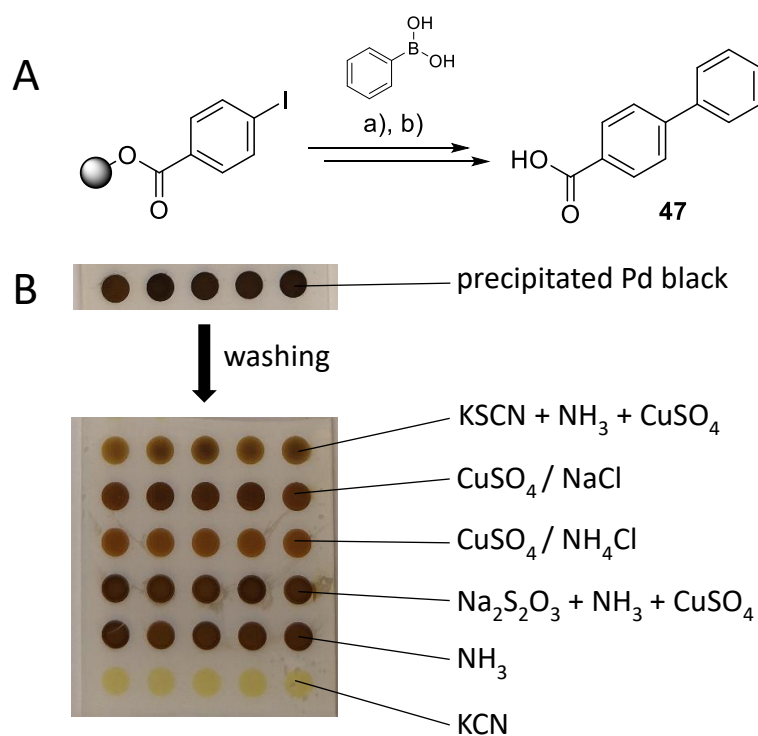


Figure 32. (A) Scheme of the first SMR reaction performed on the DMA. a) Et_3N , $\text{Pd}(\text{OAc})_2$, phenylboronic acid in $\text{NMP}/\text{H}_2\text{O}$ b) 365 nm, 2.5 mW/cm^2 , 20 minutes in H_2O (B) During the reaction, Pd-black precipitation occurs, leading to a total inhibition of UV-triggered release. Different washing solutions were applied at room temperature for 4 h, yielding KCN as the best performing. Diameter of the hydrophilic spots is 3 mm.

As it can be seen in Figure 32, solution (6) had the best effect on palladium removal from the surface and was used from there on as washing solution. For safety reasons, the KCN solutions and all washing solutions which came in contact with them were collected separately in a beaker with NaOH pellets and diluted 1:1 (v/v) with 30% (w/w) hydrogen peroxide solution for at least 24 h before being discarded to the aqueous waste. Also no acetone or isopropanol was used in the washing steps to avoid the formation of highly explosive acetone peroxide.

The removal of palladium by treatment with KCN solution was monitored via energy-dispersive X-ray spectroscopy (EDX) and inductively coupled plasma optical emission spectrometry (ICP-OES). EDX Measurements were performed by Volker Zibat at the Laboratory for Electron Microscopy at KIT and ICP-OES analysis was performed by Thomas Bergfeldt at the Institute of Applied Materials at KIT. Figure 33 shows the results of the EDX analysis of a hydrophilic spot. Measurements were carried out on a system containing of a “LEO 1530” REM by Zeiss (Jena, Germany) and a “NORAN System SIX” EDX by Thermo Electron GmbH (Karlsruhe, Germany). Samples were coated with 5 nm platinum on an EM ACE600 by Leica (Wetzlar, Germany) prior to the analysis.

Typical peaks of carbon, oxygen and sulphur are visible in both samples from the polymer backbone. While a strong peak from the palladium could be detected in the spectrum of the sample without the KCN wash, only traces of palladium were visible after the treatment, indicating a sufficient removal of palladium.

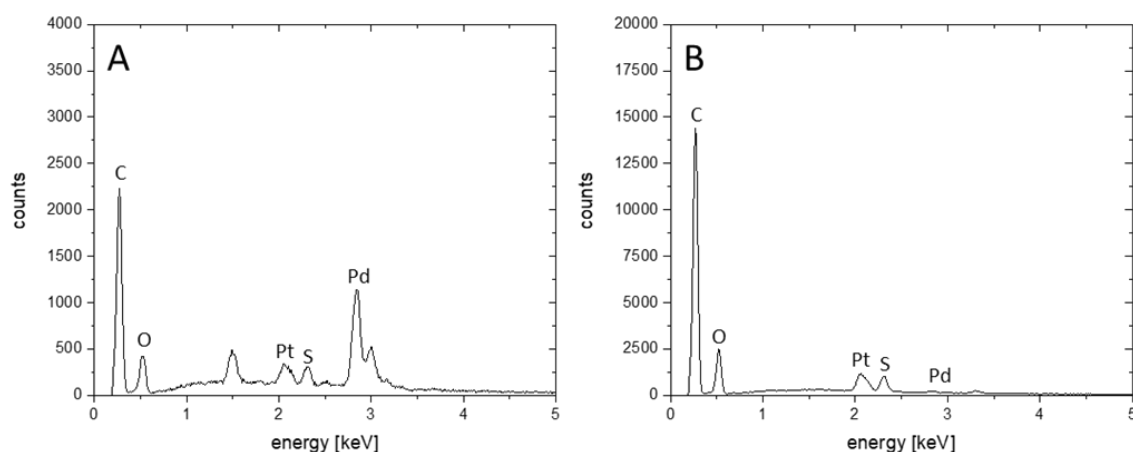


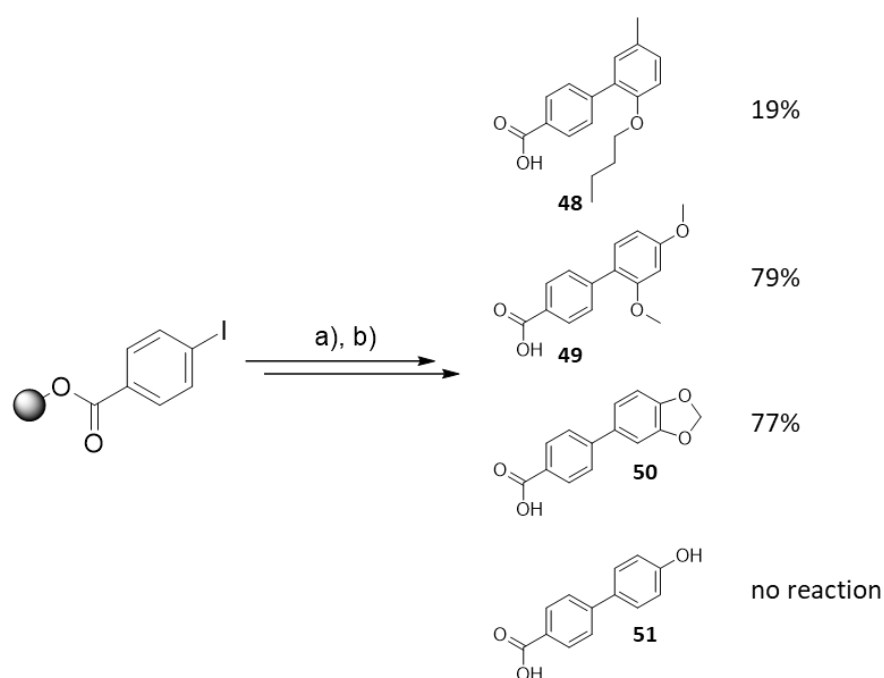
Figure 33. EDX spectra of a 3 mm round hydrophilic spot after the SMR before (A) and after (B) removal of the precipitated palladium via washing with a 0.1 M solution of KCN in DMSO/water (1:1, v/v). Signals representing carbon, oxygen and sulphur come from the polymer backbone, while platinum comes from the pretreatment of the sample.

As the UV-triggered release of the products from the surface was now possible, it was performed according to the standard protocol and analysed via LC-MS. The purity of **47** was detected as 92% (at 280 nm absorbance) with no detectable dehalogenated side product. The leftover sample after the photorelease was then handed to ICP-OES analysis to determine the palladium contamination. After correction with the dilution factor, the residual palladium content was 35 ppm. While the general goal for active pharmaceutical ingredients is a palladium level below 20 ppm, it highly depends on the performed assay if higher concentrations are problematic or not.^[159] For example, it is reported that cytotoxicity for mouse fibroblasts does not occur below 100 ppm of palladium,^[169] but 25 ppm can already give false positive results in an ELISA assay for Pad4 affinity.^[170] It should be noted that this assay seems to be very sensitive in

general, as it is even more influenced by zinc and iron ions. However, cell-based assays are supposed to be less sensitive to palladium contamination and it was decided that the palladium removal via KCN wash is sufficient for a primary screen.

In the next step, four more boronic acids were employed under the same conditions with 4-iodobenzoic acid on the surface: 2-butoxy-5-methylphenylboronic acid, 2,4-dimethoxyphenylboronic acid, 3,4-(methylenedioxy)phenylboronic acid and 4-hydroxyphenylboronic acid (see Scheme 12). After washing with KCN solution and photorelease, the outcome was analysed via LC-MS and is shown in Scheme 12. While **49** and **50** yielded purities of 79% and 77%, respectively, **48** only had a purity of 19%. For **51**, no product was detectable and the spectrum consisted solely of starting material. Impurities in the spectra almost exclusively came from the unreacted starting material and only one minor peak which could not assigned to a certain possible byproduct. As the minor impurity was the same in all 4 reactions, it's most probably coming from a reactant or solvent.

While purities of >70% would be acceptable for a high throughput primary screening, very low or no conversions to the product are a problem. Also structures containing a hydroxylated phenyl are suspected to have an estrogenic effect and are from great interest in this project. Additionally it was experienced that the liquid dispenser (Certus Flex by Gyger) was not able to handle 2 M concentrations of the reactants and clogged, most probably due to higher viscosity or precipitation. As the goal of this project was also the miniaturized synthesis and screening in 900 μm spots, the conditions for the on-chip SMR had to be improved to be suitable for liquid handling automation.



*Scheme 12. SMR on DMA with 4 different boronic acids, yielding products **48**, **49** and **50**. a) Et₃N, Pd(OAc)₂, boronic acid in NMP/H₂O b) 365 nm, 2.5 mW/cm², 20 minutes in H₂O. Percentages show detected purities of products at 280 nm absorbance in LC-MS analysis.*

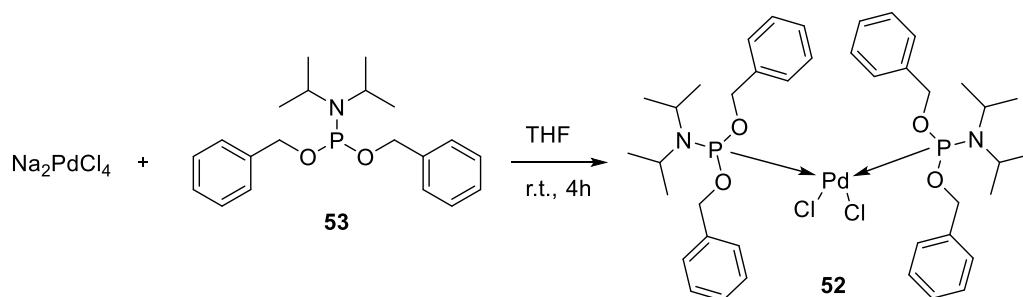
The reaction of 4-iodobenzoic acid and 4-hydroxyphenylboronic acid was chosen as model reaction and several conditions were tested (see Table 6). Generally, the boronic acid was used with a concentration of 0.5 M and the catalyst as 80 mM, both in NMP/H₂O (9:1, v/v). 3 μl of both solutions were pipetted in each 3 mm round spot.

Table 6. Overview of the tested reaction conditions for the SMR between surface-bound 4-iodobenzoic acid and 4-hydroxyphenylboronic acid.

| Base | Catalyst | Temp. | Product Formation |
|---------------------------------|---------------------------------|-------|-------------------|
| Et ₃ N | Pd(OAc) ₂ | r.t. | - |
| Et ₃ N | Pd(OAc) ₂ | 50°C | - |
| Na ₂ CO ₃ | Pd(OAc) ₂ | r.t. | traces |
| Et ₃ N | JohnPhos / Pd(OAc) ₂ | r.t. | - |
| Et ₃ N | JohnPhos / Pd(OAc) ₂ | 50°C | - |
| Na ₂ CO ₃ | JohnPhos / Pd(OAc) ₂ | r.t. | - |
| Na ₂ CO ₃ | JohnPhos / Pd(OAc) ₂ | 50°C | - |
| Et ₃ N | XPhos Pd G3 | r.t. | - |
| Na ₂ CO ₃ | XPhos Pd G3 | r.t. | - |
| Et ₃ N | Pd(dba) ₂ | r.t. | - |
| Na ₂ CO ₃ | CX-31 | r.t. | - |
| Et ₃ N | CX-31 | r.t. | - |
| Na ₂ CO ₃ | 52 | r.t. | 88% purity |
| Et ₃ N | 52 | r.t. | traces |

Since the first conditions with triethylamine and palladium acetate did work to some extent, they were used as starting point for further variations. Heating the reaction to 50°C during the reaction time of 18 h did not improve the outcome, same as the switch to sodium carbonate as base, which at least gave a weak mass signal of the desired product in the LC-MS analysis. As written in chapter 1.5.2, ligandless conditions are very limited in their use, so different ligands were employed. The most commonly used ligand P(Ph)₃ (triphenylphosphine) turned out to be not suitable, because it yielded a strong precipitation after addition of the palladium source, most probably because of its oxygen sensitivity. More sophisticated phosphine ligands such as JohnPhos and XPhos as well as N-heterocyclic carbene ligands such as CX-31 were tested with Et₃N and Na₂CO₃, but also yielded no product. Again, this may be caused by the ambient atmosphere in which the slides were handled. Even though the ligands are described as “air stable” during storage, the sensitivity against oxygen increases when they are complexed to palladium. This is also the reason why the SMR is classically conducted under inert atmosphere.

However, during literature research a new possible approach was found with the quite unknown catalyst **52**, which was said to be active at room temperature under ambient atmosphere.^[82] This catalyst was synthesized according to the literature from sodium tetrachloropalladate (Na_2PdCl_4) and dibenzyl-diisopropylphosphoramidite (**53**) in THF. After evaporation of solvent, the residue was redissolved in NMP to yield a 80 mM solution, which was employed in the model reaction, where it yielded a product purity of 88% with Na_2CO_3 as base at room temperature.



*Scheme 13. Synthesis of the catalyst **52** according to literature. After evaporation of THF, the yellow product was redissolved in NMP and used with a concentration of 80 mM.*

The new conditions for the SMR were then applied for a bigger library of starting materials. The 16 carboxylic acids (C_z) and 25 boronic acids (B_x) are presented in Table 7 and allowed for 400 different combinations. The use of both linkers **HEPL** and **FAPL** (see chapter 1.4) doubled the achievable number of compounds by releasing every combination of building blocks as carboxylic acid or amide, so the final possible library contained 800 products.

Table 7. Structures of the carboxylic acid aryl halide (C_x) and the boronic acid (B_x) entries

| Aryl Halide | H ₁ | H ₂ | H ₃ | H ₄ | X = | Boronic Acid | H ₁ | H ₂ | H ₃ | H ₄ |
|-----------------------|-----------------|----------------|----------------|----------------|---|-----------------------|---|---------------------------------------|---|-----------------|
| C₁ | H | H | Br | H | -(CH ₂) ₂ -(CO)- | B₁ | F | H | CH ₃ | H |
| C₂ | OMe | H | H | Br | -(CH ₂)- | B₂ | CH ₃ | H | OMe | H |
| C₃ | H | H | Br | H | -(CH ₂) ₃ - | B₃ | H | H | -(CO)-NH ₂ | H |
| C₄ | H | F | Br | H | -(CH ₂)- | B₄ | H | -(CH)-(CH ₃) ₂ | H | H |
| C₅ | F | H | H | Br | -(CH ₂)- | B₅ | H | OMe | H | OMe |
| C₆ | F | H | H | Br | - | B₆ | H | F | F | H |
| C₇ | H | H | Br | H | -(CH ₂)-O- | B₇ | H | H | -(CH ₂) ₂ -CH ₃ | H |
| C₈ | H | H | Br | H | -(CH ₂) ₂ - | B₈ | H | F | OMe | H |
| C₉ | H | Br | H | H | -(CH ₂) ₂ - | B₉ | H | Cl | H | F |
| C₁₀ | H | Br | H | H | -(CH ₂)- | B₁₀ | H | OH | H | H |
| C₁₁ | CF ₃ | H | Br | H | - | B₁₁ | H | OEt | H | H |
| C₁₂ | CH ₃ | H | H | Br | - | B₁₂ | H | H | O ⁱ Pr | H |
| C₁₃ | Cl | H | Br | H | -(CH ₂)- | B₁₃ | H | H | Cl | H |
| C₁₄ | OMe | H | Br | H | -(CH ₂)- | B₁₄ | H | H | CH ₃ | H |
| C₁₅ | H | H | Br | H | -(CH ₂)- | B₁₅ | H | CF ₃ | H | H |
| C₁₆ | H | H | I | H | - | B₁₆ | H | F | F | F |
| | | | | | | B₁₇ | H | H | -O-(CH ₂) ₂ -OMe | H |
| | | | | | | B₁₈ | H | H | H | H |
| | | | | | | B₁₉ | -O-(CH ₂) ₃ -CH ₃ | H | H | CH ₃ |
| | | | | | | B₂₀ | OMe | H | OMe | H |
| | | | | | | B₂₁ | H | ---O---(CH ₂)---O--- | | H |
| | | | | | | B₂₂ | H | H | CF ₃ | H |
| | | | | | | B₂₃ | H | H | OH | H |

B₂₄

B₂₅

Several combinations of the building blocks were tested with the new catalyst and base combination. First, the hydrophilic spots (3 mm, round) were treated with 5 μ l linker coupling solution per spot for 18 h. The linker coupling solution contained 0.1 M photolinker (**HEPL** or **FAPL**) and 0.1 M 1-hydroxybenzotria-

zole (HOBT) in N-methyl-2-pyrrolidone (NMP) and was freshly mixed with 5% (v/v) diisopropylcarbodiimide (DIC) before dispensing. By the end of the coupling, the DMA was rinsed with ethanol and acetone and dried in air flow. The Fmoc amine photolinker was then deprotected with 5 μ l of 20% (v/v) piperidine in NMP for 4 h and washed again. Subsequently, the aromatic halides (containing a carboxylic acid) were coupled to the linker by adding in each spot 5 μ l of a solution containing 0.1 M of the carboxylic acid, 0.01 M 4-(dimethylamino)pyridine (4-DMAP) and 5% (v/v) DIC in NMP and let react for 18 h. Washing and drying was carried out in the way described above. Volumes for the later used 900 μ m spot sizes were 150 nl in all steps.

The now attached aryl halides were employed in the SMR. In every 3 mm round spot, 3 μ l of a 80 mM solution of **52** in NMP were pipetted and incubated for 15 minutes at room temperature (30 nl for 900 μ m pattern).^[82] Subsequently, 3 μ l of a solution containing 0.5 M boronic acid derivate in NMP and 2 μ l of saturated Na₂CO₃ solution were added and the DMA was incubated in the dark at room temperature for 18 h (100 nl and 30 nl for 900 μ m pattern). The reactions were ended by washing off the mixtures with acetone and ethanol prior to immersion of the whole slide in a 0.1 M solution of KCN in DMSO/water (1:1) for 3 remove the precipitated palladium. Only water and ethanol were used for the final washing step. The waste was collected separately and treated with hydrogen peroxide and sodium hydroxide.

To monitor the synthetic success and purity of the products, 25 reactions were performed on 3 mm spots with different linkers and analyzed via LC-MS. Purity was calculated as the proportion of the product's peak integral from the summarized peaks integrals at 280 nm absorbance and is presented in Table 8. Since the starting materials absorb UV light as well and can therefore be seen in the chromatograms, the purity value also contains information about the reaction yield. There was no tested combination of starting materials that didn't lead to the desired product under these conditions.

Table 8. Purity of exemplary compounds synthesized in 3 mm spots to monitor synthetic success via LC-MS analysis. Product was identified via mass detector, while purity was calculated as the proportion of the product's peak integral from the summarized peaks integrals at 280 nm absorbance.

| Product | Entry C | Entry B | Linker | Purity | Product | Entry A | Entry B | Linker | Purity |
|---------|-----------------|-----------------|--------|--------|---------|-----------------|-----------------|--------|--------|
| 54 | C ₁₅ | B ₁₉ | HEPL | 90% | 67 | C ₁₆ | B ₂₃ | FAPL | 79% |
| 55 | C ₁₅ | B ₂₀ | HEPL | 87% | 68 | C ₁₅ | B ₂₃ | FAPL | 87% |
| 56 | C ₁₅ | B ₂₁ | HEPL | 91% | 69 | C ₆ | B ₂₃ | FAPL | 55% |
| 57 | C ₆ | B ₂₃ | HEPL | 87% | 70 | C ₇ | B ₂₃ | FAPL | 65% |
| 58 | C ₁₅ | B ₂₃ | HEPL | 97% | 71 | C ₁₆ | B ₂₁ | FAPL | 76% |
| 59 | C ₁₆ | B ₁₈ | HEPL | 95% | 72 | C ₁₅ | B ₂₁ | FAPL | 94% |
| 60 | C ₉ | B ₁₆ | HEPL | 89% | 73 | C ₆ | B ₂₁ | FAPL | 79% |
| 61 | C ₉ | B ₇ | HEPL | 84% | 74 | C ₇ | B ₂₁ | FAPL | 86% |
| 62 | C ₁₅ | B ₁₆ | HEPL | 88% | 75 | C ₁₆ | B ₂₂ | FAPL | 78% |
| 63 | C ₁₅ | B ₇ | HEPL | 85% | 76 | C ₁₅ | B ₂₂ | FAPL | 89% |
| 64 | C ₉ | B ₁₄ | HEPL | 90% | 77 | C ₆ | B ₂₂ | FAPL | 66% |
| 65 | C ₃ | B ₁₄ | HEPL | 88% | 78 | C ₇ | B ₂₂ | FAPL | 84% |
| 66 | C ₁₆ | B ₂₃ | HEPL | 88% | | | | | |

2.2.3.2 YES-Assay

The goal of this project was to screen the newly synthesized biphenyls for their activity against the human estrogen receptor hER α . For this, the yeast estrogen screening (YES) assay was chosen, which is based on the recombinant yeast strain *Arxula adenivorans* (purchased from new_diagnostics GmbH, Berlin, Germany). Genes for the hER α receptor, dsRED and regulators were integrated into its genome, which yields a detectable fluorescence when an estrogenic active compound is present. The intensity of the fluorescence signal correlates with the concentration and affinity of the compound to the hER α receptor and is sometimes compared to a calibration curve made with 17 β -estradiol to quantify the effect. Therefore, the results of the assay can be given in estradiol-equivalents. Since the calibration curve needs to be done in parallel to every experiment, it can serve as internal positive control. Using a yeast based assay has several advantages: While the yeast strain can be continuously cultured to support a constant demand, it can also be purchased in a lyophilized state where it can be stored and quickly reconstituted when needed. In the latter case, no sterile conditions are needed, so its handling is very convenient. Another advantage is the robustness of the assay. It is commonly employed to determine the content of endocrine activity in various samples and is stable against complex matrices or certain amounts of organic solvents. For example,

the planar YES assay can be performed on a developed TLC plate to investigate hormonal activity of separated compounds coming from wastewater, soil or lotion extracts.^[171, 172]

In a preliminary experiment, the applicability of the YES-assay on the droplet microarray was tested with 17 β -estradiol (E₂) as positive control in concentrations of 100, 50, 25, 10, 5, 2.5 and 1.25 $\mu\text{g/L}$. For this, E₂ was dissolved in ethanol to a concentration of 1 mg/L and diluted with water. As a negative sample, deionized water was used. 4 blocks with each 3 repetitions of the calibration curve and a checkerboard pattern (using the 100 $\mu\text{g/L}$ positive control and water) were printed (see Figure 34).

The yeast was purchased lyophilized and had to be reconstituted with the included medium prior to use. In every 900 μm round spot, 100 nl sample and 50 nl of yeast suspension were dispensed by a Certus Flex (Fritz Gyger, Gwatt, Switzerland) and the slide was put on a wetted piece of tissue in a sealed petri dish and incubated for 48 h at 37°C. The detected signals of dsRED in fluorescence microscopy (BZ-X800 by Keyence, Osaka, Japan) were analysed via ImageJ-Software and the “Array Analyser” plug-in. Results are shown in Figure 34.

While the average background signal of spots containing yeast and deionized water was 19505 AU (\pm 2065), the lowest concentration of E₂ with 1.25 $\mu\text{g/L}$ (4.59 nM) had an intensity of 23401 AU (\pm 3490) and was therefore only slightly higher than the background signal. Spots with 2.5 $\mu\text{g/L}$ (9.18 nM) sample concentration were already clearly above (33163 AU \pm 9064) this level.

Remarkably, the average fluorescence of spots with the highest sample concentration (100 $\mu\text{g/L}$) didn't differ significantly from the second highest concentration (277257 AU \pm 42877 and 268628 AU \pm 37576). This is most probably caused by the high concentration of ethanol in this sample (10%, v/v), leading to cell death or diminished metabolic activity. Figure 34 shows the top half of the slide, so the two topmost blocks are very close to the edge. The whole area of experiments was surrounded by one row of spots filled with pure medium to avoid edge effects, but since ethanol is very volatile, it would have been possible to evaporate faster from the outer spots than from the inner spots. With a rapid decreasing concentration of ethanol on this two outer blocks, the yeast was less impaired and could develop a stronger fluorescence signal as compared to the spots which are located more in the center of the DMA. The Z-factor was calculated with the signals from all the highest concentrations (100 $\mu\text{g/L}$) as positive control and yielded 0.58, indicating the assay is “excellent” with a satisfyingly broad signal range.^[173]

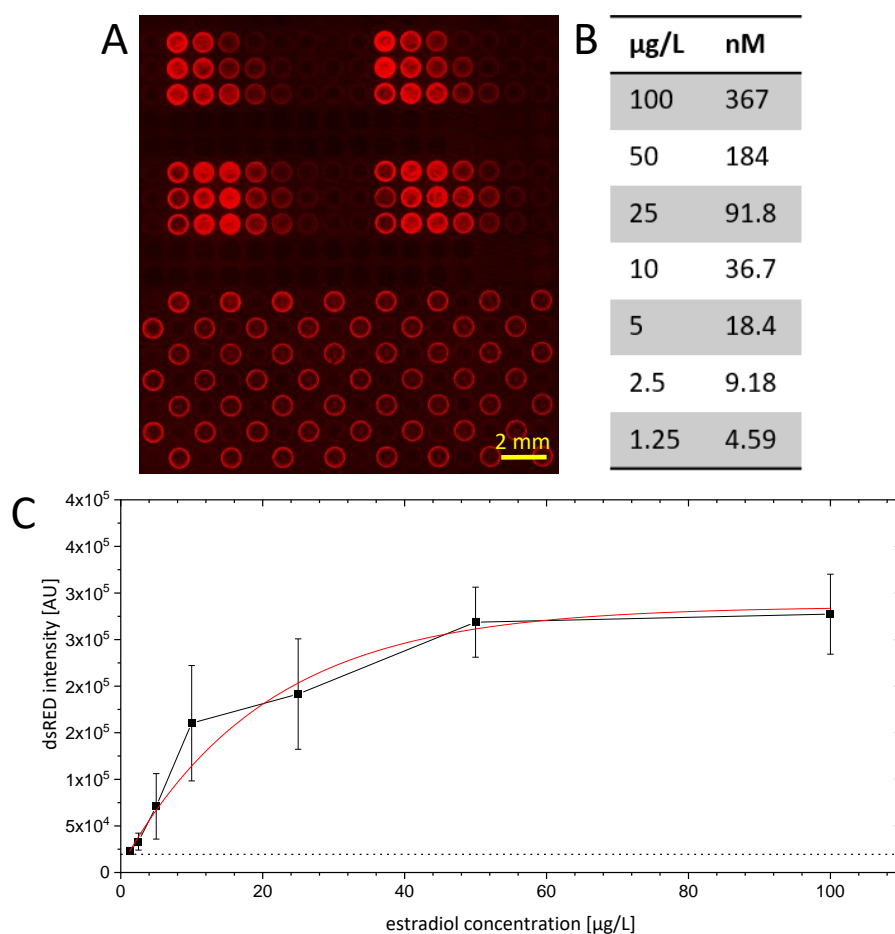


Figure 34. Preliminary test of the YES-assay on DMA with 17β -estradiol as positive control. $100\ \mu\text{l}$ of sample and $50\ \mu\text{l}$ of yeast suspension were dispensed in every spot and incubated for 48 h at 37°C . (A) Fluorescence microscopy picture of the DMA featuring $900\ \mu\text{m}$ round spots. 4 blocks with each 3 repetitions of a calibration curve and a checkerboard pattern are visible. (B) Concentrations of the positive controls. (C) Detected fluorescence intensity and standard deviation of all calibration spots plotted against the sample concentration of 17β -estradiol. Red line shows an exponential fit. Black dotted line represents the average of all background spots with deionized water as sample.

The used DMA pattern for the library synthesis offers round hydrophilic spots in the size of $900\ \mu\text{m}$ and a center-to-center distance of $1125\ \mu\text{m}$. With $18 \times 64 = 1152$ spots and the size of a standardized microscopic glass slide ($7.6\ \text{cm} \times 2.6\ \text{cm} = 19.8\ \text{cm}^2$) it achieves a density of $58\ \text{spots/cm}^2$ with a volume of $150\ \text{nl}$ each. This allows for an over four times higher throughput and thirty times less sample volume as compared to a 1536-well plate ($14\ \text{wells/cm}^2$, $5\ \mu\text{l}$ per well). The experimental design on the DMA was planned to screen 800 different compounds per slide and have a positive control and a negative control for each background. To avoid edge effects, the outmost spots were not used for experiments and were filled with deionized water. The design of the slide can be seen in Figure 35A. Aryl halide building blocks containing a carboxylic acid (**C_x**) were attached row-wise to the photolinkers and the boronic acids (**B_x**) were added column-wise to obtain all possible combinations in an array. Also every building block **C_x** was screened

without being modified by the reaction. After washing off the reaction mixture and removal of precipitated palladium via KCN solution, the DMA was irradiated with UV light (365 nm, 2.5 mW/cm², 20 min) and the spots were filled with the yeast suspension. 17 β -Estradiol solution with a concentration of 50 μ g/L was used as a positive control and dispensed multiple times. Deionized water was used as negative control. After an incubation time of 48 h at 37 °C, the dsRED signal was read out in a fluorescence microscope. As it can be seen in Figure 35B, only the positive control gave a fluorescent signal, indicating that the yeast was generally active but none of the synthesized compounds showed activity in this assay.

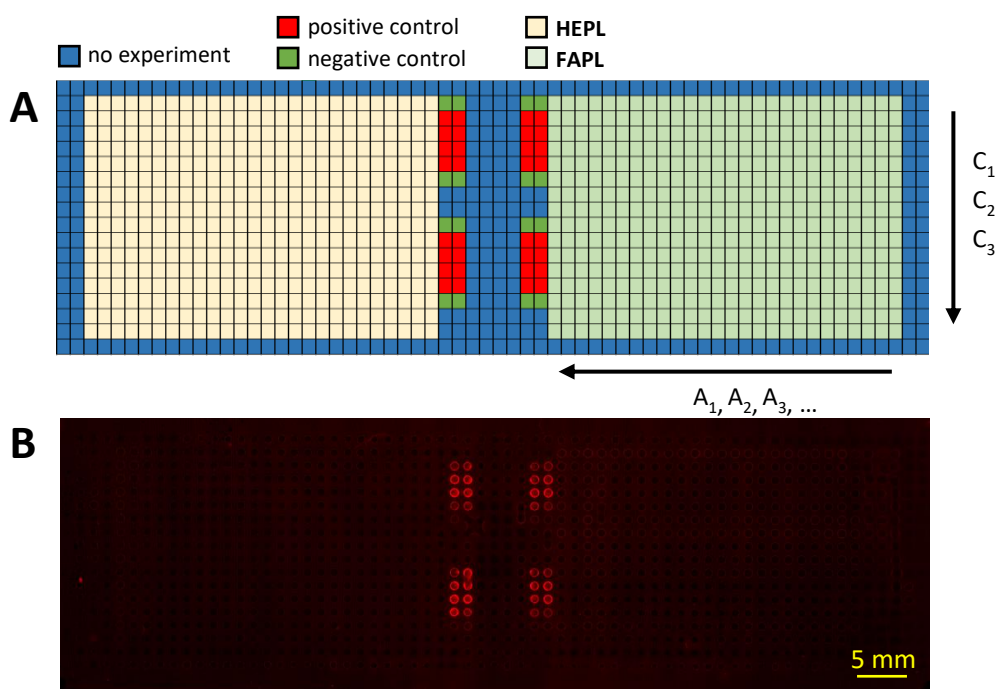


Figure 35. (A) Experimental design of the DMA for the library synthesis on 900 μ m spots. The 16 x 25 = 400 compound library was released once as carboxylic acid (from HEPL) and once as carboxamide (from FAPL), leading to 800 different compounds. (B) Fluorescent microscopy image of the YES assay with no found active compounds.

Besides the possibility that indeed not a single one of the 800 synthesized compounds has an estrogenic effect, they may have been not available at all for the yeast cells, e.g. because of a failed synthesis. While the success of this type of reaction was already demonstrated on larger spots (3 mm), it was not monitored yet on the smaller patterns. To overcome this, the whole library needs to be analyzed on-chip by MALDI-ToF as the next step in the future.

2.2.3.3 MALDI-ToF from Conductive Droplet Microarrays

Copying the droplet array onto a MALDI compatible surface via sandwiching was presented in chapter 2.2.1.2.5, but this process is laborious, time-consuming and needs special equipment, such as the sandwiching device shown in Figure 27. To remove this intermediate step, the whole DMA formation and compound synthesis should already be performed on a suitable conductive surface.

For this, the manufacturing protocol of the glass-supported DMA had to be adapted for ITO-coated glass slides. In contrast to glass, the activation of ITO could not be conducted with aqueous solutions of hydrochloric acid and sodium hydroxide, since ITO is sensitive to acids. The slides were instead immersed in 3 M KOH in methanol for 4 h to increase the amount of free hydroxyl groups on the surface.^[174] After washing with deionized water, they were immersed in 2% (v/v) 3-(trimethoxysilyl)propyl methacrylate in toluene for 18 h at room temperature and washed with acetone prior of curing the silane layer at 80 °C for 24 h. Polymerization of HEMA-co-EDMA onto this substrate, esterification with 4-pentynoic acid and photolithographic patterning with cysteaminium chloride and PFDT was then conducted according to the protocol for the standard glass-supported slides. This yielded a droplet microarray on a conductive surface (cDMA). If two hydrophilic spots (900 μm, round) in the distance of 2 cm were filled with water, the conductivity between them was detected with a continuity tester of a common multimeter by bringing each tip in contact with one droplet. This effect was not detectable on DMA produced on glass surface, even when the two droplets were closer together.

In a preliminary experiment for MALDI-ToF analysis, doxorubicin was used as reference substance and applied via automated liquid dispensing onto the DMA as a solution of 10 mg/ml (17.2 mM) in 10% (v/v) acetonitrile in water. 75 nl of this sample solution were printed in every spot of the cDMA, followed by 75 nl matrix mixture, consisting of a saturated solution of α-cyano-4-hydroxycinnamic acid (CHCA) and 2,5-dihydroxybenzoic acid (DHB) in 10% (v/v) acetonitrile in water (containing 0.1% TFA, v/v).^[135] After drying in vacuum, the slide was handed to Sergiy Afonin from the Department of Molecular Biophysics (IBG-2, KIT) for MALDI-ToF analysis. As it can be seen in Figure 36, the corresponding mass of doxorubicin was clearly detected as sodium adduct ($[M+Na^+]$, calculated: 566.16 m/z, detected: 566.07 m/z), indicating the suitability of the cDMA for MALDI-ToF analysis.

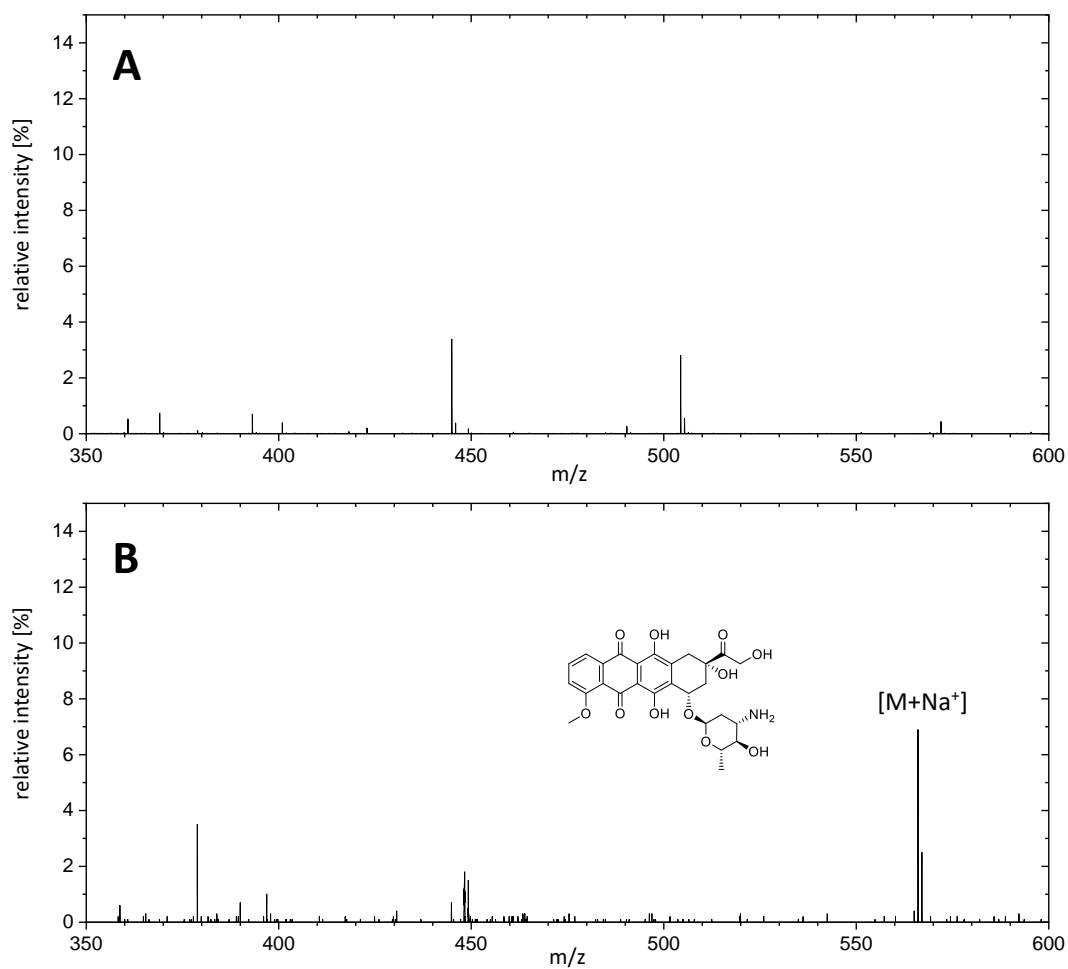


Figure 36. Mass spectrum of matrix background (A) and doxorubicin (B), obtained by MALDI-ToF from a 900 μm sized hydrophilic spot from a conductive droplet microarray (cDMA). Doxorubicin solution was mixed with matrix solution (CHCA/DHB) on-chip and dried in vacuum. Mass signal corresponds to the sodium adduct ($[M+Na^+]$, calculated: 566.16 m/z, detected: 566.07 m/z).

2.2.4 Conclusion

Integration of both synthesis and screening of compound libraries to a miniaturized platform allows for a straightforward hyphenation of biology and chemistry with a drastically decreased consumption of reagents, solvents and biomaterial.

The droplet microarray, which is based on hydrophilic spots on a superhydrophobic background, was already employed in miniaturized high-throughput biological experiments, but was lacking the possibility to be combined with parallel chemical synthesis. In this chapter, the nanoporous HEMA-*co*-EDMA coating of the DMA was utilized as anchor point for solid phase synthesis with every hydrophilic spot serving as a microvessel which held the reaction solutions in place without merging or cross contamination. Starting materials were attached to the solid phase via a UV-cleavable linker and used for various reactions, such as the Ugi reaction (chapter 2.2.1.2.4 and 2.2.2), which led to a 588-compound library. A model system with CHO-K1 cells and chlorambucil demonstrated that the cells in the hydrophilic spots were only affected by the linker-bound drug when UV-light triggered the release, while the drug had no effect without this trigger. Via control of UV-irradiation, the released concentration could be controlled spatially and quantitatively.

Next, several synthetic challenges were investigated: The attempted synthesis of sequence-defined oligomers via cycles of Ugi and thiol-ene reactions turned out to be not possible on the DMA under the tested conditions, most probably because of not accessible reactive sides on the surface. However, thermally induced hydrothiolation of alkenes and a copper catalysed azide-alkyne cycloaddition reaction was proven to work on the platform.

Utilization of the DMA for palladium-catalysed cross coupling reactions was successfully demonstrated by the synthesis of an 800-compound library of biphenyls via the Suzuki-Miyaura reaction. Furthermore, this library was then screened for estrogenic effects in a yeast based assay on the same chip. The construction of a conductive droplet microarray on an ITO slide demonstrated on-chip MALDI-ToF analysis for future analysis of the products.

Summarized, this chapter established the use of droplet microarrays for miniaturized and parallel solid phase synthesis with subsequent on-chip screening of the resulting compound libraries. Selective reactions were demonstrated, a yeast based assay was conducted and the whole platform was improved to be compatible with on-chip MALDI-ToF analysis.

3 Summary

Superhydrophobic surfaces are not just theoretically interesting, but can also be applied to solve complex problems such as miniaturization and parallelization of chemistry and biological experiments. After giving an introduction about the relevant theoretical background in chapter 1, this thesis presents a new and simple method for the reversible switching of surface wettability in chapter 2.1. An inherently hydrophilic nanoporous HEMA-co-EDMA polymer coating on a glass slide was treated with a fluorinated trichloroalkylsilane, which lowered the surface energy to turn the surface superhydrophobic due to the drastic change in surface chemistry. Despite of the high stability of such silane modifications, the previous hydrophilic state could be restored by treatment with fluoride anions in the form of tetrabutylammonium fluoride (TBAF). Both silanization and desilanization could be performed in less than 2 minutes and over several cycles, showing full reversibility, which was proven via WCA, ToF-SIMS and AFM analysis. This method was also employed for other silanes such as trichlorododecylsilane and trimethylchlorosilane, as well as for a smooth surface of a silicon wafer. In the latter case, the desilanization process was not as fast as compared to the polymer coating (as determined via WCA analysis), most probably due to the lower accessibility of the reaction sites on the smooth surface. When the desilanization solution was applied via automated liquid dispenser or a brush, hydrophilic-hydrophobic patterns could be created on the surface. Such dispensed patterns can be used, for example, to create arrays of microliter- or nanoliter-sized droplets.

Similar droplet microarrays constructed on porous HEMA-co-EDMA coatings and patterned via photolithography were already introduced for miniaturized biological screenings in our research group, but their use for chemistry was not fully explored. In chapter 2.2, such microarrays were investigated as substrates for solid phase synthesis of compound libraries in the low nanomolar range with the possibility to screen them on the same chip in a biological assay. A UV-cleavable linker was utilized for attachment of starting materials and controlled release of products without addition of contaminating cleaving agents. First, chlorambucil was employed as model compound and attached to the polymer surface via a photocleavable linker inside the 3 mm round hydrophilic spots, surrounded by superhydrophobic borders consisting of fluorinated porous polymer. Via different times of UV irradiation, concentration of the compound could be varied in the 5 μ l water droplet until it reached its maximum of 954 μ M after 15 minutes.

Using the same model compound, selectivity and biocompatibility of the cleavage conditions were investigated in chapter 2.2.1.2.3 with CHO-K1 cells as model organism. The chlorambucil-sensitive cell line was cultured on hydrophilic spots which were modified with linker-bound chlorambucil and half of the spots were irradiated with UV light at 365 nm for 15 minutes. Only on the irradiated spots, the chlorambucil

was released and induced apoptosis of the cells. Without irradiation, the cell viability remained on the same high level as for the control samples (no model drug, irradiated and non-irradiated). This demonstrates the selective and controlled release of the linker-bound compound by UV-irradiation, which does not diminish the viability of the cells.

To show the possibility of downsizing, a 588-compound library was synthesized on 1 mm spots by the Ugi reaction in chapter 2.2.1.2.4, after exemplary compounds were synthesized in larger spots (3 mm) to analyze the reaction outcome via LC-MS. It was shown that copying the small droplets of the microarray onto a conductive surface via sandwiching allowed for MALDI-ToF analysis of the products. This demonstrated for the first time the use of droplet microarrays for miniaturized compound synthesis on solid phase with a subsequent release of the products for analysis or screening.

During several attempts to synthesize a library of sequence-defined oligomers on the DMA via alternating Ugi and thiol-ene reactions in chapter 2.2.2, no product from the second Ugi cycle was detected. However, attachment of succinic acid to the linker as starting material increased the purities of the first Ugi products, compared to the amine-approach in the chapter before. Combination of 13 starting materials yielded 40 different products, which all were analyzed via LC-MS and offered a terminal alkene group. While the subsequent addition of 3-mercaptopropionic acid was successful, no second Ugi reaction was possible under various conditions. A different linkage to the new carboxylic acid functionality was tested by incorporating an alkyne via propargylamine, followed by copper catalyzed addition of 2-azidoacetic acid. Both reactions performed successfully, but no second Ugi reaction took place. In a last attempt, cysteamine was added to the terminal alkene to offer a different functionality on the surface, but also yielded no detectable product formation.

Even though the attempted library of oligomers was not achieved, two new reaction types were proven to work on the DMA: Thermally initiated hydrothiolation of alkenes and the copper catalysed azide-alkyne cycloaddition reaction (CuAAC). This shows the possibility to “click” building blocks together for future syntheses of compound libraries.

In chapter 2.2.3, an additional metal-catalysed reaction was demonstrated for library synthesis on droplet microarrays: An 800-compound library of biphenyls was synthesized via the palladium-catalysed Suzuki-Miyaura reaction and screened on-chip for estrogenic activity in a yeast-based assay. Several catalysts were screened to find the best performing under ambient atmosphere on DMA, before 41 building blocks (16 aryl bromides, 25 aryl boronic acids) were combined to 400 different combinations in sub-nanomolar amounts. Usage of two different UV-cleavable linkers allowed to double the library size by releasing every compound as either carboxylic acid or carboxamide. A suitable removal strategy for precipitated palladium after the synthesis was found and analysis of residual palladium was conducted via energy-dispersive X-ray spectroscopy (EDX) and inductively coupled plasma optical emission spectrometry (ICP-OES).

The full library was screened in a yeast-based cellular assay, but none of the synthesized compound showed activity on the estrogen receptor, which may be caused by failed synthesis, insufficient uptake into the cells or an actual lack of bioactivity. While the latter two can be addressed in the future via target-based screening approaches, investigation of synthetic success via mass spectrometry needed an adaptation of the DMA platform to be compatible with such techniques. By constructing the DMA onto an ITO slide instead of glass, the platform was rendered conductive and suitable for future on-chip MALDI-ToF analysis of the reaction products.

Summarized, this work presents new ways of controlling surface wettability and introduced the polymer-based droplet microarray as suitable substrate for solid phase synthesis of miniaturized compound libraries, followed by their on-chip screening.

4 Outlook

While many methods and strategies are presented in this thesis, it was impossible to cover the whole scope, so future research needs to be conducted:

More research needs to be done on the synthesis of compound libraries with consecutive on-chip analysis of products and their purification. While mass spectrometry only gives a qualitative information, methods for on-chip quantification of products must be found, ideally without even releasing the compounds from the porous surface. Currently, every compound library has to be synthesized twice: Once for analysis of products and once for the biological screening. This is a common drawback in miniaturized high-throughput approaches, since the analysed batch never gets screened and the screened batch was never analysed. Non-destructive analytical techniques such as NMR, IR, Raman or UV/VIS spectroscopy might solve this issue and should be in focus. On the other hand, the increase of throughput combined with the significant miniaturization of the synthesis, analysis and application, is a completely new concept, which cannot be directly compared to the traditional one-by-one synthesis, purification and biological experiment. With the increase in throughput, not all analytical methods become compatible, since the analysis time per sample becomes more relevant and might be even further increased by a minute amount of analyte.

Also, strategies for high throughput and parallel purification of crude products have to be developed to improve the purity of the obtained compound library. The solid phase synthesis approach already allowed us to wash off excess reagents and some side products, but could not remove all impurities. Ideally, several purification methods are available in the future to choose the most suitable one for every single reaction or library synthesis. For example, extraction of side products may be possible by either immersion of the whole DMA in a suitable solvent or sandwiching with a second DMA containing the solvent in the spots.

Also a deeper understanding about the behaviour of the polymer coating should be gained, such as the swelling properties by different solvents, variation of crosslinkage, distribution and accessibility of functional groups or the chemical stability against all possible reaction conditions. During this, alternative coatings could be introduced and compared in their physical and chemical properties. The toolbox of chemists, consisting of chemical reactions, purification strategies and analytical methods, needs to grow further and further.

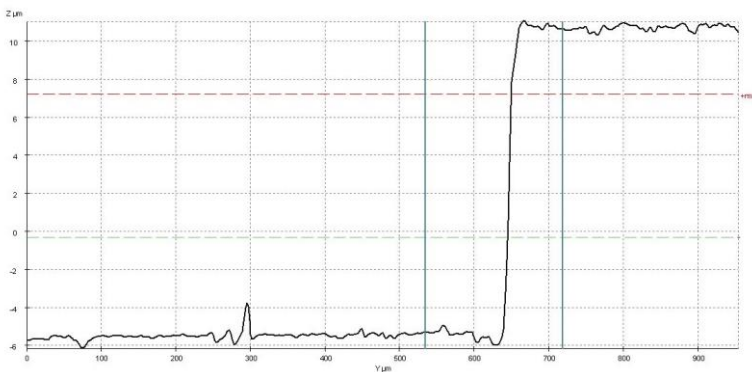
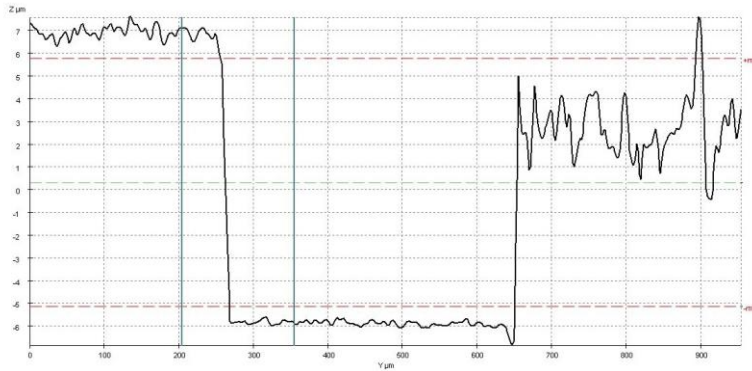
In this thesis, first steps were made into a new direction of miniaturized solid phase synthesis for high throughput screenings. With further research and development, it might help and inspire many other scientists in the field of drug discovery.

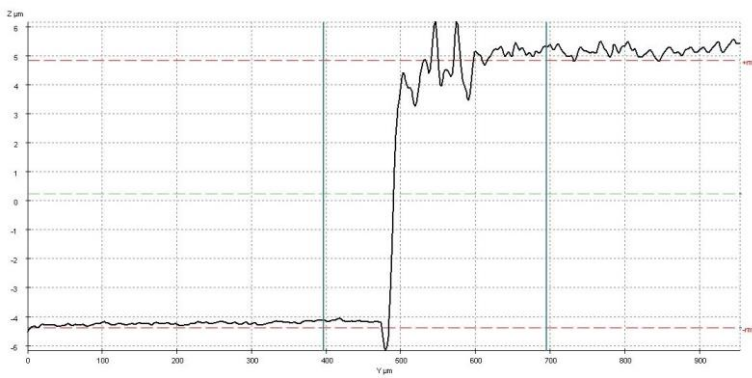
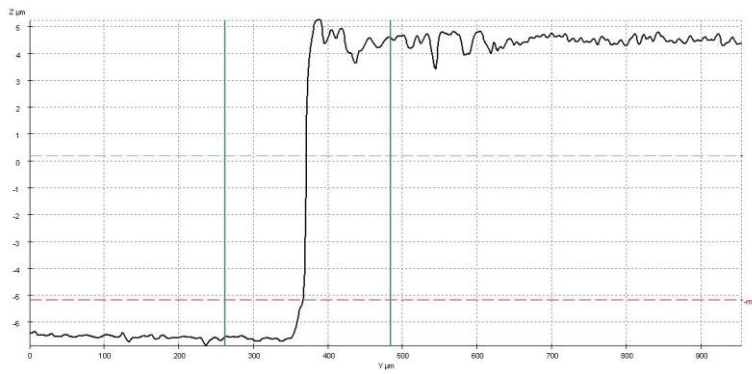
5 Appendix

5.1 Spectra

5.1.1 Thickness of Polymer Coating via Optical Profilometry

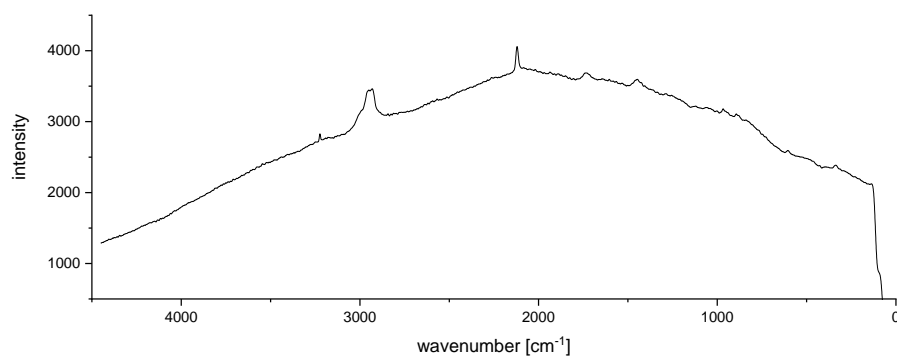
Four slides were manufactured according to the standard protocol and scratched with a spatula to spatially remove the polymer layer. The edges of the polymer were then analyzed via optical profilometry by Paul Schreiber from Institute of Applied Materials at KIT on a ContourX-500 by Bruker (Ettlingen, Germany). Pictures below are screenshots from the analysis software and show the profile of the parts with scratched off polymer.



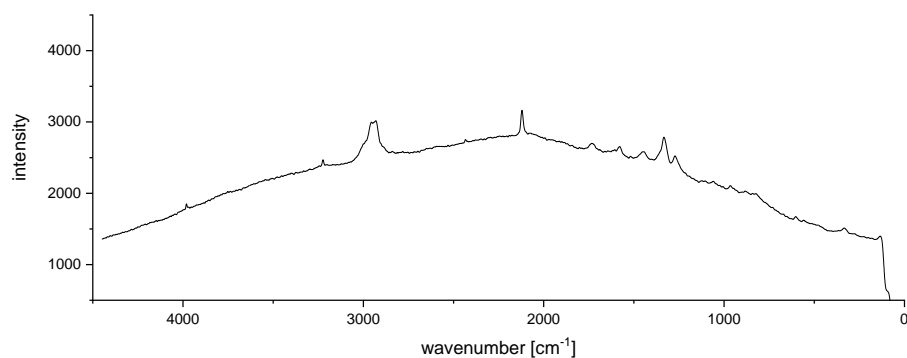


5.1.2 Raman Spectra and LC-MS Chromatograms of Chapter 2.2.1

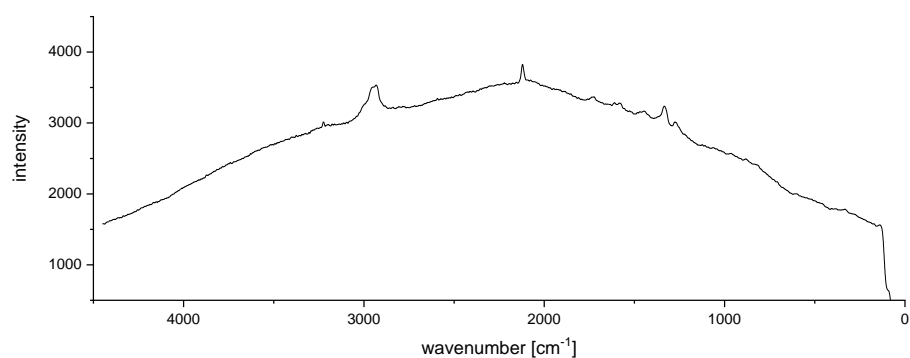
Raman microscopy was performed by Stefan Heissler on a Hyperion 3000 by Bruker (Ettlingen, Germany; IFG, KIT). Illumination was executed by a laser beam at 532 nm and 2 mW intensity. Raw spectra are shown below.



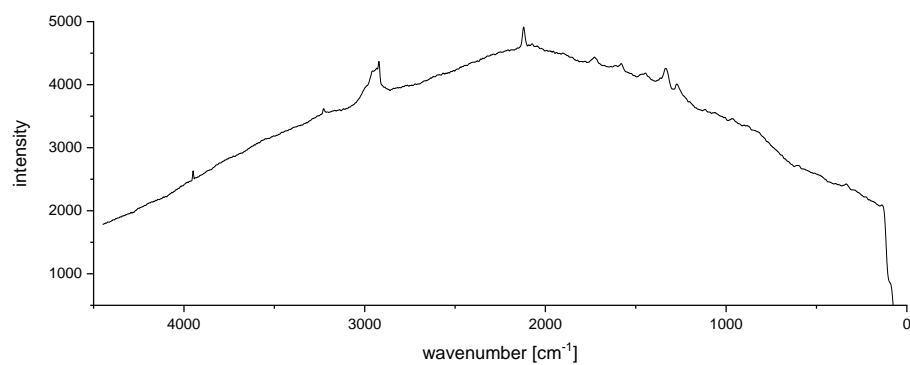
Supporting Spectrum 1. Raman spectrum of a hydrophilic spot of a freshly produced droplet microarray with free amino groups from cysteamine.



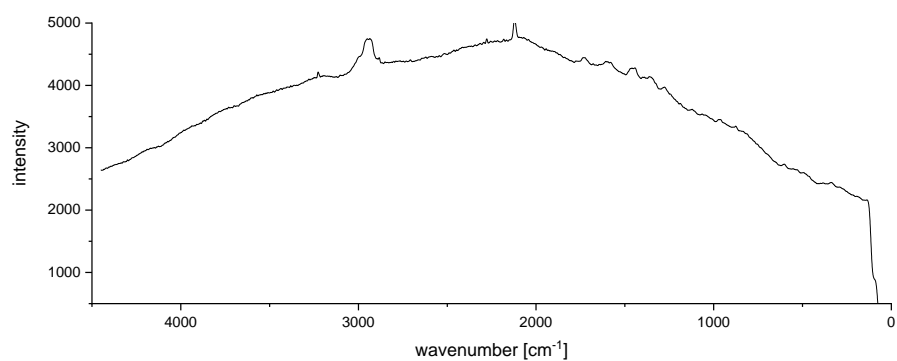
Supporting Spectrum 2. Hydrophilic spot after Hydroxyethyl photolinker (HEPL) was attached via Steglich esterification.



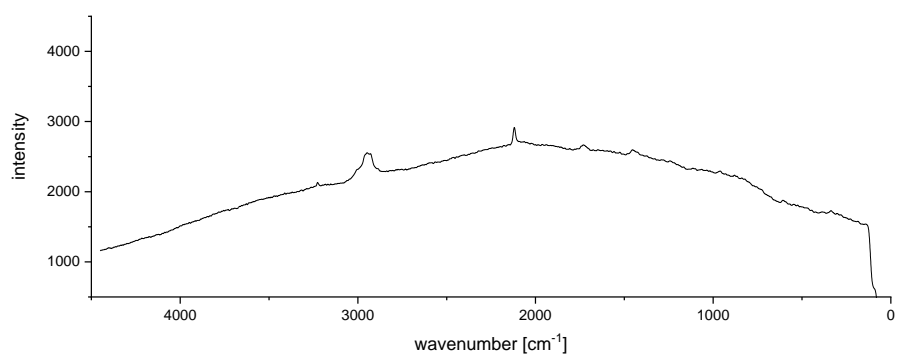
Supporting Spectrum 3. Hydrophilic spot after Fmoc-Gly-OH was coupled to linker via DIC and HOBt.



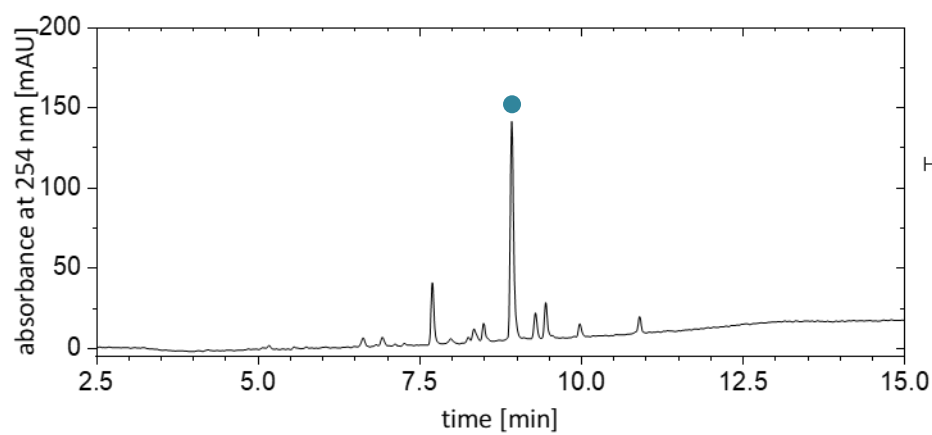
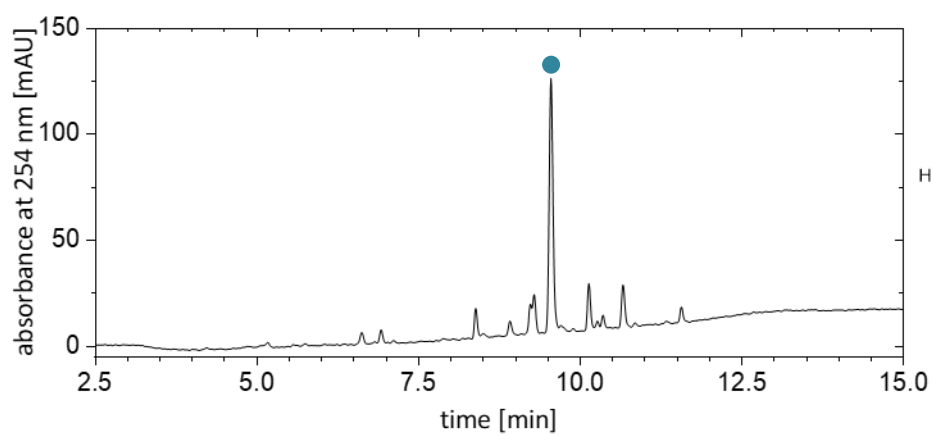
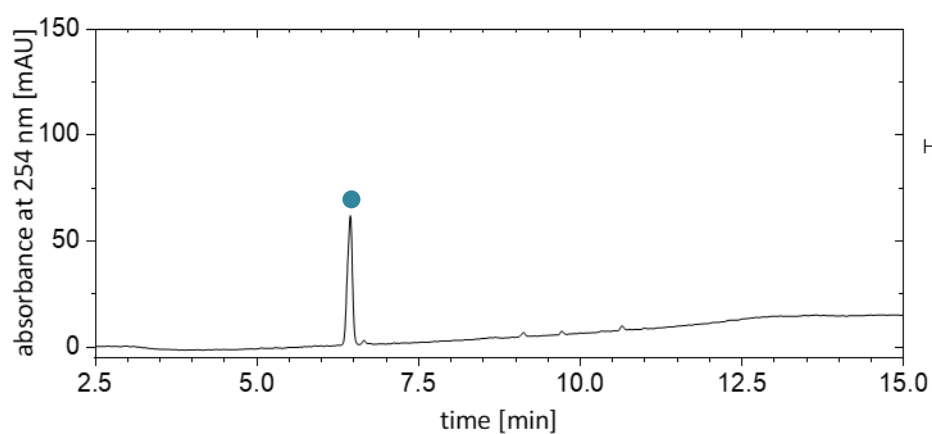
Supporting Spectrum 4. Hydrophilic spot after Fmoc group was removed by 20 % (v/v) piperidine in NMP.

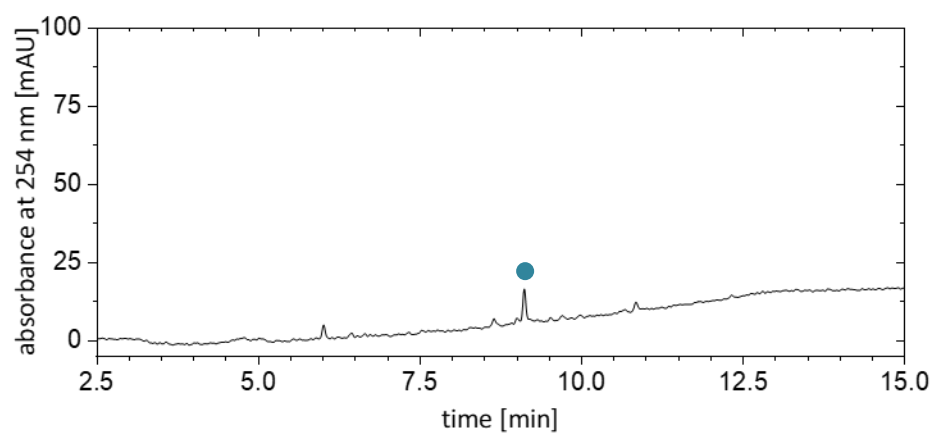
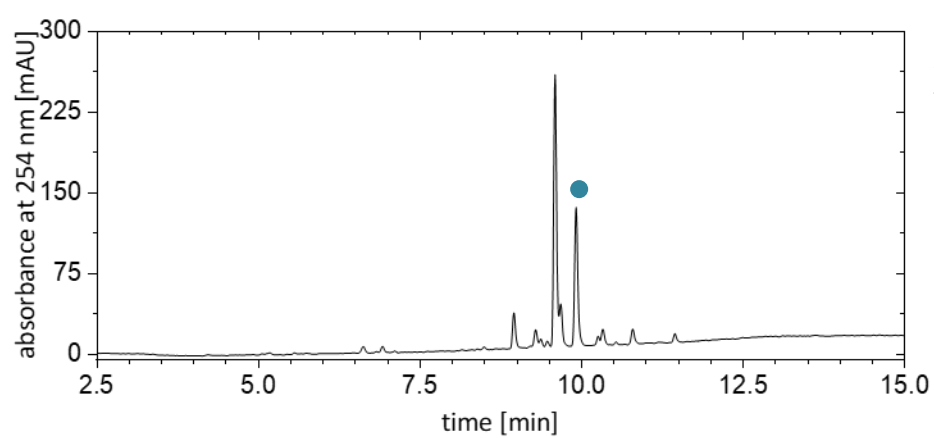
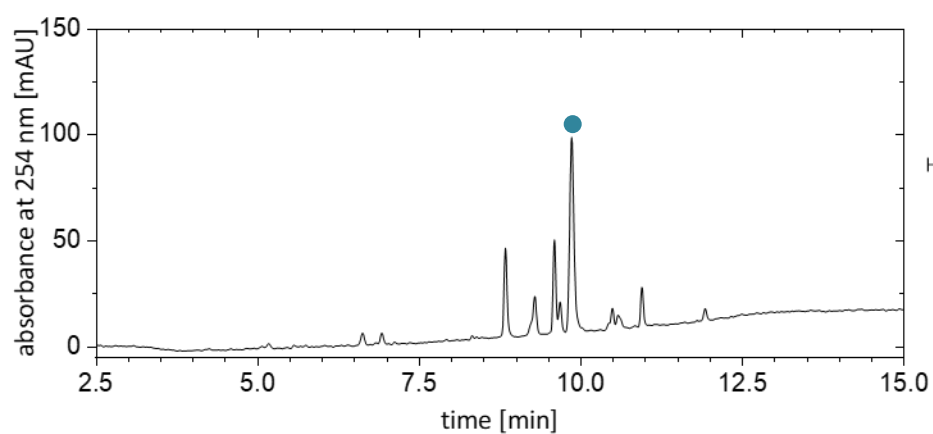


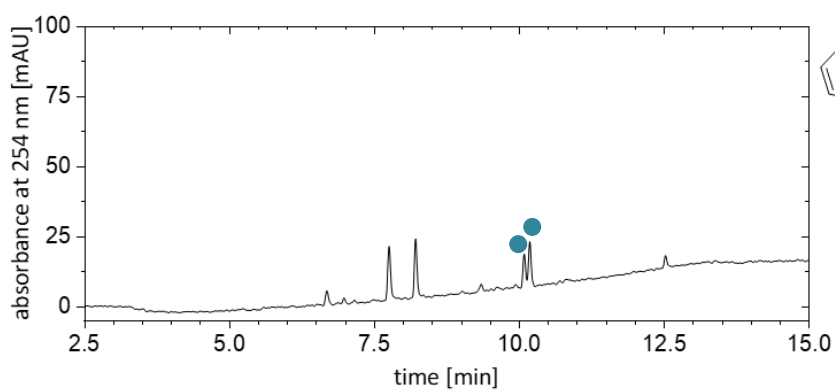
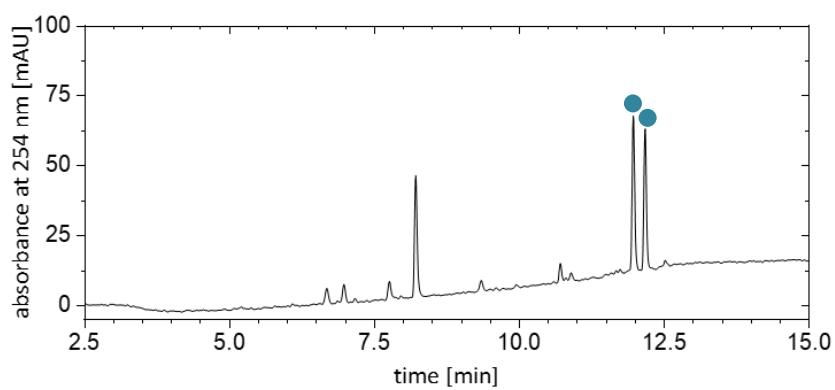
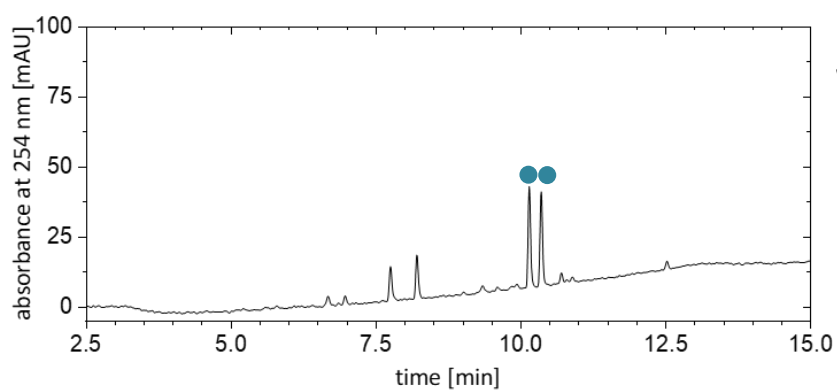
Supporting Spectrum 5. The hydrophilic spots were irradiated for 15 minutes at 365 nm (2.5 mW/cm²).

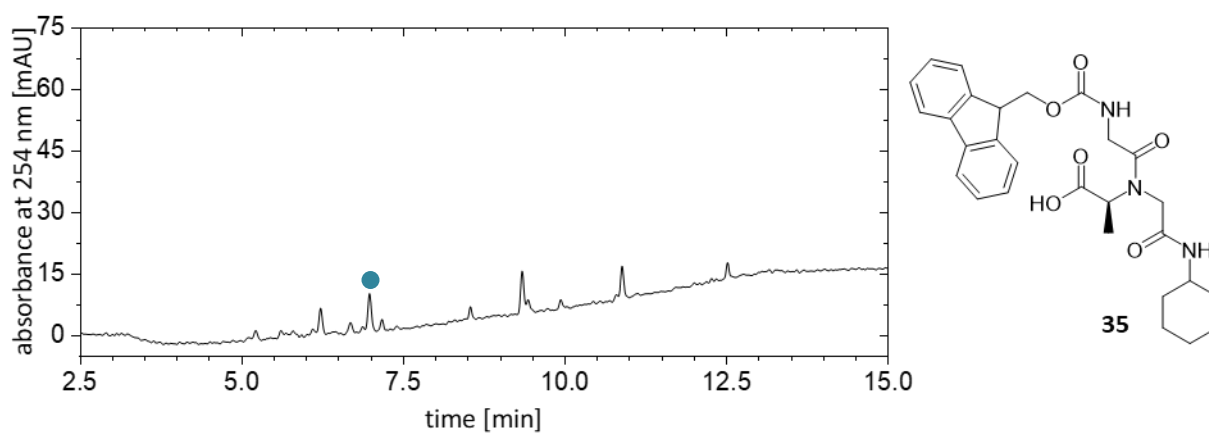
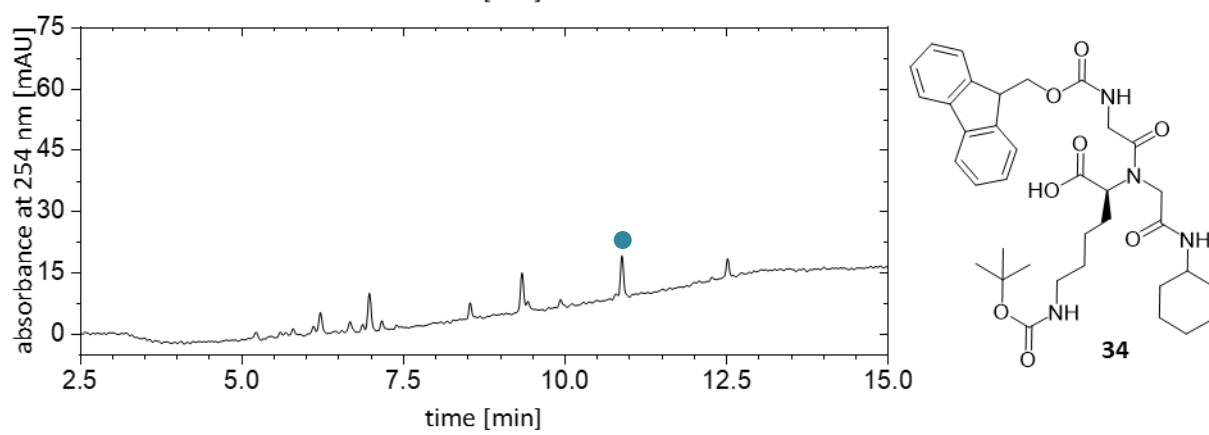
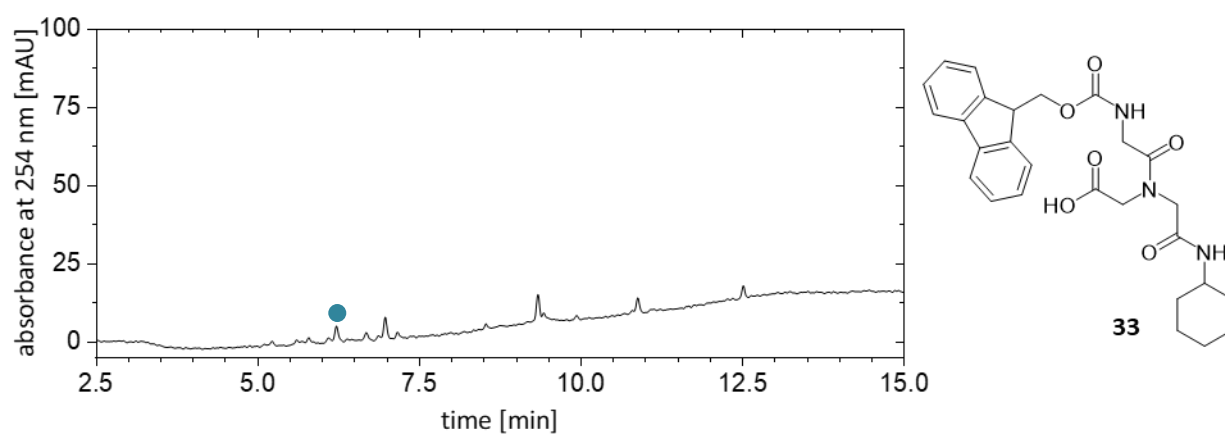


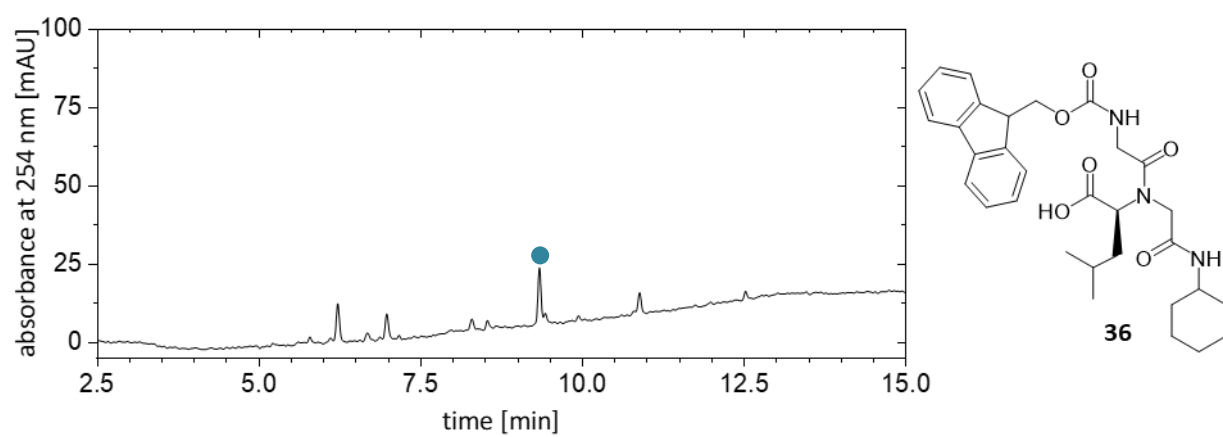
Supporting Spectrum 6. Raman spectrum of the superhydrophobic border.



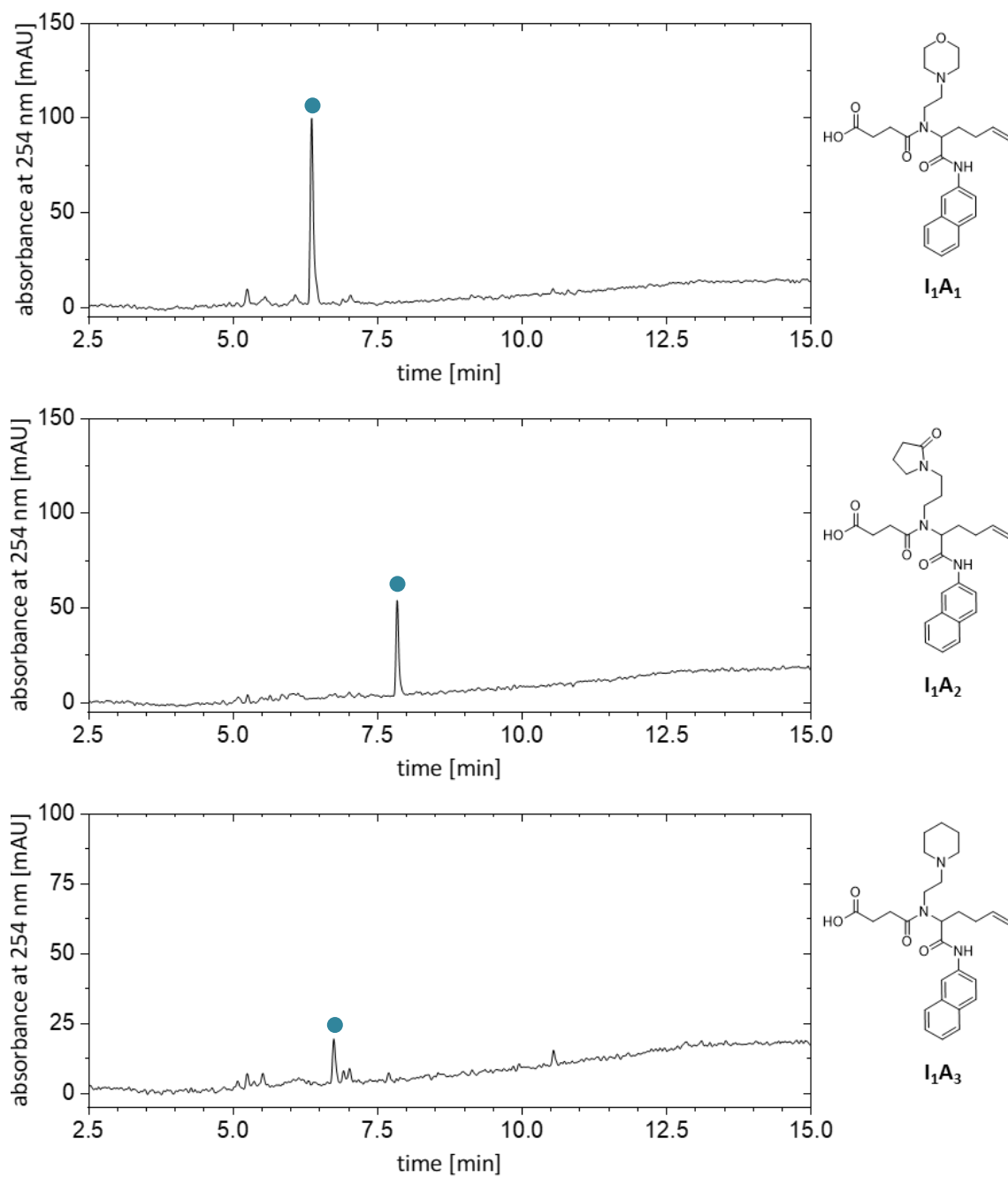


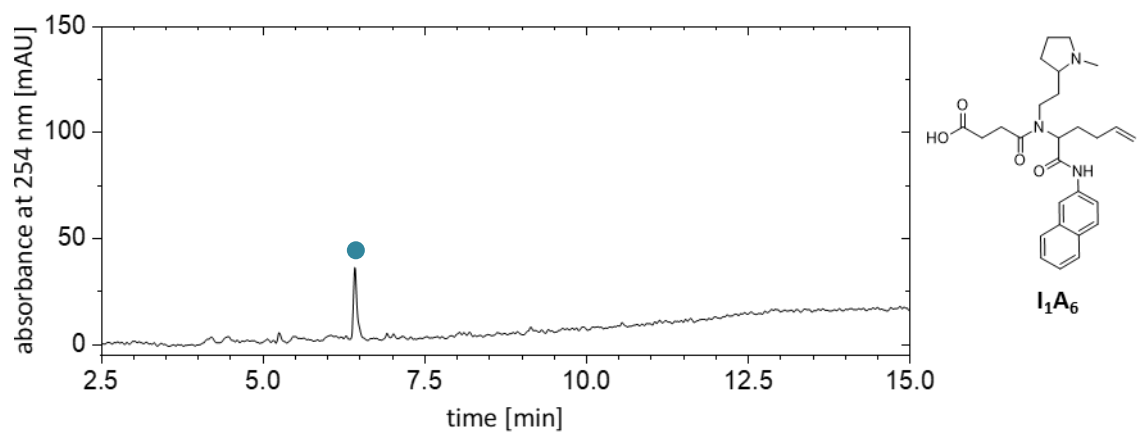
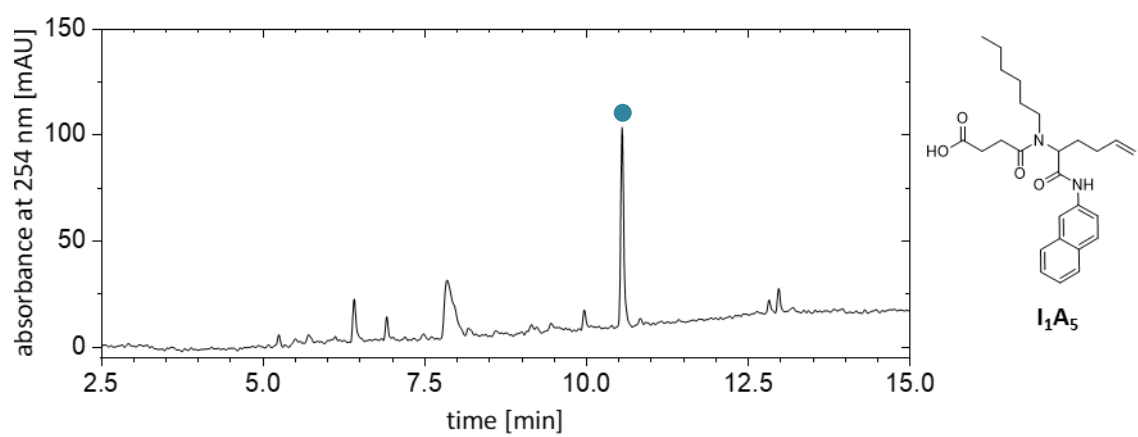
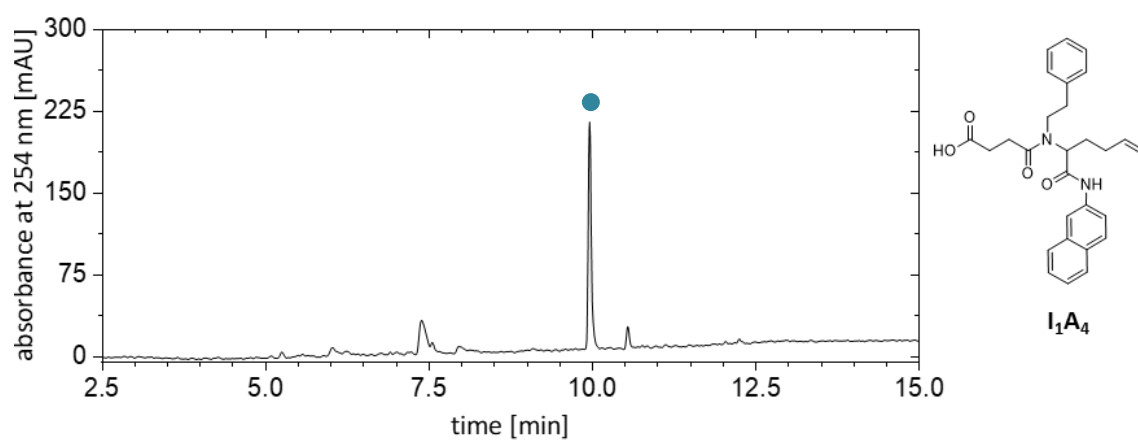


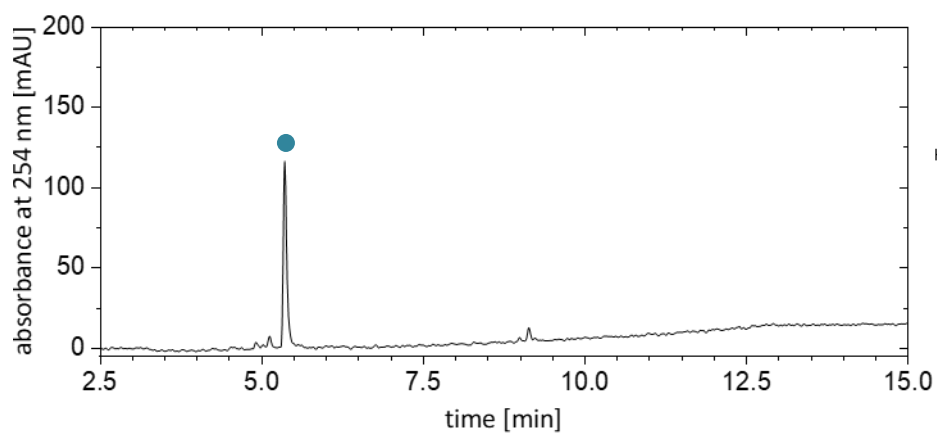
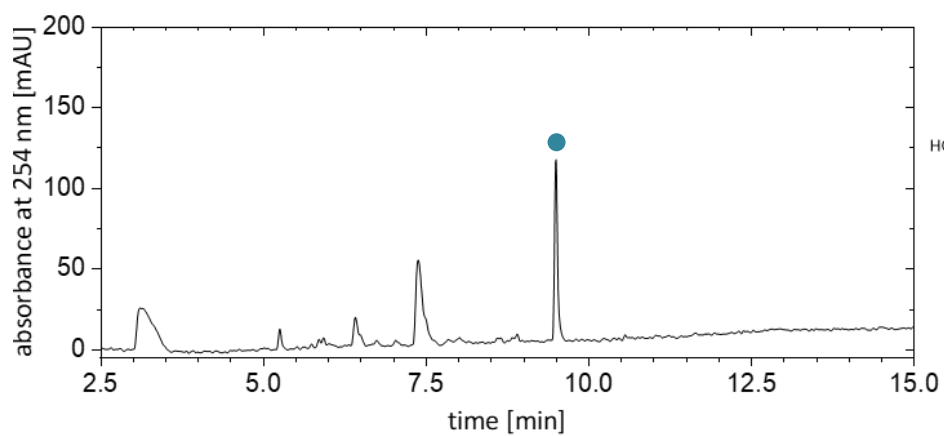
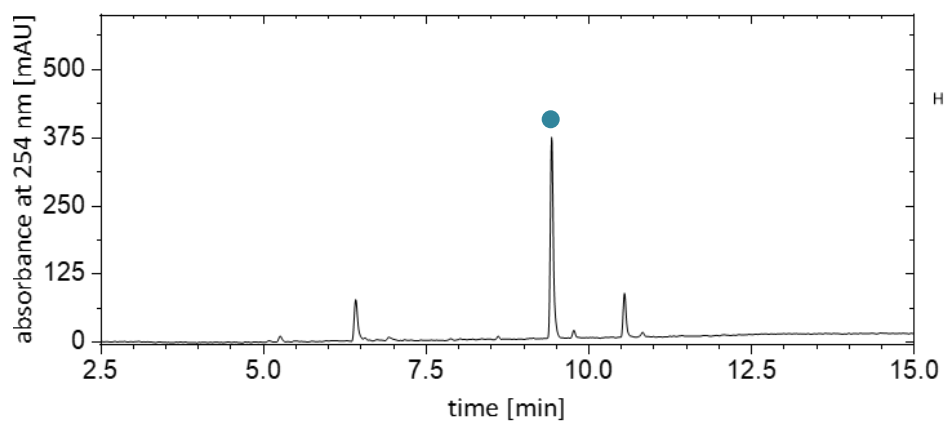


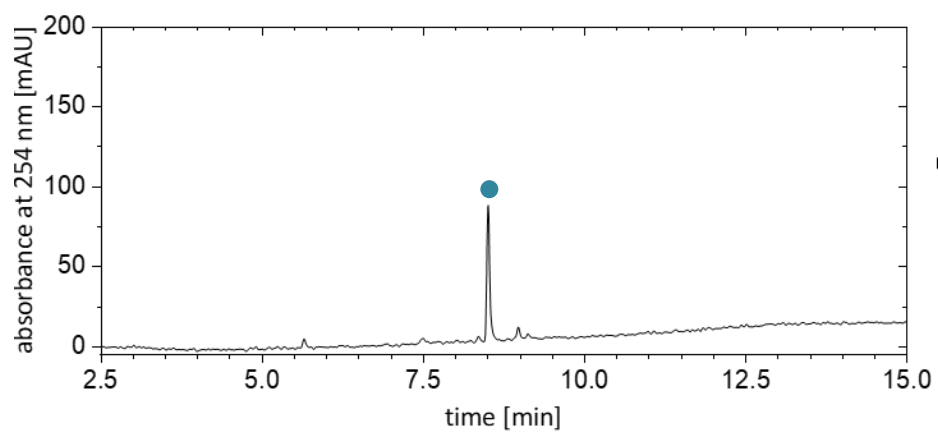
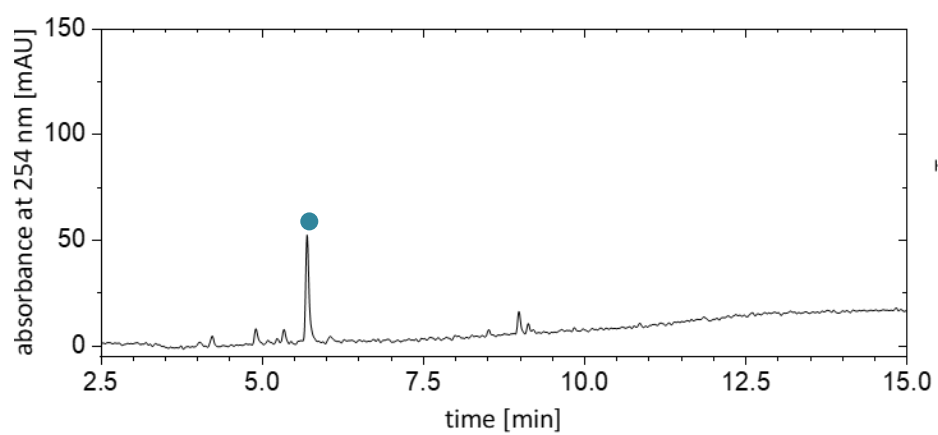
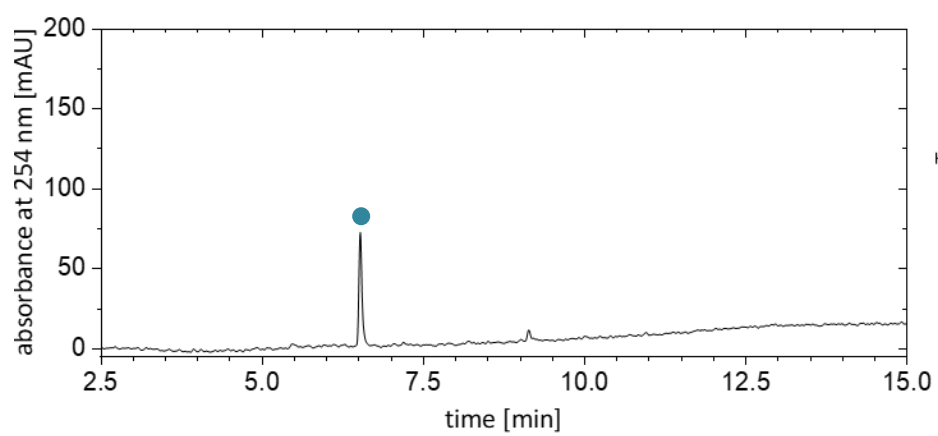


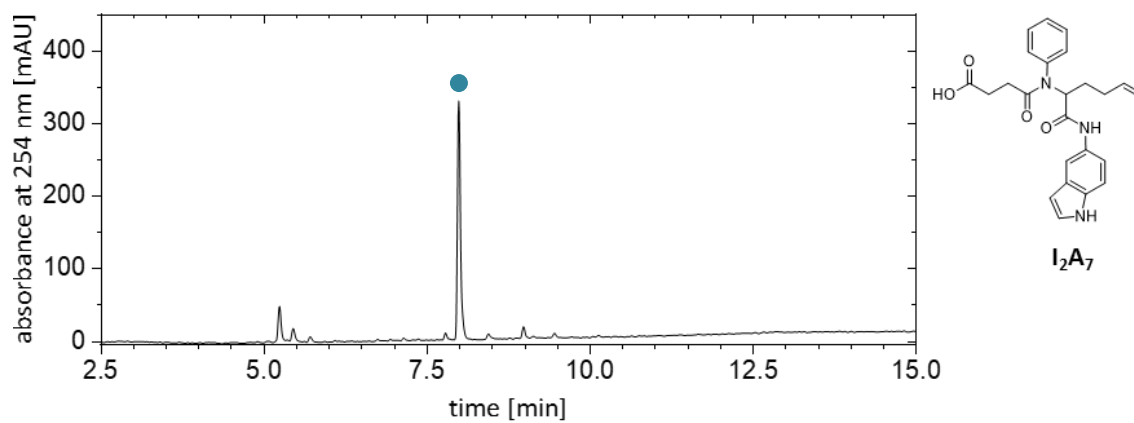
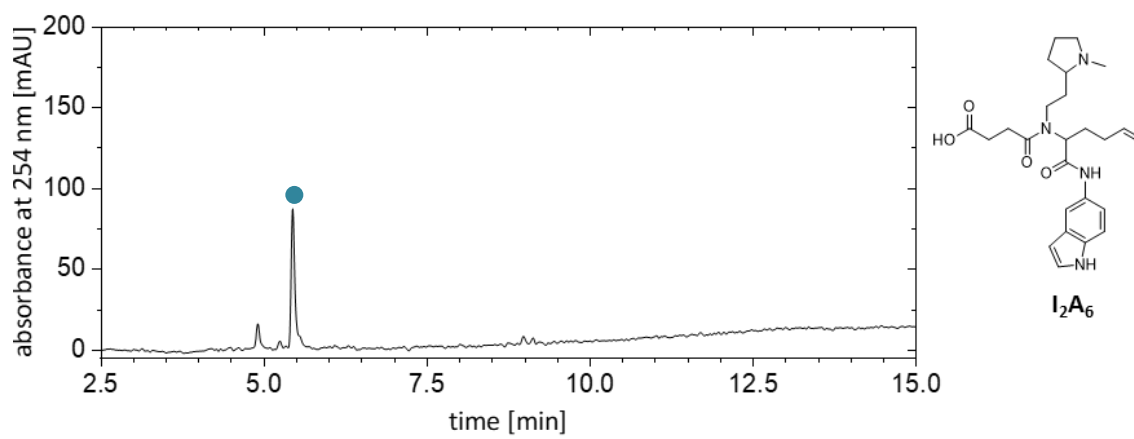
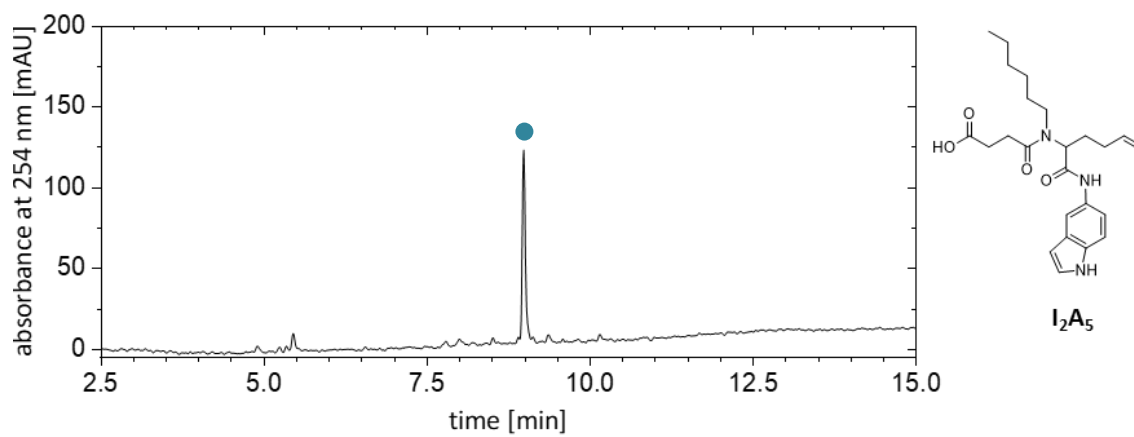
5.1.3 LC-MS Chromatograms of Chapter 2.2.2

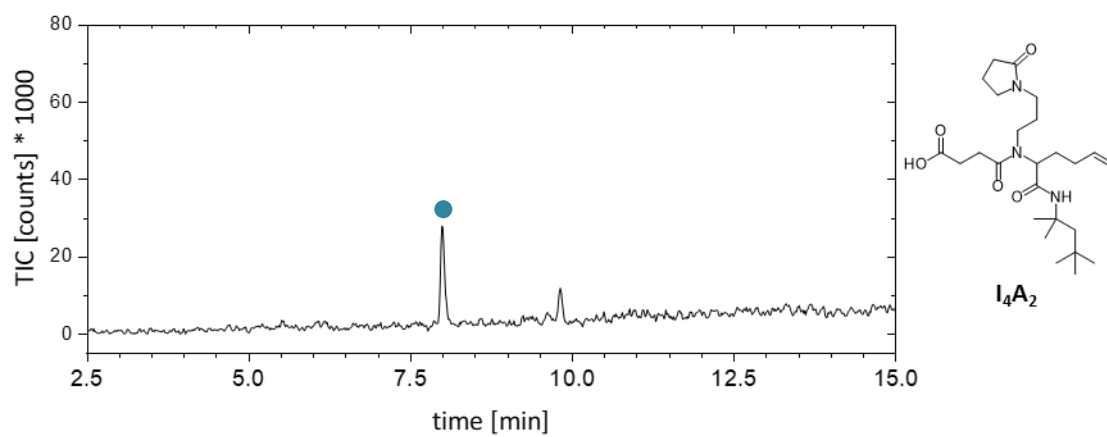
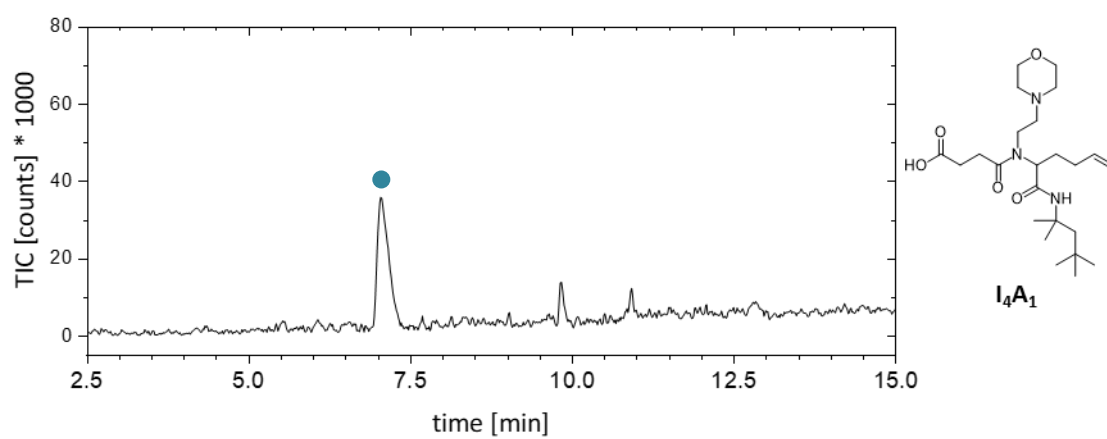
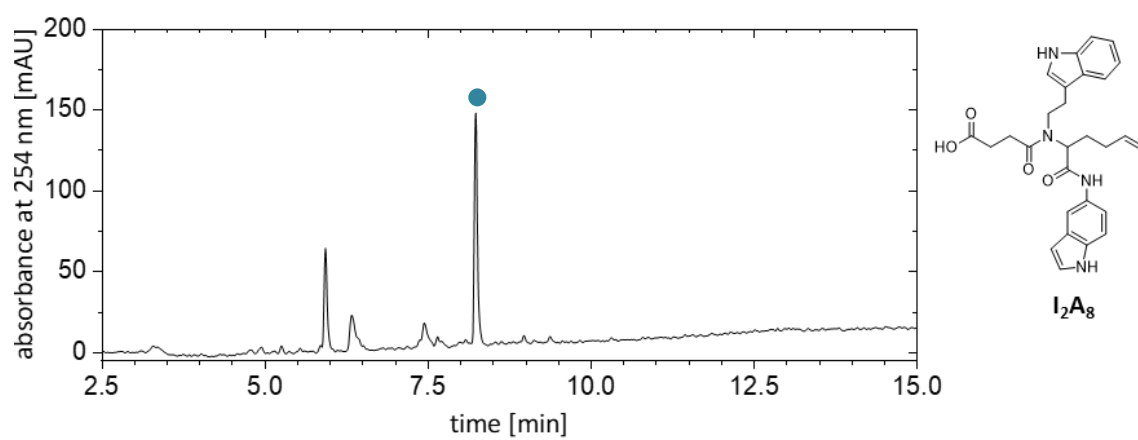


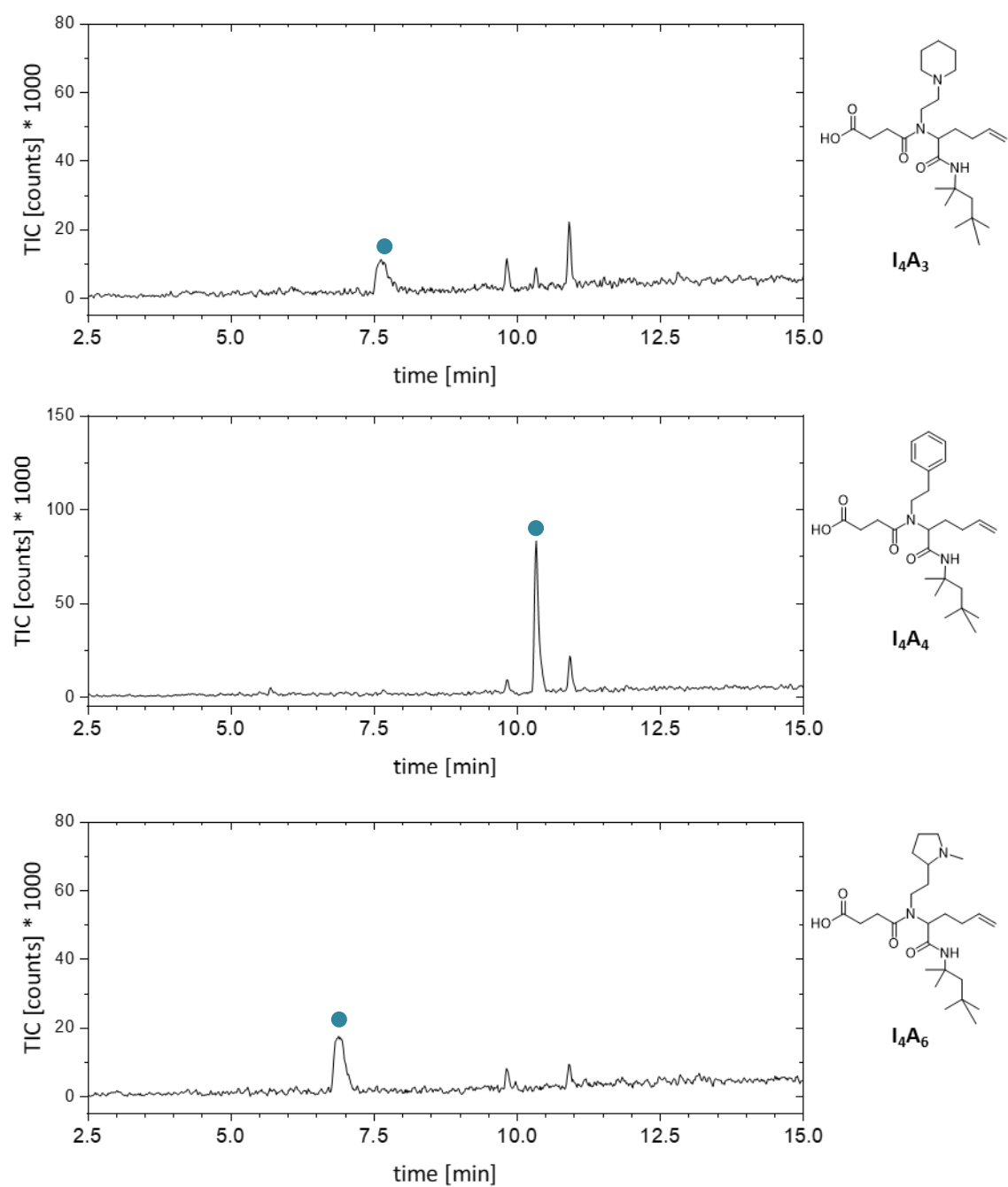


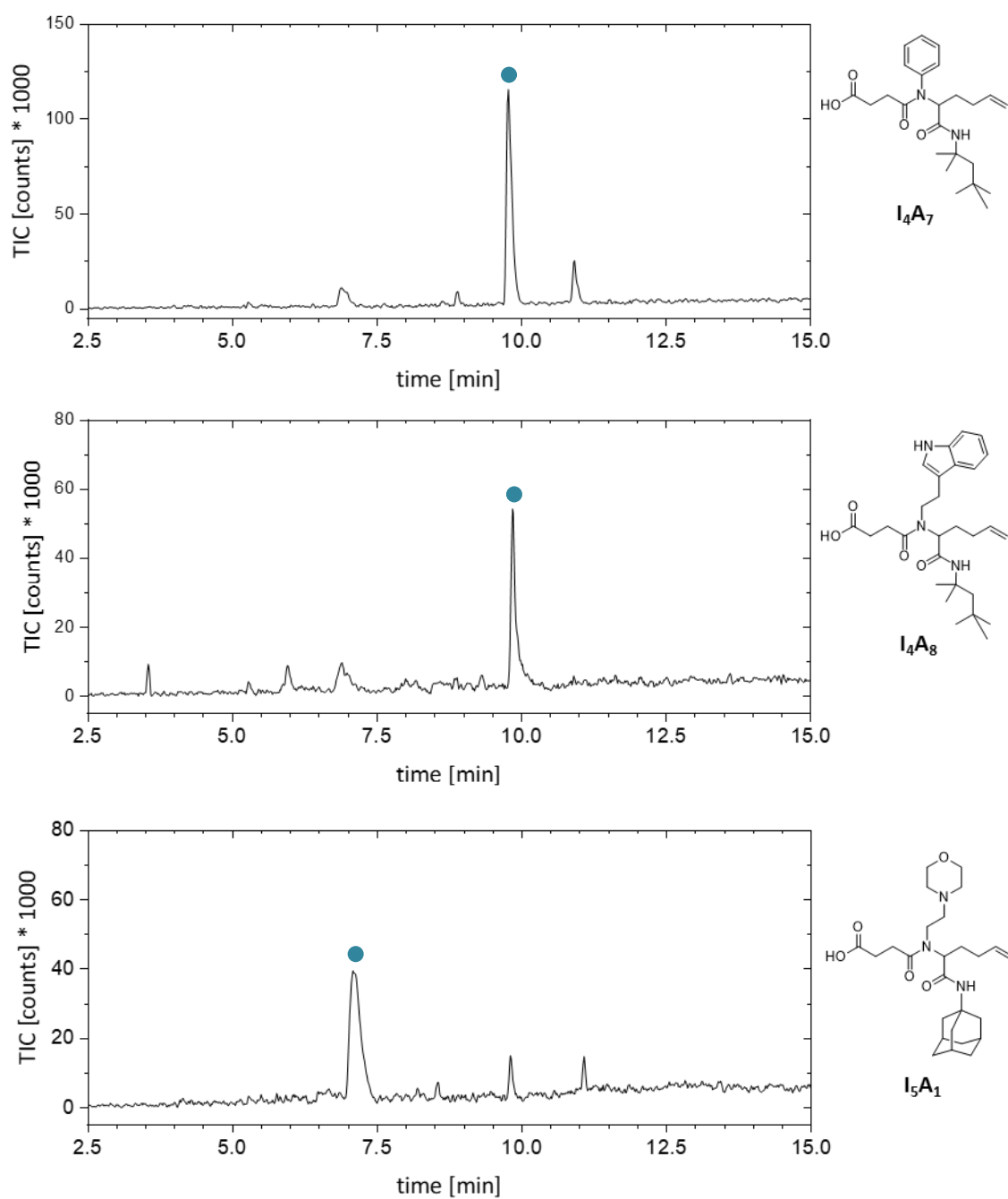


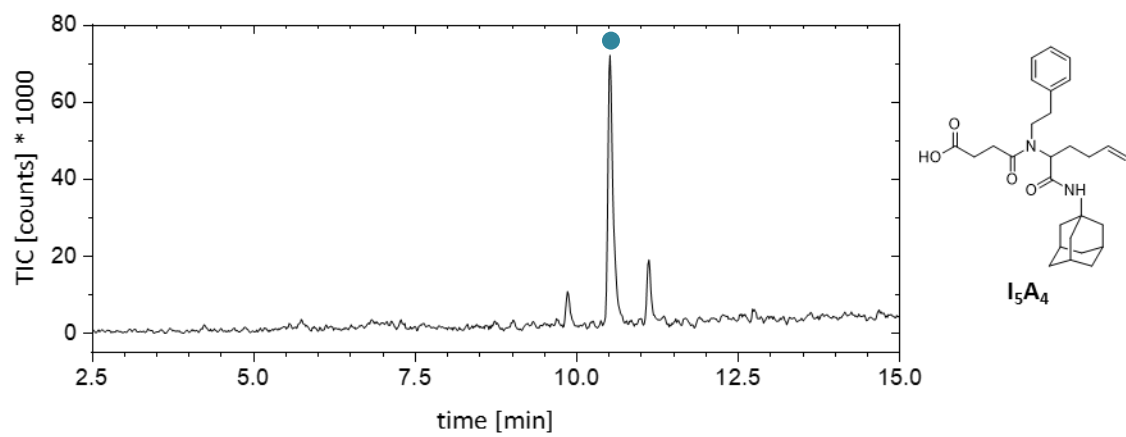
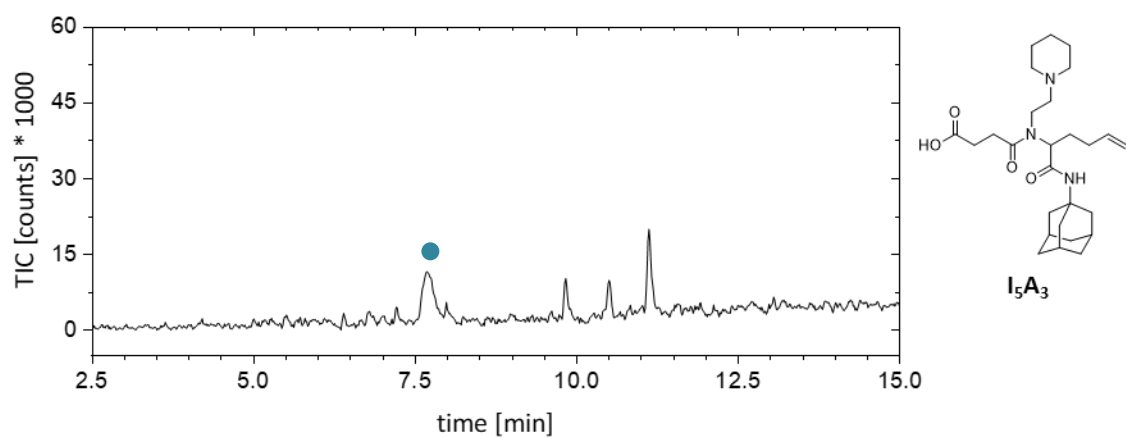
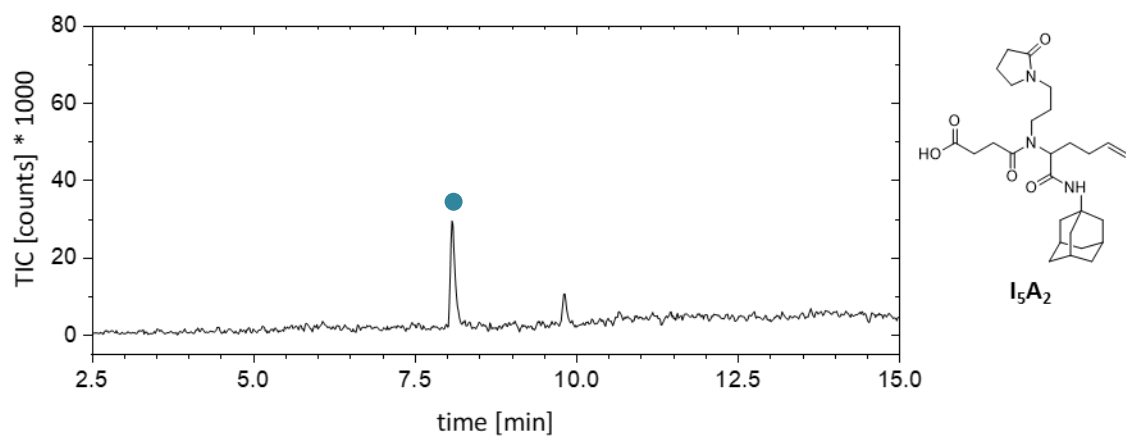


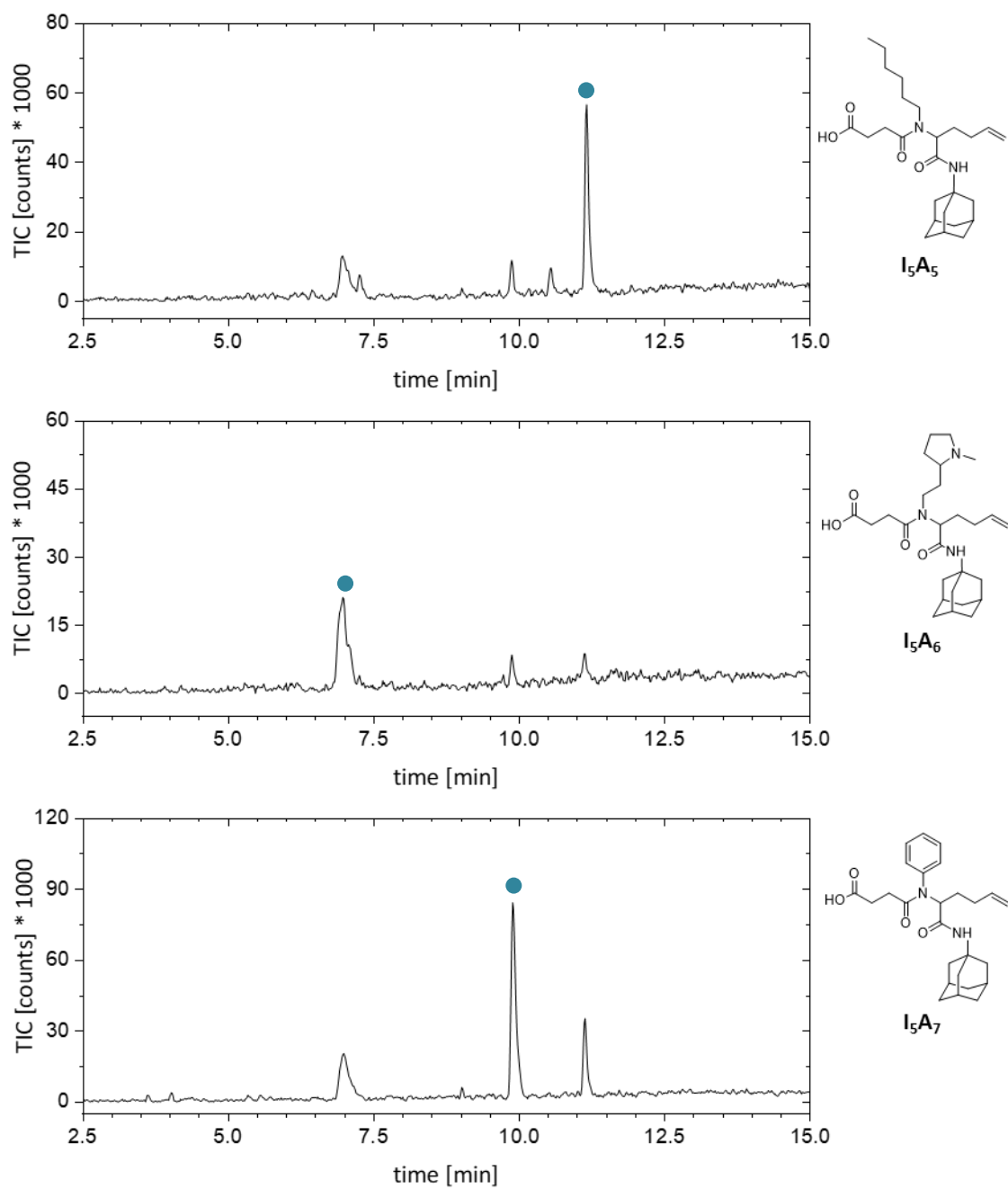


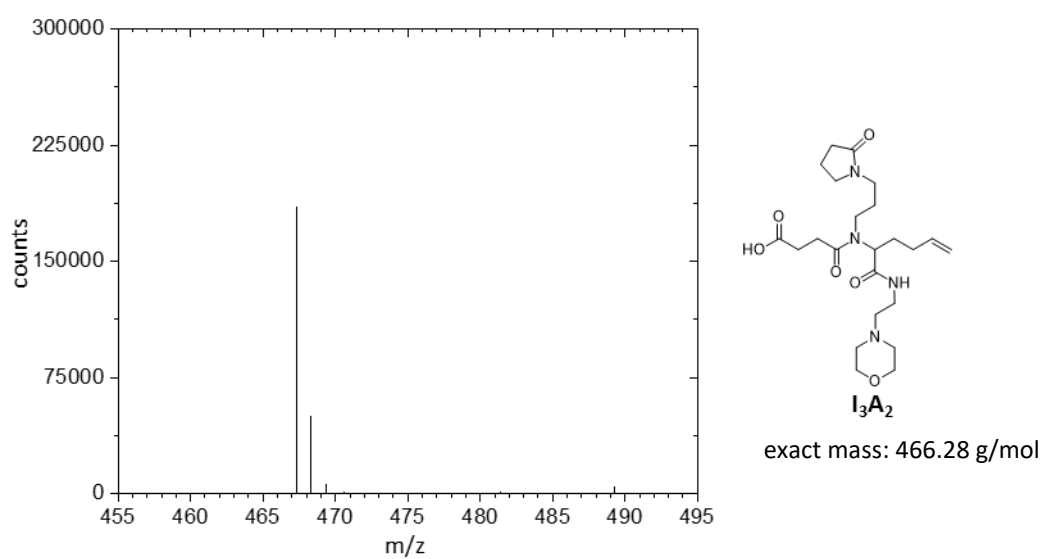
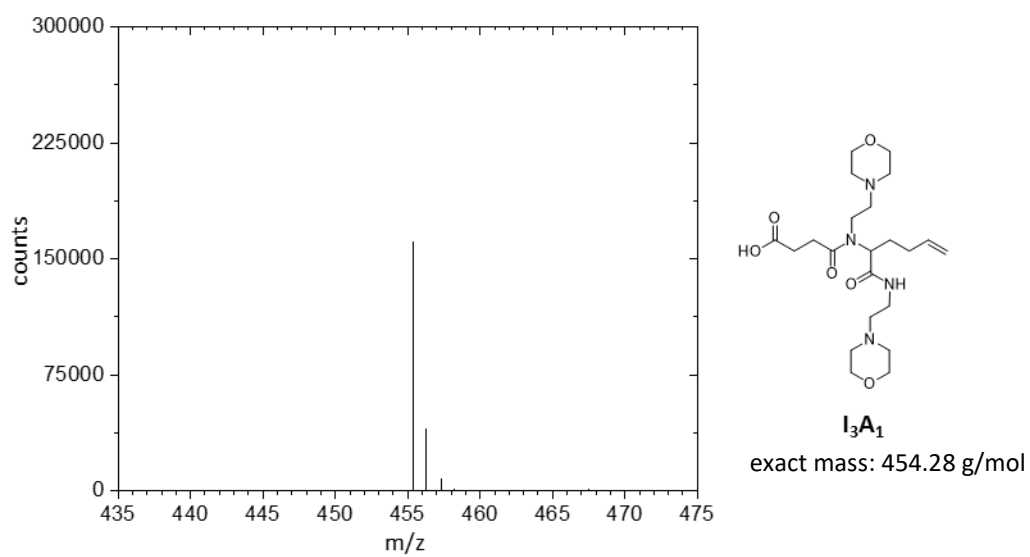
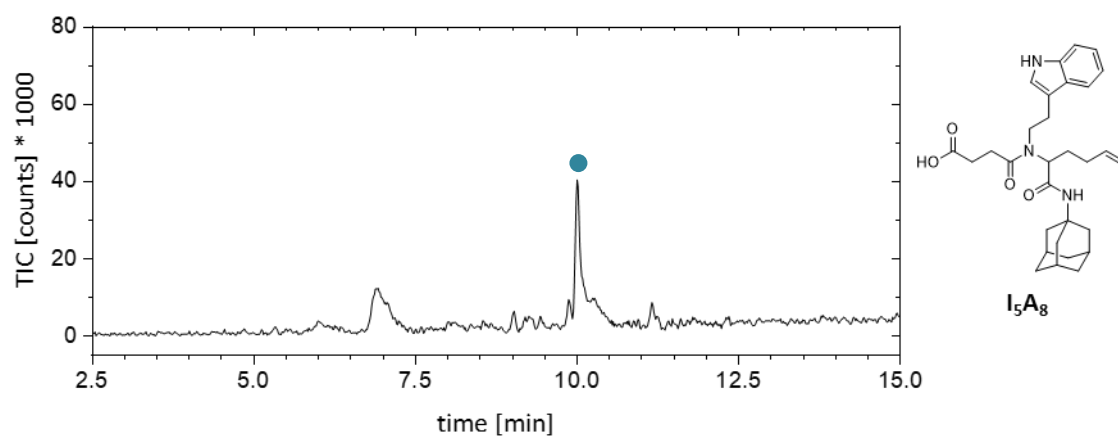


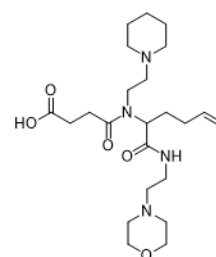
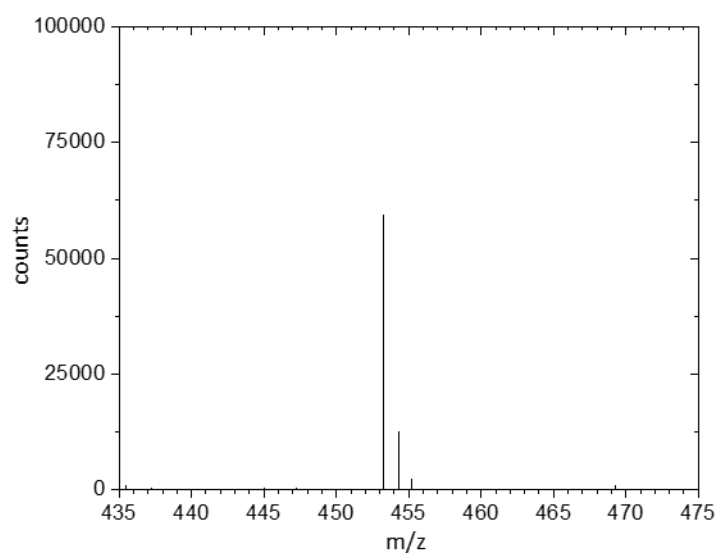




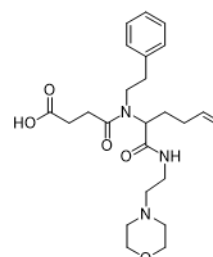
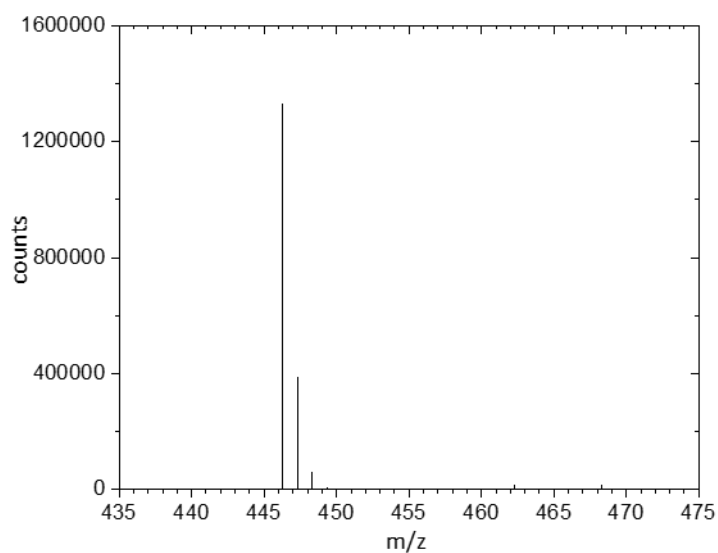




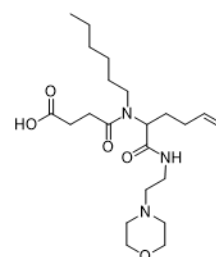
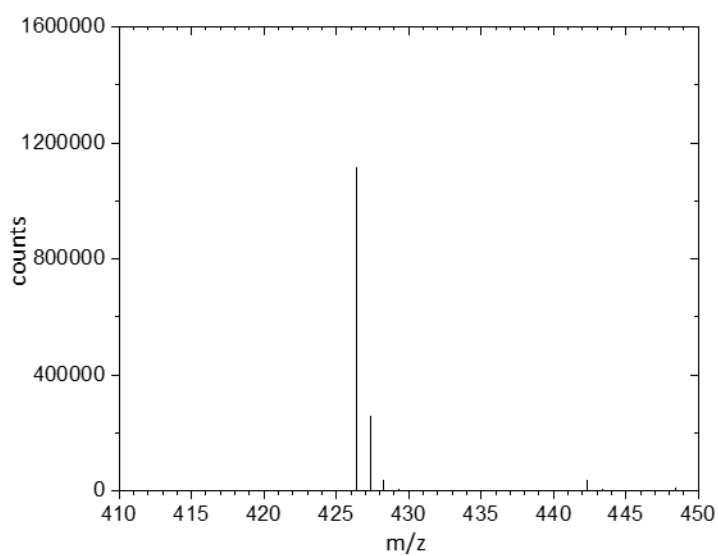




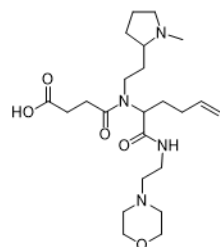
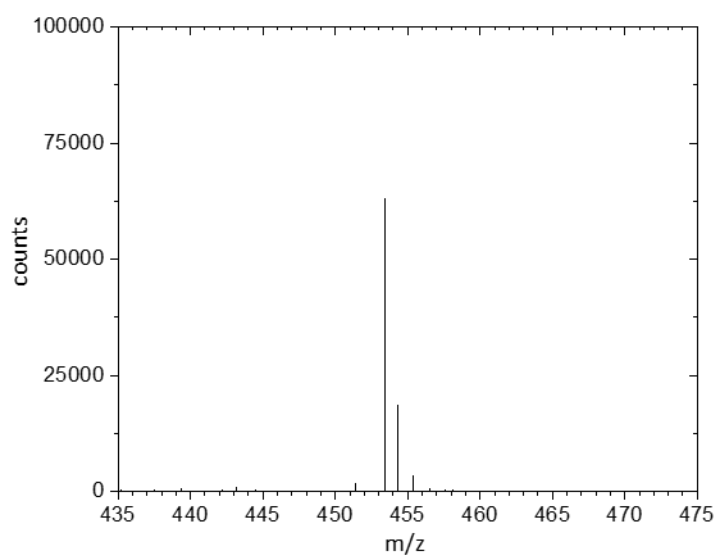
I₃A₃
exact mass: 452.30 g/mol



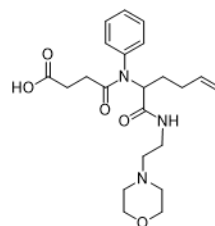
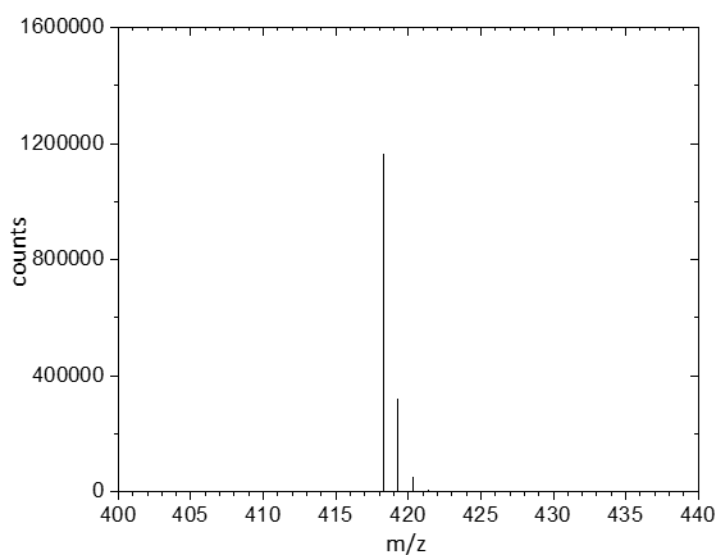
I₃A₄
exact mass: 445.26 g/mol



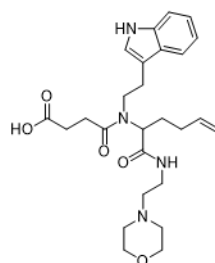
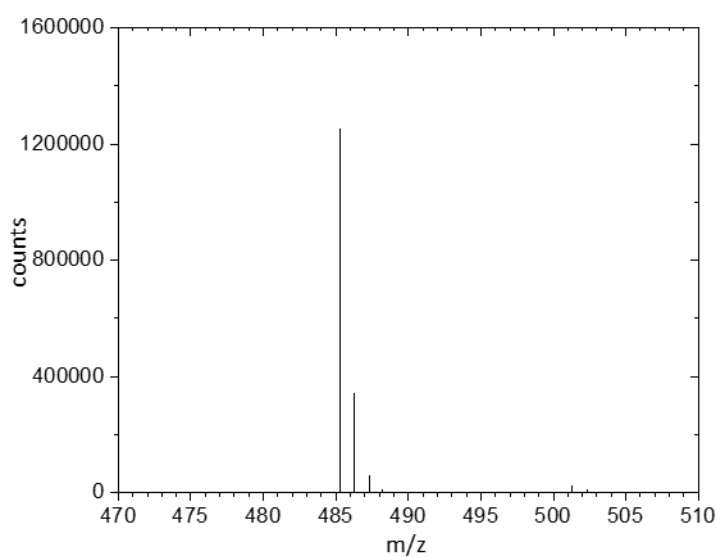
I₃A₅
exact mass: 425.29 g/mol

**I₃A₆**

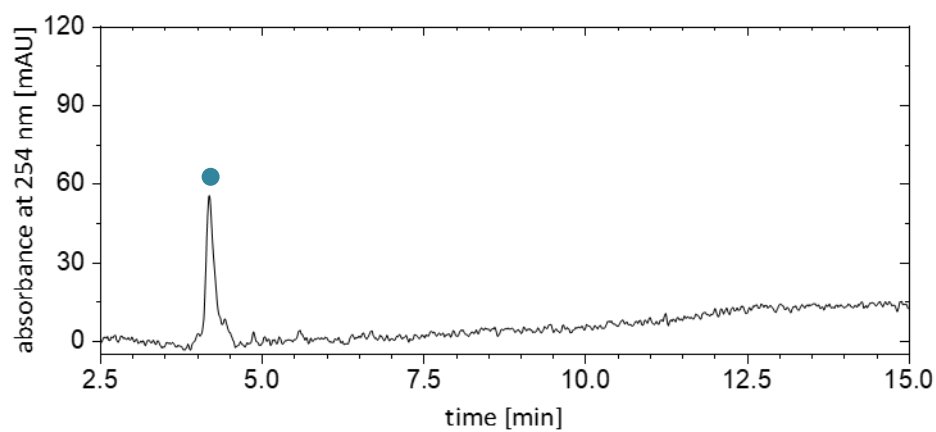
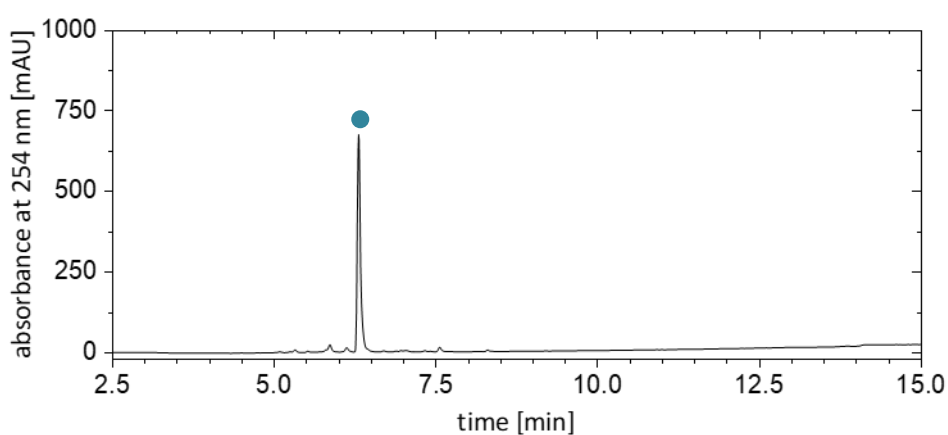
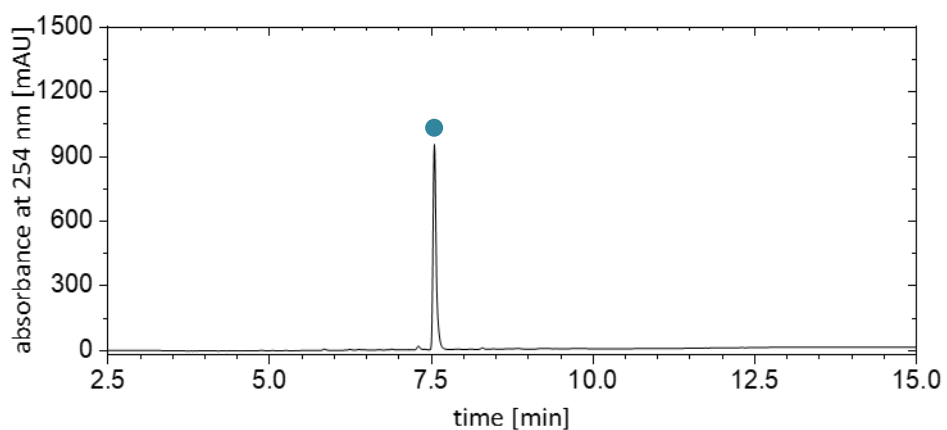
exact mass: 452.30 g/mol

**I₃A₇**

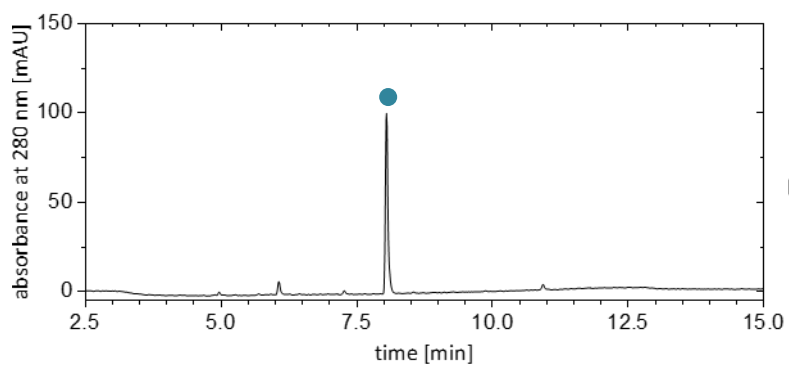
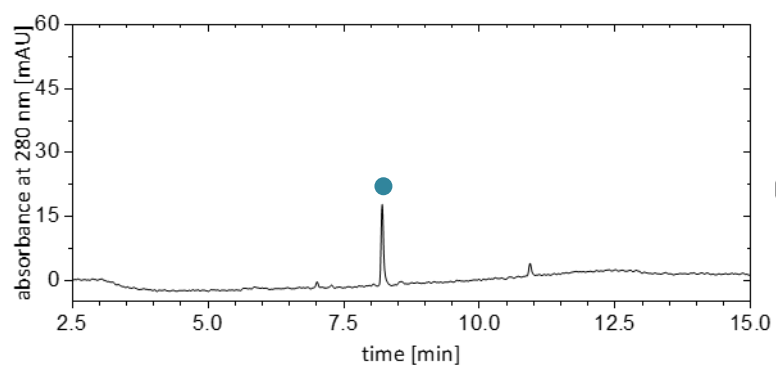
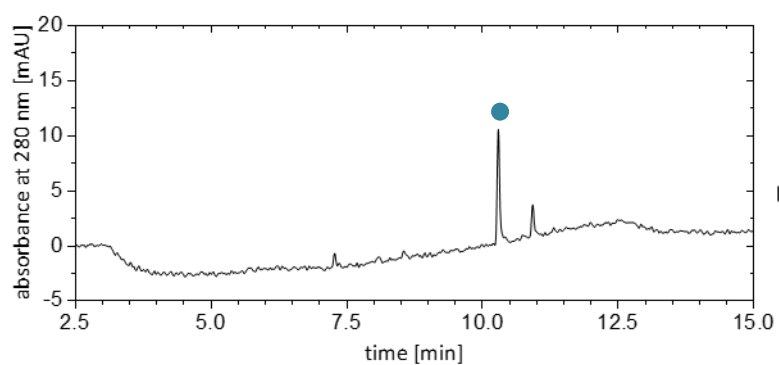
exact mass: 417.23 g/mol

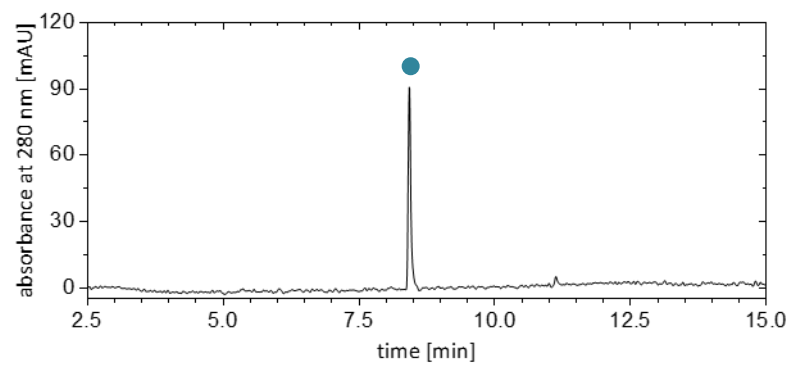
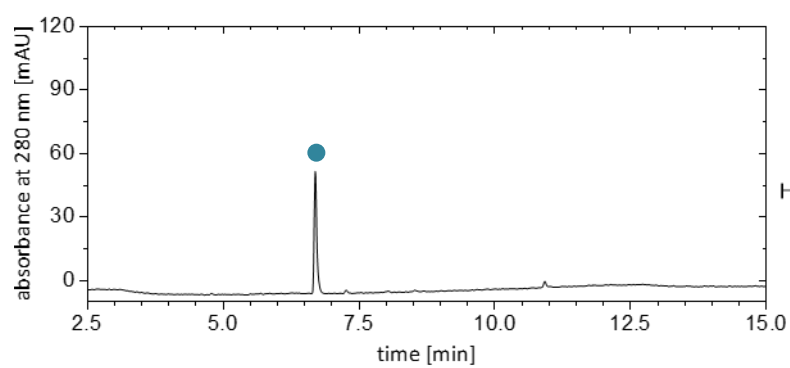
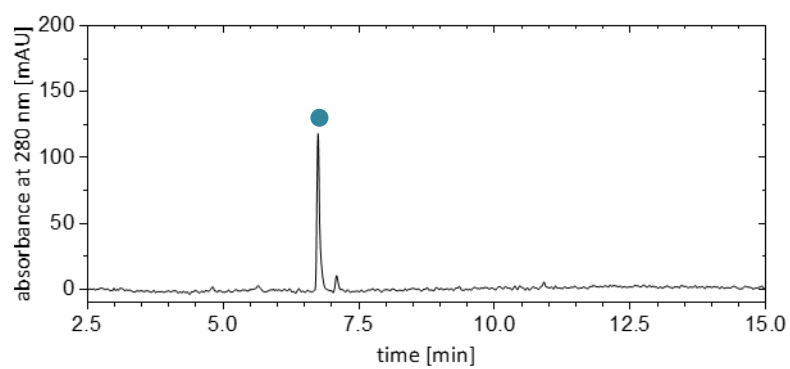
**I₃A₈**

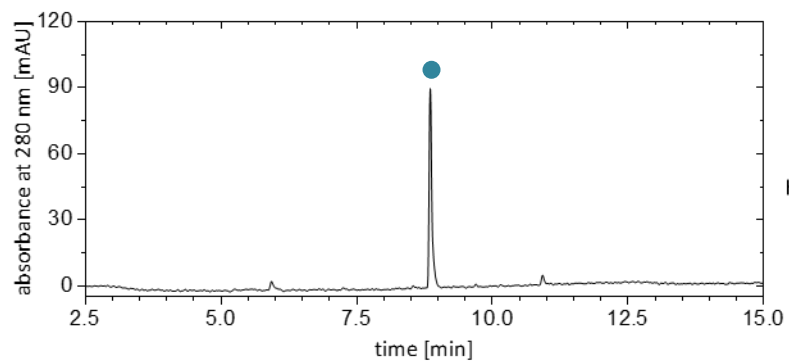
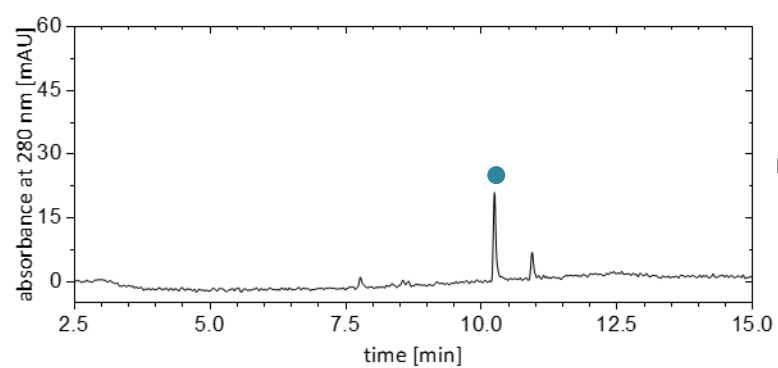
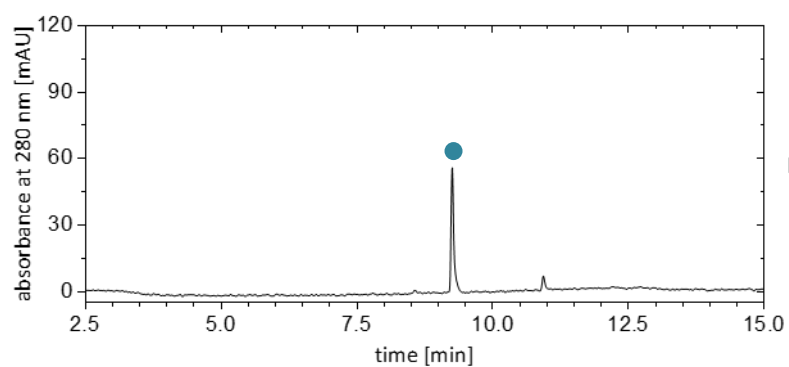
exact mass: 484.27 g/mol

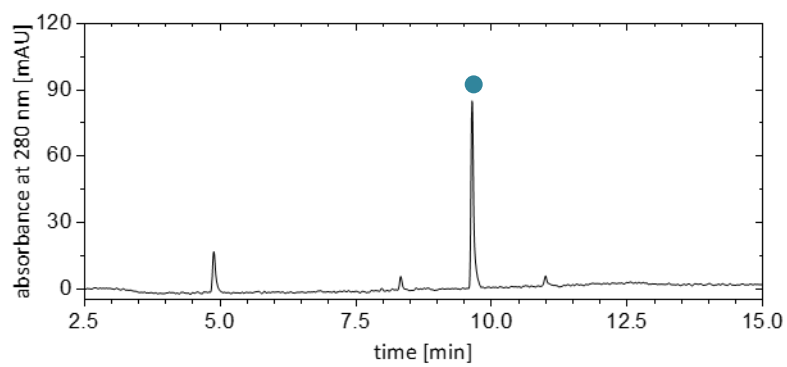
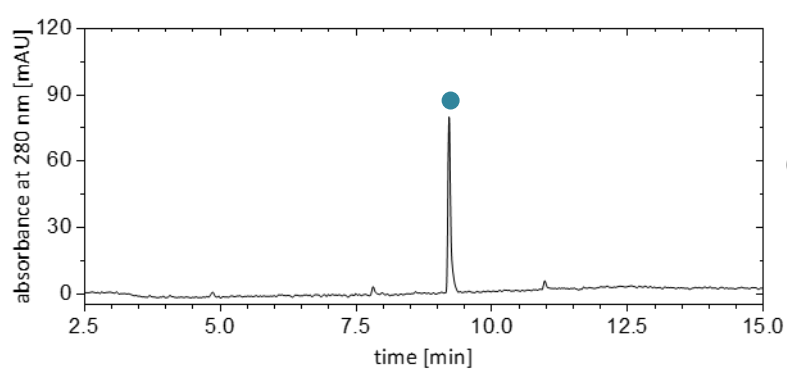
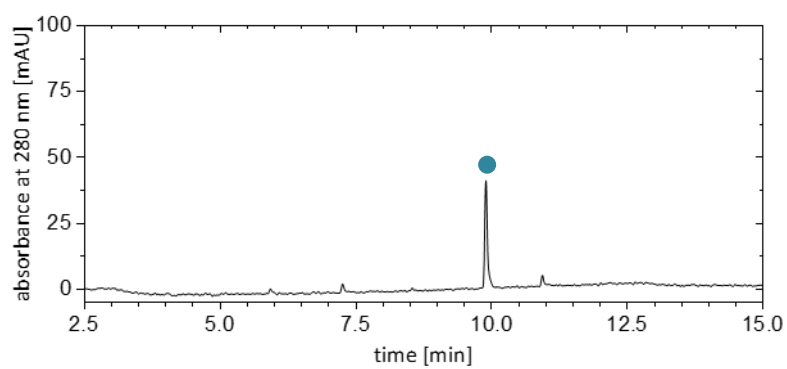


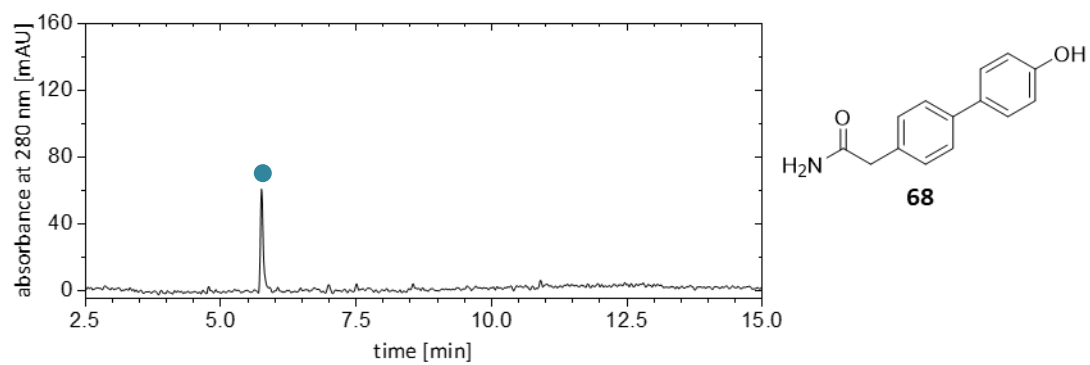
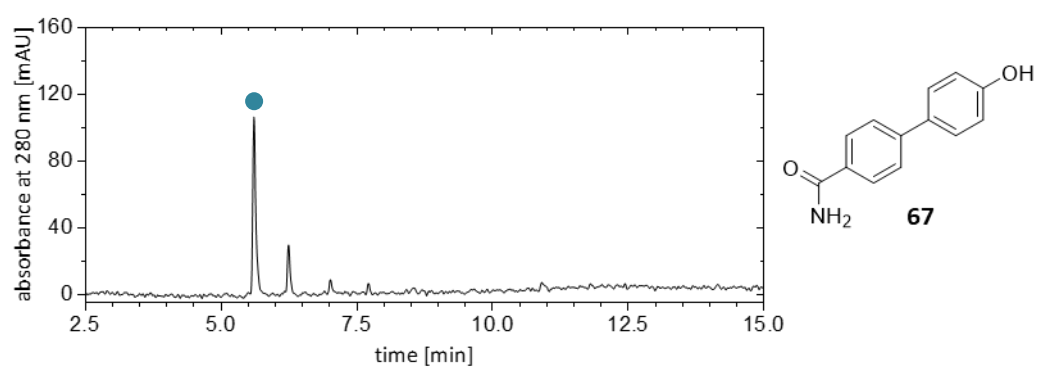
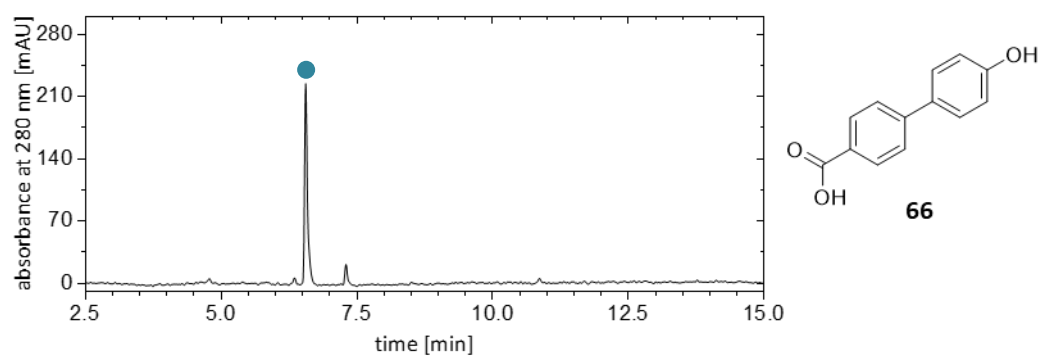
5.1.4 LC-MS Chromatograms of Chapter 2.2.3

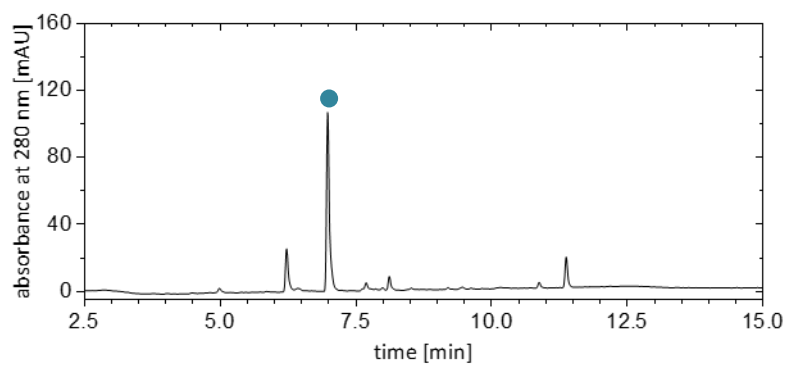
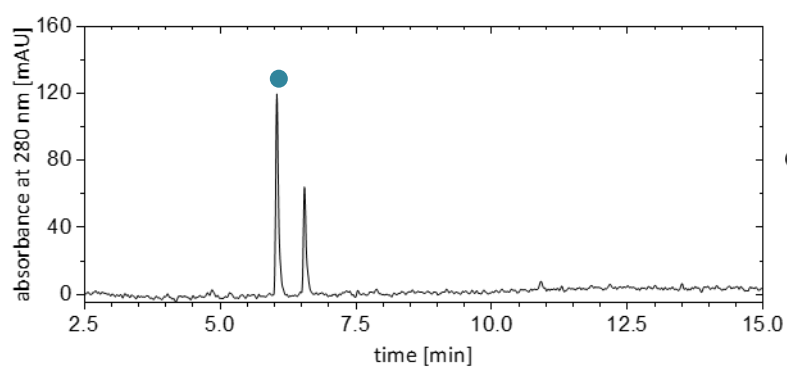
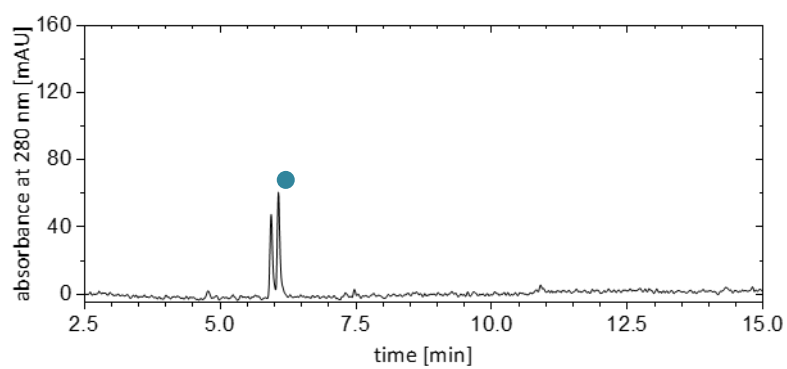


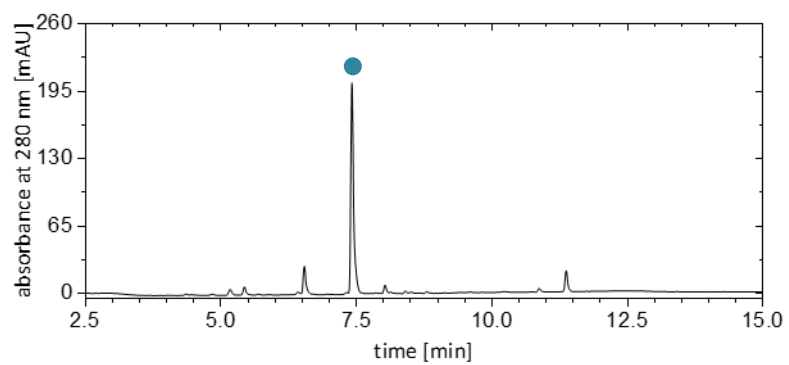
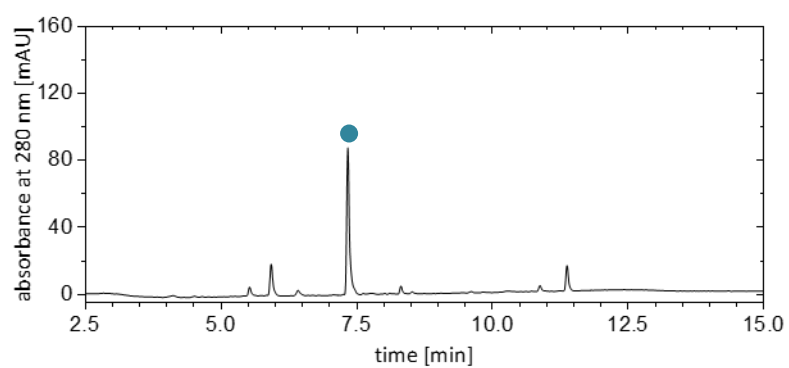
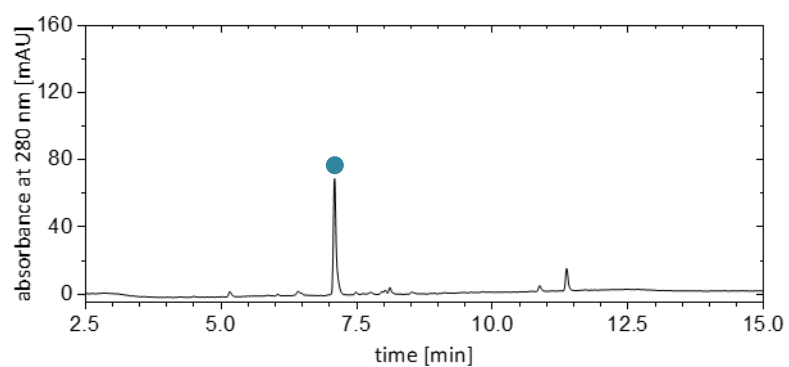


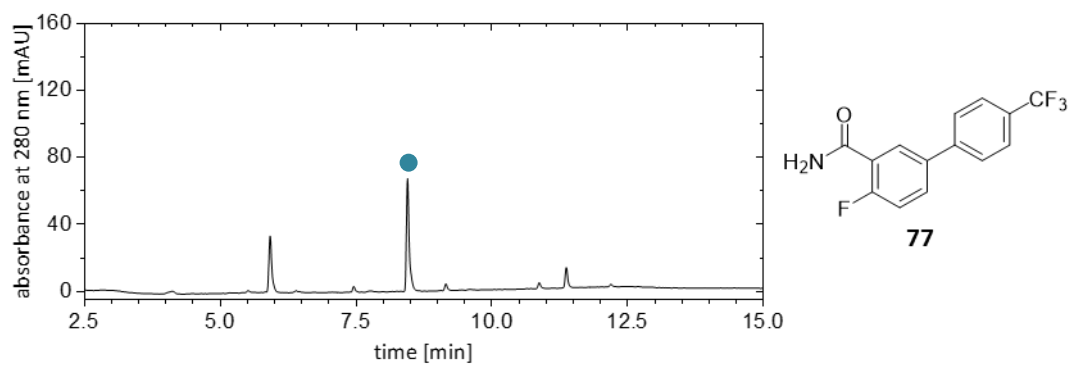
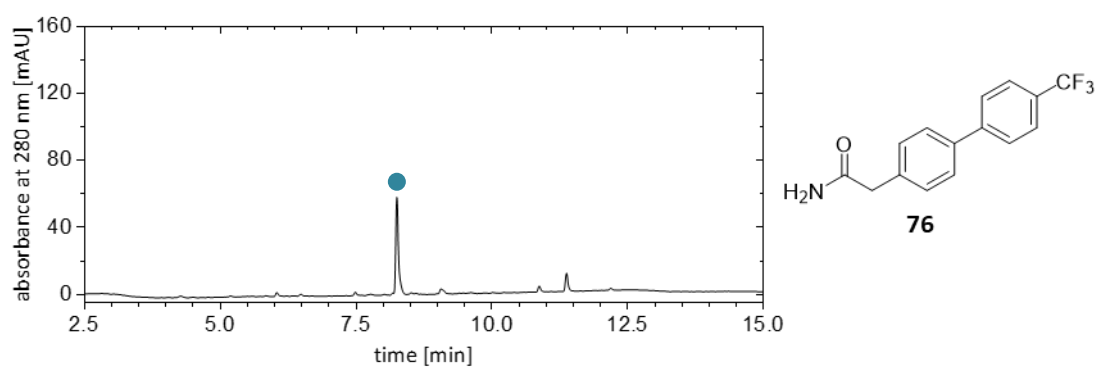
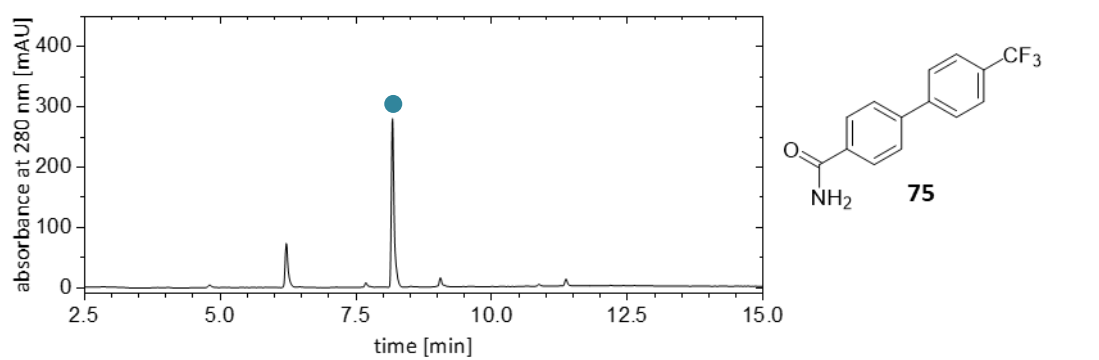


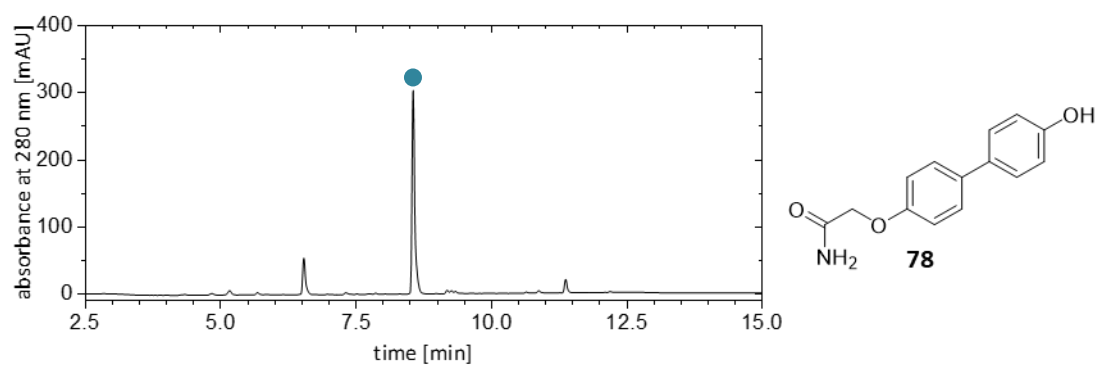












5.2 Bibliography

- [1] M. Brehm, *Establishing Combinatorial Solid Phase Synthesis on Droplet Microarrays*, unpublished master thesis, Karlsruhe Institute of Technology **2017**.
- [2] A. Rosenfeld, M. Brehm, A. Welle, V. Trouillet, S. Heissler, M. Benz, P. A. Levkin, *Mater. Today Bio* **2019**, *3*, 100022.
- [3] M. Brehm, J. M. Scheiger, A. Welle, P. A. Levkin, *Adv. Mater. Interfaces* **2020**, *7*, 1902134.
- [4] M. Brehm, S. Heissler, S. Afonin, P. A. Levkin, *Small* **2020**, *16*, 1905971.
- [5] T. Young, *Philos. Trans. R. Soc. London* **1805**, *95*, 65-87.
- [6] R. N. Wenzel, *Ind. Eng. Chem.* **1936**, *28*, 988-994.
- [7] A. B. D. Cassie, S. Baxter, *Trans. Faraday Soc.* **1944**, *40*, 546-551.
- [8] S. Wang, L. Jiang, *Adv. Mater.* **2007**, *19*, 3423-3424.
- [9] T. A. Otitoju, A. L. Ahmad, B. S. Ooi, *J. Ind. Eng. Chem.* **2017**, *47*, 19-40.
- [10] P. A. Levkin, F. Svec, J. M. J. Fréchet, *Adv. Funct. Mater.* **2009**, *19*, 1993-1998.
- [11] W. Barthlott, C. Neinhuis, *Planta* **1997**, *202*, 1-8.
- [12] D. Öner, T. J. McCarthy, *Langmuir* **2000**, *16*, 7777-7782.
- [13] T. Baldacchini, J. E. Carey, M. Zhou, E. Mazur, *Langmuir* **2006**, *22*, 4917-4919.
- [14] H. Li, X. Wang, Y. Song, Y. Liu, Q. Li, L. Jiang, D. Zhu, *Angew. Chem. Int. Ed.* **2001**, *40*, 1743 - 1746.
- [15] A. Ahuja, J. A. Taylor, V. Lifton, A. A. Sidorenko, T. R. Salamon, E. J. Lobaton, P. Kolodner, T. N. Krupenkin, *Langmuir* **2008**, *24*, 9-14.
- [16] S. Pan, A. K. Kota, J. M. Mabry, A. Tuteja, *J. Am. Chem. Soc.* **2013**, *135*, 578-581.
- [17] S. Parvate, P. Dixit, S. Chattopadhyay, *J. Phys. Chem. B* **2020**, *124*, 1323-1360.
- [18] F. L. Geyer, E. Ueda, U. Liebel, N. Grau, P. A. Levkin, *Angew. Chem. Int. Ed.* **2011**, *50*, 8424-8427.
- [19] F. Svec, J. M. J. Fréchet, *Chem. Mater.* **1995**, *7*, 707-715.
- [20] D. Zahner, J. Abagat, F. Svec, J. M. J. Fréchet, P. A. Levkin, *Adv. Mater.* **2011**, *23*, 3030-3034.
- [21] M. A. Brumbach, Neal, *Encyclopedia of Electrochemistry*, Wiley, Weinheim, **2007**.
- [22] B. Neises, W. Steglich, *Angew. Chem. Int. Ed.* **1978**, *17*, 522-524.
- [23] R. M. Bär, S. Widmaier, P. A. Levkin, *RSC Adv.* **2016**, *6*, 98257-98266.
- [24] A. N. Efremov, E. Stanganello, A. Welle, S. Scholpp, P. A. Levkin, *Biomaterials* **2013**, *34*, 1757-1763.
- [25] A. A. Popova, S. M. Schillo, K. Demir, E. Ueda, A. Nesterov-Mueller, P. A. Levkin, *Adv. Mater.* **2015**, *27*, 5217-5222.
- [26] A. A. Popova, C. Depew, K. M. Permana, A. Trubitsyn, R. Peravali, J. Á. G. Ordiano, M. Reischl, P. A. Levkin, *SLAS Technol.* **2016**, *22*, 163-175.
- [27] A. A. Popova, K. Demir, T. G. Hartanto, E. Schmitt, P. A. Levkin, *RSC Adv.* **2016**, *6*, 38263-38276.
- [28] T. Tronser, A. A. Popova, M. Jaggy, M. Bastmeyer, P. A. Levkin, *Adv. Healthc. Mater.* **2017**, *6*, 1700622.
- [29] T. Tronser, K. Demir, M. Reischl, M. Bastmeyer, P. A. Levkin, *Lab Chip* **2018**, *18*, 2257-2269.

- [30] A. A. Popova, D. Marcato, R. Peravali, I. Wehl, U. Schepers, P. A. Levkin, *Adv. Funct. Mater.* **2018**, *28*, 1703486.
- [31] A. A. Popova, S. Dietrich, W. Huber, M. Reischl, R. Peravali, P. A. Levkin, *SLAS Technol.* **2020**, 2472630320934432.
- [32] A. I. Neto, K. Demir, A. A. Popova, M. B. Oliveira, J. F. Mano, P. A. Levkin, *Adv. Mater.* **2016**, *28*, 7613-7619.
- [33] A. Rosenfeld, C. Oelschlaeger, R. Thelen, S. Heissler, P. A. Levkin, *Mater. Today Bio* **2020**, *6*, 100053.
- [34] M. Benz, M. R. Molla, A. Böser, A. Rosenfeld, P. A. Levkin, *Nat. Commun.* **2019**, *10*, 2879.
- [35] R. B. Merrifield, *J. Am. Chem. Soc.* **1963**, *85*, 2149-2154.
- [36] https://www.nobelprize.org/nobel_prizes/chemistry/laureates/1984/ (downloaded 08.09.2017).
- [37] L. M. Gierasch, *Pept. Sci.* **2006**, *84*, 433-434.
- [38] B. Gutte, R. B. Merrifield, *J. Biol. Chem.* **1971**, *246*, 1922-1941.
- [39] A. Marglin, *Pept. Sci.* **2008**, *90*, 200-202.
- [40] C. B. Reese, *Org. Biomol. Chem.* **2005**, *3*, 3851-3868.
- [41] K. Burgess, *Solid-Phase Organic Synthesis*, Wiley, Weinheim, **2004**.
- [42] R. Haag, A. Hebel, J.-F. Stumbé, *Handbook of Combinatorial Chemistry*, Wiley, Weinheim, **2002**.
- [43] F. Guillier, D. Orain, M. Bradley, *Chem. Rev.* **2000**, *100*, 2091-2158.
- [44] J. Clayden, N. Greeves, S. Warren, *Organic Chemistry*, OUP Oxford, Oxford, **2012**.
- [45] J. A. Barltrop, P. Schofield, *Tetrahedron Lett.* **1962**, *3*, 697-699.
- [46] C.-H. Park, R. S. Givens, *J. Am. Chem. Soc.* **1997**, *119*, 2453-2463.
- [47] C. G. Bochet, *J. Chem. Soc., Perkin Trans. 1* **2002**, 125-142.
- [48] C. H. Bamford, R. G. W. Norrish, *J. Chem. Soc.* **1935**, 1504-1511.
- [49] J. A. Barltrop, P. J. Plant, P. Schofield, *Chem. Commun.* **1966**, 822-823.
- [50] S. Walbert, W. Pfeleiderer, U. E. Steiner, *Helv. Chim. Acta* **2001**, *84*, 1601-1611.
- [51] A. Patchornik, B. Amit, R. B. Woodward, *J. Am. Chem. Soc.* **1970**, *92*, 6333-6335.
- [52] J. F. Cameron, J. M. J. Frechet, *J. Am. Chem. Soc.* **1991**, *113*, 4303-4313.
- [53] S. M. Sternson, S. L. Schreiber, *Tetrahedron Lett.* **1998**, *39*, 7451-7454.
- [54] C. P. Holmes, *J. Org. Chem.* **1997**, *62*, 2370-2380.
- [55] C. P. Holmes, D. G. Jones, *J. Org. Chem.* **1995**, *60*, 2318-2319.
- [56] K. Qvortrup, V. V. Komnatnyy, T. E. Nielsen, *Org. Lett.* **2014**, *16*, 4782-4785.
- [57] I. Ugi, C. Steinbrückner, *Angew. Chem.* **1960**, *72*, 267-268.
- [58] I. Ugi, *Angew. Chem. Int. Ed.* **1962**, *1*, 8-21.
- [59] M. A. Fouad, H. Abdel-Hamid, M. S. Ayoup, *RSC Adv.* **2020**, *10*, 42644-42681.
- [60] A. Dömling, W. Wang, K. Wang, *Chem. Rev.* **2012**, *112*, 3083-3135.
- [61] M. C. Pirrung, K. D. Sarma, *J. Am. Chem. Soc.* **2004**, *126*, 444-445.
- [62] J.-C. Bradley, K. Baig Mirza, T. Osborne, A. Williams, K. Owens, *J. Vis. Exp.* **2008**, 942.

- [63] R. O. Rocha, M. O. Rodrigues, B. A. D. Neto, *ACS Omega* **2020**, *5*, 972-979.
- [64] G. A. Medeiros, W. A. da Silva, G. A. Bataglioni, D. A. C. Ferreira, H. C. B. de Oliveira, M. N. Eberlin, B. A. D. Neto, *Chem. Commun.* **2014**, *50*, 338-340.
- [65] J. Zhang, P. Yu, S.-Y. Li, H. Sun, S.-H. Xiang, J. Wang, K. N. Houk, B. Tan, *Science* **2018**, *361*, eaas8707.
- [66] A. Dömling, I. Ugi, *Angew. Chem. Int. Ed.* **2000**, *39*, 3168-3210.
- [67] W. Keung, F. Bakir, A. P. Patron, D. Rogers, C. D. Priest, V. Darmohusodo, *Tetrahedron Lett.* **2004**, *45*, 733-737.
- [68] T. Godet, Y. Bonvin, G. Vincent, D. Merle, A. Thozet, M. A. Ciufolini, *Org. Lett.* **2004**, *6*, 3281-3284.
- [69] N. P. Tripolitsiotis, M. Thomaidi, C. G. Neochoritis, *Eur. J. Org. Chem.* **2020**, *2020*, 6525-6554.
- [70] A. Ilyin, V. Kysil, M. Krasavin, I. Kurashvili, A. V. Ivachtchenko, *J. Org. Chem.* **2006**, *71*, 9544-9547.
- [71] Z. Ma, Z. Xiang, T. Luo, K. Lu, Z. Xu, J. Chen, Z. Yang, *J. Comb. Chem.* **2006**, *8*, 696-704.
- [72] Z. Xiang, T. Luo, K. Lu, J. Cui, X. Shi, R. Fathi, J. Chen, Z. Yang, *Org. Lett.* **2004**, *6*, 3155-3158.
- [73] S. C. Solleder, K. S. Wetzels, M. A. R. Meier, *Polym. Chem.* **2015**, *6*, 3201-3204.
- [74] M. Hartweg, C. J. C. Edwards-Gayle, E. Radvar, D. Collis, M. Reza, M. Kaupp, J. Steinkoenig, J. Ruokolainen, R. Rambo, C. Barner-Kowollik, I. W. Hamley, H. S. Azevedo, C. R. Becer, *Polym. Chem.* **2018**, *9*, 482-489.
- [75] N. Miyaura, K. Yamada, A. Suzuki, *Tetrahedron Lett.* **1979**, *20*, 3437-3440.
- [76] N. Miyaura, A. Suzuki, *J. Chem. Soc., Chem. Commun.* **1979**, 866-867.
- [77] N. R. Lee, R. T. H. Linstadt, D. J. Gloisten, F. Gallou, B. H. Lipshutz, *Org. Lett.* **2018**, *20*, 2902-2905.
- [78] The Nobel Prize in Chemistry 2010, Nobel Media AB, <https://www.nobelprize.org/prizes/chemistry/2010/summary/> (retrieved 21.12.2020).
- [79] R. Franzén, *Can. J. Chem.* **2000**, *78*, 957-962.
- [80] M. M. Heravi, E. Hashemi, *Tetrahedron* **2012**, *68*, 9145-9178.
- [81] A. Chatterjee, T. R. Ward, *Catal. Lett.* **2016**, *146*, 820-840.
- [82] M. Guo, Q. Zhang, *Tetrahedron Lett.* **2009**, *50*, 1965-1968.
- [83] C. Liu, X. Rao, Y. Zhang, X. Li, J. Qiu, Z. Jin, *Eur. J. Org. Chem.* **2013**, *2013*, 4345-4350.
- [84] L. Kürti, B. Czakó, *Strategic Applications of Named Reactions in Organic Synthesis: Background and Detailed Mechanisms*, Elsevier Science, Amsterdam, **2005**.
- [85] G. B. Smith, G. C. Dezeny, D. L. Hughes, A. O. King, T. R. Verhoeven, *J. Org. Chem.* **1994**, *59*, 8151-8156.
- [86] G. W. Kabalka, V. Namboodiri, L. Wang, *Chem. Commun.* **2001**, 775-775.
- [87] J. Sherwood, J. H. Clark, I. J. S. Fairlamb, J. M. Slattery, *Green Chem.* **2019**, *21*, 2164-2213.
- [88] X. Li, H. Zhang, Q. Hu, B. Jiang, Y. Zeli, *Synth. Commun.* **2018**, *48*, 3123-3132.
- [89] R. Martin, S. L. Buchwald, *Acc. Chem. Res.* **2008**, *41*, 1461-1473.
- [90] J. P. Knowles, A. Whiting, *Org. Biomol. Chem.* **2007**, *5*, 31-44.
- [91] J.-S. Ouyang, Y.-F. Li, F.-D. Huang, D.-D. Lu, F.-S. Liu, *ChemCatChem* **2018**, *10*, 371-375.
- [92] C. A. Fleckenstein, H. Plenio, *Chem. Soc. Rev.* **2010**, *39*, 694-711.
- [93] M. R. Molla, A. Böser, A. Rana, K. Schwarz, P. A. Levkin, *Bioconjugate Chem.* **2018**, *29*, 992-999.

- [94] A. O. Pedersen, J. Jacobsen, *Eur. J. Biochem.* **1980**, *106*, 291-295.
- [95] L. Feng, S. Li, Y. Li, H. Li, L. Zhang, J. Zhai, Y. Song, B. Liu, L. Jiang, D. Zhu, *Adv. Mater.* **2002**, *14*, 1857-1860.
- [96] J. Yong, J. Huo, F. Chen, Q. Yang, X. Hou, *PCCP* **2018**, *20*, 25140-25163.
- [97] R. Blossey, *Nat. Mater.* **2003**, *2*, 301.
- [98] E. Vazirinasab, R. Jafari, G. Momen, *Surf. Coat. Technol.* **2018**, *341*, 40-56.
- [99] I. Banerjee, R. C. Pangule, R. S. Kane, *Adv. Mater.* **2011**, *23*, 690-718.
- [100] E. Ueda, P. A. Levkin, *Adv. Mater.* **2013**, *25*, 1234-1247.
- [101] C. Dorrrer, J. Rhe, *Adv. Mater.* **2008**, *20*, 159-163.
- [102] S. Wang, Y. Song, L. Jiang, *J. Photoch. Photobio. C.* **2007**, *8*, 18-29.
- [103] W. Zhu, X. Feng, L. Feng, L. Jiang, *Chem. Commun.* **2006**, 2753-2755.
- [104] H. Liu, L. Feng, J. Zhai, L. Jiang, D. Zhu, *Langmuir* **2004**, *20*, 5659-5661.
- [105] S. Wang, X. Feng, J. Yao, L. Jiang, *Angew. Chem. Int. Ed.* **2006**, *45*, 1264-1267.
- [106] L. M. Siewierski, W. J. Brittain, S. Petrash, M. D. Foster, *Langmuir* **1996**, *12*, 5838-5844.
- [107] W. Jiang, G. Wang, Y. He, X. Wang, Y. An, Y. Song, L. Jiang, *Chem. Commun.* **2005**, 3550-3552.
- [108] X. Du, J. Li, A. Welle, L. Li, W. Feng, P. A. Levkin, *Adv. Mater.* **2015**, *27*, 4997-5001.
- [109] G. Godeau, T. Darmanin, F. Guittard, *J. Appl. Polym. Sci.* **2016**, *133*.
- [110] Y. Aono, A. Hirata, H. Tokura, *Appl. Surf. Sci.* **2016**, *371*, 530-537.
- [111] T. D. Nelson, R. D. Crouch, *Synthesis* **1996**, *1996*, 1031-1069.
- [112] J. Wu, J. Xia, W. Lei, B.-p. Wang, *Sci. Rep.* **2013**, *3*, 3268.
- [113] R. D. Crouch, *Synth. Commun.* **2013**, *43*, 2265-2279.
- [114] L. Pauling, *The Nature of the Chemical Bond and the Structure of Molecules and Crystals*, Cornell University Press, New York, **1960**.
- [115] J. A. DiMasi, H. G. Grabowski, R. W. Hansen, *J. Health Econ.* **2016**, *47*, 20-33.
- [116] R. Frank, *J. Immunol. Methods* **2002**, *267*, 13-26.
- [117] H. E. Blackwell, *Curr. Opin. Chem. Biol.* **2006**, *10*, 203-212.
- [118] F. Deiss, W. L. Matochko, N. Govindasamy, E. Y. Lin, R. Derda, *Angew. Chem. Int. Ed.* **2014**, *53*, 6374-6377.
- [119] P. M. Lpez-Prez, E. Grimsey, L. Bourne, R. Mikut, K. Hilpert, *Front. Chem.* **2017**, *5*, 25-25.
- [120] A. Kramer, T. Keitel, K. Winkler, W. Stcklein, W. Hhne, J. Schneider-Mergener, *Cell* **1997**, *91*, 799-809.
- [121] K. Hilpert, D. F. H. Winkler, R. E. W. Hancock, *Nat. Protoc.* **2007**, *2*, 1333.
- [122] M. Beyer, A. Nesterov, I. Block, K. Knig, T. Felgenhauer, S. Fernandez, K. Leibe, G. Torralba, M. Hausmann, U. Trunk, V. Lindenstruth, F. R. Bischoff, V. Stadler, F. Breitling, *Science* **2007**, *318*, 1888-1888.
- [123] V. Stadler, T. Felgenhauer, M. Beyer, S. Fernandez, K. Leibe, S. Gttler, M. Grning, K. Knig, G. Torralba, M. Hausmann, V. Lindenstruth, A. Nesterov, I. Block, R. Pipkorn, A. Poustka, F. R. Bischoff, F. Breitling, *Angew. Chem. Int. Ed.* **2008**, *47*, 7132-7135.

- [124] A. Rosenfeld, M. Brehm, A. Welle, V. Trouillet, S. Heissler, M. Benz, P. A. Levkin, *Mater. Today Bio* **2019**, 100022.
- [125] H. A. Kenny, M. Lal-Nag, E. A. White, M. Shen, C.-Y. Chiang, A. K. Mitra, Y. Zhang, M. Curtis, E. M. Schryver, S. Bettis, A. Jadhav, M. B. Boxer, Z. Li, M. Ferrer, E. Lengyel, *Nat. Commun.* **2015**, *6*, 6220.
- [126] M. H. Beresini, Y. Liu, T. D. Dawes, K. R. Clark, L. Orren, S. Schmidt, R. Turincio, S. W. Jones, R. A. Rodriguez, P. Thana, D. Hascall, D. P. Gross, N. J. Skelton, *J. Biomol. Screen.* **2014**, *19*, 758-770.
- [127] B. C. Duffy, L. Zhu, H. Decornez, D. B. Kitchen, *Biorg. Med. Chem.* **2012**, *20*, 5324-5342.
- [128] A. Kramer, U. Reineke, L. Dong, B. Hoffmann, U. Hoffmüller, D. Winkler, R. Volkmer-Engert, J. Schneider-Mergener, *J. Pept. Res.* **1999**, *54*, 319-326.
- [129] T. Ast, N. Heine, L. Germeroth, J. Schneider-Mergener, H. Wenschuh, *Tetrahedron Lett.* **1999**, *40*, 4317-4318.
- [130] W. Feng, L. Li, E. Ueda, J. Li, S. Heißler, A. Welle, O. Trapp, P. A. Levkin, *Adv. Mater. Interfaces* **2014**, *1*, 1400269.
- [131] C. N. Robson, J. Alexander, A. L. Harris, I. D. Hickson, *Cancer Res.* **1986**, *46*, 6290-6294.
- [132] I. Akritopoulou-Zanze, *Curr. Opin. Chem. Biol.* **2008**, *12*, 324-331.
- [133] J.-C. Bradley, K. B. Mirza, T. Osborne, A. Williams, K. Owens, *J. Vis. Exp.* **2008**, 942.
- [134] S. Marcaccini, T. Torroba, *Nat. Protoc.* **2007**, *2*, 632.
- [135] S. Laugesen, P. Roepstorff, *J. Am. Soc. Mass. Spectrom.* **2003**, *14*, 992-1002.
- [136] A. A. Popova, C. Depew, K. M. Permana, A. Trubitsyn, R. Peravali, J. Á. G. Ordiano, M. Reischl, P. A. Levkin, *SLAS Technol.* **2017**, *22*, 163-175.
- [137] J. Yao, J. R. Scott, M. K. Young, C. L. Wilkins, *J. Am. Soc. Mass. Spectrom.* **1998**, *9*, 805-813.
- [138] N. Goldman, P. Bertone, S. Chen, C. Dessimoz, E. M. LeProust, B. Sipos, E. Birney, *Nature* **2013**, *494*, 77.
- [139] J.-F. Lutz, M. Ouchi, D. R. Liu, M. Sawamoto, *Science* **2013**, 341.
- [140] W. A. Braunecker, K. Matyjaszewski, *Prog. Polym. Sci.* **2007**, *32*, 93-146.
- [141] G. Moad, E. Rizzardo, S. H. Thang, *Aust. J. Chem.* **2005**, *58*, 379-410.
- [142] M. Maric, *Curr. Org. Chem.* **2018**, *22*, 1264-1284.
- [143] A. Szekely, M. Klusmann, *Chem. Asian J.* **2019**, *14*, 105-115.
- [144] B. Schmidt, C. Barner-Kowollik, *Nat. Chem.* **2013**, *5*, 990-992.
- [145] D. M. M. Jaradat, *J. Amino Acids* **2018**, *50*, 39-68.
- [146] S. D. Ganesh, N. Saha, O. Zandraa, R. N. Zuckermann, P. Saha, *Polym. Bull.* **2017**, *74*, 3455-3466.
- [147] T. S. Burkoth, A. T. Fafarman, D. H. Charych, M. D. Connolly, R. N. Zuckermann, *J. Am. Chem. Soc.* **2003**, *125*, 8841-8845.
- [148] L. Q. Wen, G. Edmunds, C. Gibbons, J. B. Zhang, M. R. Gadi, H. L. Zhu, J. Q. Fang, X. W. Liu, Y. Kong, P. G. Wang, *Chem. Rev.* **2018**, *118*, 8151-8187.
- [149] C.-H. Wong, S. C. Zimmerman, *Chem. Commun.* **2013**, *49*, 1679-1695.
- [150] S. C. Solleder, R. V. Schneider, K. S. Wetzel, A. C. Boukis, M. A. R. Meier, *Macromol. Rapid Commun.* **2017**, *38*, 1600711.
- [151] T. T. Trinh, L. Oswald, D. Chan-Seng, J.-F. Lutz, *Macromol. Rapid Commun.* **2014**, *35*, 141-145.

- [152] Y. Hibi, M. Ouchi, M. Sawamoto, *Nat. Commun.* **2016**, *7*, 11064.
- [153] P. Espeel, L. L. G. Carrette, K. Bury, S. Capenberghs, J. C. Martins, F. E. Du Prez, A. Madder, *Angew. Chem. Int. Ed.* **2013**, *52*, 13261-13264.
- [154] S. C. Solleder, D. Zengel, K. S. Wetzel, M. A. R. Meier, *Angew. Chem. Int. Ed.* **2016**, *55*, 1204-1207.
- [155] T. F. Niu, L. Gu, W. B. Yi, C. Cai, *ACS Comb. Sci.* **2012**, *14*, 309-315.
- [156] E. T. Sletten, M. Nuño, D. Guthrie, P. H. Seeberger, *Chem. Commun.* **2019**, *55*, 14598-14601.
- [157] N. Schneider, D. M. Lowe, R. A. Sayle, M. A. Tarselli, G. A. Landrum, *J. Med. Chem.* **2016**, *59*, 4385-4402.
- [158] D. G. Brown, J. Boström, *J. Med. Chem.* **2016**, *59*, 4443-4458.
- [159] S. M. Mennen, C. Alhambra, C. L. Allen, M. Barberis, S. Berritt, T. A. Brandt, A. D. Campbell, J. Castañón, A. H. Cherney, M. Christensen, D. B. Damon, J. Eugenio de Diego, S. García-Cerrada, P. García-Losada, R. Haro, J. Janey, D. C. Leitch, L. Li, F. Liu, P. C. Lobben, D. W. C. MacMillan, J. Magano, E. McInturff, S. Monfette, R. J. Post, D. Schultz, B. J. Sitter, J. M. Stevens, I. I. Strambeanu, J. Twilton, K. Wang, M. A. Zajac, *Org. Process Res. Dev.* **2019**, *23*, 1213-1242.
- [160] Gelbe Liste - Losartan, Medizinische Medien Informations GmbH, https://www.gelbe-liste.de/wirkstoffe/Losartan_26097 (retrieved 12.6.2020).
- [161] Römpf Online - Flurbiprofen, Georg Thieme Verlag, <https://roempp.thieme.de/lexicon/RD-06-01477> (retrieved 12.6.2020).
- [162] Gelbe Liste - Telmisartan, Medizinische Medien Informations GmbH, https://www.gelbe-liste.de/wirkstoffe/Telmisartan_5064 (retrieved 12.6.2020).
- [163] R. J. Edsall, H. A. Harris, E. S. Manas, R. E. Mewshaw, *Biorg. Med. Chem.* **2003**, *11*, 3457-3474.
- [164] K. Connor, K. Ramamoorthy, M. Moore, M. Mustain, I. Chen, S. Safe, T. Zacharewski, B. Gillesby, A. Joyeux, P. Balaguer, *Toxicol. Appl. Pharmacol.* **1997**, *145*, 111-123.
- [165] R. Frei, A. S. Breitbach, H. E. Blackwell, *Chem. Sci.* **2012**, *3*, 1555-1561.
- [166] C. A. Nogueira, A. P. Paiva, P. C. Oliveira, M. C. Costa, A. M. R. da Costa, *J. Hazard. Mater.* **2014**, *278*, 82-90.
- [167] S. Wang, A. Chen, Z. Zhang, J. Peng, *Environ. Prog. Sustain* **2014**, *33*, 913-917.
- [168] A. Azizitorghabeh, J. Wang, J. A. Ramsay, A. Ghahreman, *Miner. Eng.* **2021**, *160*, 106689.
- [169] A. Milheiro, K. Nozaki, C. J. Kleverlaan, J. Muris, H. Miura, A. J. Feilzer, *Odontology* **2016**, *104*, 136-142.
- [170] J. C. Hermann, Y. Chen, C. Wartchow, J. Menke, L. Gao, S. K. Gleason, N.-E. Haynes, N. Scott, A. Petersen, S. Gabriel, B. Vu, K. M. George, A. Narayanan, S. H. Li, H. Qian, N. Beatini, L. Niu, Q.-F. Gan, *ACS Med. Chem. Lett.* **2012**, *4*, 197-200.
- [171] S. Buchinger, D. Spira, K. Bröder, M. Schlüsener, T. Ternes, G. Reifferscheid, *Anal. Chem.* **2013**, *85*, 7248-7256.
- [172] D. Spira, G. Reifferscheid, S. Buchinger, *JPC-J Planar Chromat.* **2013**, *26*, 395-401.
- [173] J.-H. Zhang, T. D. Y. Chung, K. R. Oldenburg, *J. Biomol. Screen.* **1999**, *4*, 67-73.
- [174] R. Ginzburg-Turgeman, J.-B. Guion, D. Mandler, *J. Solid State Electrochem.* **2011**, *15*, 2401-2407.